Florian Riedlsperger (BSc)

Thermodynamic Precipitation Kinetic Simulation in Martensitic Cr-Steels

MASTER'S THESIS

to achieve the university degree of

Diplom-Ingenieur

Master's degree programme: Mechanical Engineering

submitted to

Graz University of Technology

Supervisor

Univ.-Prof. Dipl.-Ing. Dr. techn. Bernhard Sonderegger

Institute of Materials Science and Welding

Faculty of Mechanical Engineering and Economic Sciences
Graz University of Technology

Graz, October 2016

AFFIDAVIT

I declare that I have authored this thesis independently, that I have not used other than the declared sources/resources, and that I have explicitly indicated all material which has been quoted either literally or by content from the sources used. The text document uploaded to TUGRAZonline is identical to the present master‘s thesis dissertation.

Date

Signature

"*One has the impression, that modern physics is based on assumptions, that somehow resemble the smile of a cat which is not there.*"

"*Man hat den Eindruck, dass die moderne Physik auf Annahmen beruht, die irgendwie dem Lächeln einer Katze gleichen, die gar nicht da ist.*"

Albert Einstein

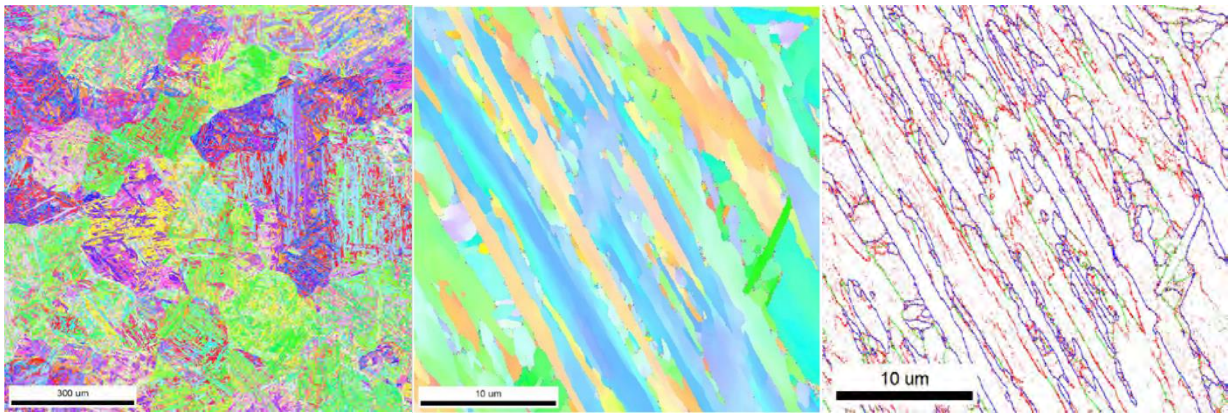

"*Energy is in fact the substance, from which all elementary particles, all atoms and therefore all things are made, and energy is that which moves. … Energy may be called the fundamental cause for all changes in the world.*"

"*Die Energie ist tatsächlich der Stoff, aus dem alle Elementarteilchen, alle Atome und daher überhaupt alle Dinge gemacht sind, und gleichzeitig ist die Energie auch das Bewegende. … Die Energie kann als Ursache für alle Veränderungen in der Welt angesehen werden.*"

Werner Heisenberg (Physics and Philosophy, 1958)

Abstract

This diploma thesis deals with the thermodynamic simulation of microstructural changes taking place in martensitic chromium steels during creep, focusing mainly on material Gr. 91/ P91. Situation in welded and non-welded condition will be considered.

Experimental investigations and literature study served to achieve updated input parameters for thermodynamic precipitation kinetic modelling, producing more diverse, physically-based and accurate results compared to an existing IWS MatCalc model from 2015. Additional measurements and data from literature helped to assess and validate the reached quality of simulation. On basis of this verified simulation results, backstress calculations were conducted, demonstrating and quantifying the material's resistance to plastic deformation, distinguishing between stronger and weaker zones of microstructure.

Die vorliegende Diplomarbeit handelt von der thermodynamischen Simulation mikrostruktureller Veränderungen in martensitischem Chrom-Stahl während eines Kriechvorgangs, wobei das Hauptaugenmerk auf der Materialsorte Gr. 91/ P91-Stahl in geschweißtem und in ungeschweißtem Zustand liegt.

Experimentelle Untersuchungen und Literaturrecherche dienten einer Aktualisierung von Inputparametern für eine thermodynamische Ausscheidungskinetiksimulation, wodurch vielfältigere, physikalischere and genauere Ergebnisse erzielt werden konnten im Vergleich mit einem bestehenden IWS MatCalc-Modell aus dem Jahr 2015. Zusätzliche Messungen und Daten aus der Literatur halfen schließlich bei Bewertung und Validierung der erreichten Simulationsqualität. Ausgehend von diesen verifizierten MatCalc Simulationsergebnissen wurden Backstress-Berechnungen durchgeführt, wodurch der Widerstand des Materials gegen plastische Deformation demonstriert und quantifiziert werden konnte. Dabei wurde wiederum zwischen stärkeren und schwächeren Zonen in der Mikrostruktur unterschieden.

Acknowledgements

First of all, I want to thank my family in Austria (my father Herbert and my brother Philipp Cem) that they were always fully behind my choice of becoming an engineer despite all the challenges on that rough and long way. In memory of my beloved mother Deniz Gürsen, who passed away to early, my family and relatives in Turkey (such as Ayfer, Cihan, Ceylan, Necip, Aygül, Mehmet) have become more important than ever before. I appreciate their mental support very much, especially when recharging my batteries in Istanbul after months of hard work in Graz.

I also want to thank my devoted friend Toni for encouraging and motivating me for university and private life in Graz in good such as in bad times.

Moreover, I want to thank my supervisor, Prof. Bernhard Sonderegger, and the head of the Institute of Materials Science and Welding (IWS), Prof. Christof Sommitsch, for offering me the opportunity to write my thesis on a highly interesting topic embedded in an industry project.

I particularly have to express sincere gratitude to Prof. Bernhard Sonderegger for his excellent support and patience during my work, including weekly meetings, fruitful discussions, useful advice and never-ending inspiration for accomplishing further tasks.

The whole IWS modelling group (Surya, Bernadette, Dilek, Bernhard Krenmayr, Romain, David, Mateusz and others) created a very comfortable and nice atmosphere in the office. I always felt warmly welcome, and my colleagues helped me to find solutions for many scientific problems, sometimes just by sending literature to me or by debating issues. Thank you!

Finally, I am grateful to the IWS laboratory staff (Thomas, Gernot and Kurt) for assisting me many times when it came to preparing and polishing specimen.

Financial support from Mitsubishi Heavy Industries (MHI) Japan is thankfully acknowledged related to the project "*Development of a creep strength estimation method on microstructural simulation in modified 9Cr-1Mo steels*".

Content

1.) Introduction

1.1) Objective of Master Thesis

This thesis describes improvements in the simulation of creep resistant martensitic 9 % Cr steel in MatCalc software, carried out at the Institute for Materials Science and Welding, Graz University of Technology, Austria, between January and July 2016 within the project "*Development of a creep strength estimation method based on microstructural simulation in mod. 9Cr-1Mo steels"* by Florian Riedlsperger under supervision of Univ.-Prof. Bernhard Sonderegger. This projected is embedded in a cooperation with Mitsubishi Heavy Industries (MHI), Japan.

The objective of the thesis lies in **modelling** the evolution of **precipitates** in steel during creep.

The document will both deal with **base metal** (short name: BM) results such as with results from a simulated **fine-grained heat affected zone** (short name: FGHAZ), meaning that the microstructure was before affected by a welding cycle.

First of all, external content from **literature** is presented and physical backgrounds will be explained. The literature study (chapter 3) also involves the status of the TU Graz MatCalc model from 2015 within the context of a previous project for MHI (model 0 written by S. Vujic). Furthermore, strengthening mechanisms are discussed and the theory of backstress will be introduced.

In the experimental part (chapter 4) the methods of **measurements** (EBSD, TEM) and **simulations** are shown (models 1 and 2) and it is demonstrated how they differ from each other. Model 0 will be improved by adjusting parameters on basis of 2015 findings (leading to model 1).

In chapter 5 about results, microstructural data is **analyzed** in an innovative way, contributing then to the more advanced MatCalc model 2. All simulation results will be revealed, predominantly concerning precipitation kinetic calculations.

The chapter discussion, where MatCalc results are compared to literature material and to 2016 measurements, served to assess the quality of models and **validate** them (chapter 6).

The thesis will conclude with a summary and perspectives for possible future tasks (chapter 7).

As an appendix (chapter 8), the comprehensive MatCalc script for model 2 was added, including a documentation written on the right side of the script code.

Finally, on the last pages the bibliography (chapter 9) can be found.

1.2) Properties of Martensitic Chromium Steel

Grade 91 steel is also known as P91 chromium steel and represents one of the most wide-spread steels for high temperature applications in thermal power plants. Examples for realized components made out of Gr. 91 are superheaters, steam pipes, boilers and blades for steam turbines. [1]

1.2.1) Microstructure and Manufacturing

P91 microstructure consists of tempered martensite, which means that austenitization and quenching (=normalizing) as well as tempering are the necessary steps of heat treatment for manufacturing. During air cooling in the normalizing process, austenite in the absence of diffusion rapidly transforms into martensite, which is marked by a highly strained body-centered cubic lattice. [2] Martensite, which is very hard and brittle, can be further subdevided into a microstructure of packets, blocks and laths (for a good visualization see figure 1a). [3] Tempering, in contrast, is responsible for development of low-angle subgrain boundaries that give back ductility to the material, and for precipitation of secondary phases, like chromium carbide or MX particles e.g. (figure 1b). [3] [2]

1.2.2) Assets of P91

P91 is characterized by considerable toughness and resistance against thermal loads, stability against oxidation, high creep strength and last but not least by low production costs in comparison to austenitic steels, for instance. High thermal conductivity, but low thermal expansion also rank amongst the biggest advantages. [4]

1.2.3) Issue of Welding

Unfortunately, concern is growing about the long-term creep behavior of Gr. 91 weldments. Especially exposure to a local welding peak temperatures above Ac_3 and the use of processes that create a large heat-affected zone is regarded as critical. [5] In this area, the stability of microstructure is undermined by formation of prior austenitic grains without lath structure that are often smaller than 10 µm and act like highways for diffusion. As a result, in the FGHAZ so-called type IV cracking may take place during creep, which is connected to formation and growth of voids until damage. In this zone, precipitate evolution during service and subgrain coarsening are accelerated, too. This makes the creep strength drop dramatically in FGHAZ, increasing the risk of early damage and associated failure. [5] [6]

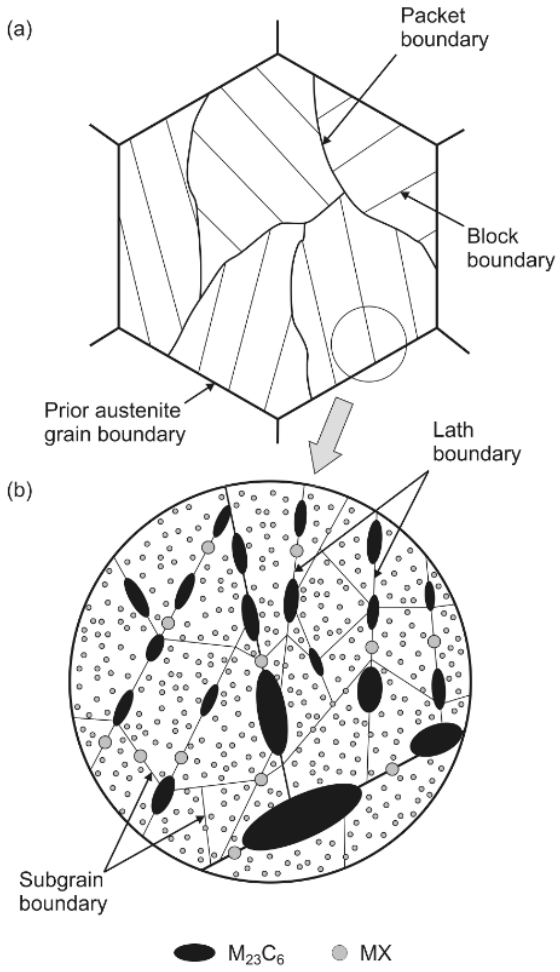

Figure 1) Tempered martensite in 9- 12 % Cr steels: PAGB, packets, blocks, laths, subgrains and possible precipitates [3]

1.2.4) Importance for Environment

Being aware of climate change and environmental problems, many countries started trying to reduce CO_2 emissions and also air pollution. As renewable energy at the moment is not completely able to replace fossile energies, modern coal and gas power plants- besides pumped hydroelectric energy storage (PHES)- remain important to compensate for fluctuations in the power supply system. Their operation proves to be more flexible and independent from weather conditions. By increasing service temperature (from 530 to 600 °C) and pressure (from 180 to 300 bar), the degree of effectiveness of thermal power plants could be considerably improved in the last years from 30- 35 % to around 42- 47 %, going hand in hand with around 30 % less CO_2. [7] Innovative and safe materials are part of this steady progress. Optimizing thermodynamic design [8] and making use of district heating are other possible measures for maximizing effectiveness.

Additionally, efforts for carbon capture and storage have been made, realizing 13 projects world wide (in the year 2015) for test purposes [9], so far with questionable success due to high costs. Future applications for Gr. 91 steel or its successor P92 might lie in heat exchanger pipes for solar thermal power plants. For instance, such a concentrated solar tower power plant (Ivanpah) with around 400 MW in performance has recently been built in California, USA [10].

As a result, heat-resistent martensitic steel that nowadays is predominantly used in fossile or nuclear power plants could soon play an important role for the expansion of solar energy, too.

2.) Literature Study

2.1) Character and Role of Precipitates

To a significant part, creep resistant steels owe their good creep properties to precipitates. These precipitates may decorate different places in the material and serve to hinder dislocations from movement, increasing the strength. The involved mechanisms will be explained in chapter 3.5. However, the microstructure does not show a static behavior, but is constantly evolving under high temperature and stress. This limits the reliability of Gr. 91 steel over long periods of time.

The most common precipitates dominating the microstructure are as follows:

- $M_{23}C_6$: This carbide enriched with chromium plays a central role for creep strength. It has a cubic crystal structure and was reported to nucleate after tempering predominantly at prior austenitic grain boundaries and at martensitic lath boundaries. Regrettably, its high coarsening tendency during service at elevated temperatures is regarded as problematic for maintaining long-term creep strength [4] [2] [3]

- MX: These nitrides or carbides include vanadium nitride VN, niobium carbid NbC and mixed forms. After tempering these cubic particles in as-received condition can be found at dislocations, in the bulk material or on subgrain boundaries. MX precipitates stand out for their long stability in creep conditions. Coarsening is comparably low. Unfortunately, a negative interaction with a possible modified Z phase after long service times was observed. Modified Z phase may grow at the expense of VN. [4] [2] [3]

- Laves phase: The role of this intermetallic phase $(Fe,Cr,Si)_2(W,Mo)$ with hexagonal structure for precipitation strengthening is disputed. Fact is that it forms during service after several hundreds or thousands of hours, being located at grain boundaries or subgrain boundaries and showing a fast coarsening tendency. Moreover, Laves phase seems to harm

the effect of solid solution hardening (see more details in chapter 3.5.5) because of consuming the chemical elements of W or Mo during long-term creep. [4] [2] [7]

- Aluminium nitride: Aluminium is added to Gr. 91 steels since it provides advantages for manufacturing processes (especially casting and forming). Unfortunately, it has been found out by [11] that aluminium nitride harms the long-term creep resistance of Gr. 91 steel because of promoting prior austenitic grain refinement. [12] also warn that aluminium nitride tends to consume vanadium nitride particles during service and decreases the phase fraction of all MX precipitates, which negatively affects precipitation strengthening.

- Modified Z phase: The more chromium is contained in the martensitic steel, the higher the risk is estimated for precipitation of modified Z phase particles during long-term creep. As a result, 11- 12 % Cr steels are more threatened. Nevertheless, they have also been detected in 9 % Cr steels. [13] They are made responsible for creep strength reduction because of consuming MX particles and coarsening dramatically fast. Chemical formula of modified Z phase, which has a tetragonal structure, is Cr(V,Nb)N. [14] [2]

2.2) Microstructural Data (External)

This section comprises a literature study on P91 steels with different chemical compositions. The microstructural data will cover as-received, aged and creep loaded conditions. Furthermore, the study contains data of base material and FGHAZ. The presented data were later compared to MatCalc simulation results and helped to assess the quality of MatCalc modelling. The introduced tables were taken from the literature review for MHI project 2016 created by Bernhard Krenmayr and Bernhard Sonderegger [15].

Following abbreviations were used for specification:

- AR: as-received
- FGHAZ: fine grain heat affected zone
- PWHT: post weld heat treated
- GB: grain boundary
- LB: lath boundary
- LI: lath interior
- CO: cuboidal
- IR: irregular
- UF: until fracture

The chemical composition of Gr. 91 steels in the literature review slightly varied (see table 1).

No.	C	Si	Mn	P	S	Cr	Mo	V	Nb	N	Ni	Al	Ti	Zr	Cu	W	Ref.
Min	0.06	0.18	0.25	-	-	7.90	0.80	0.16	0.05	0.025	-	-	-	-	-		[16]
Max	0.15	0.56	0.66	0.025	0.012	9.60	1.10	0.27	0.11	0.080	0.43	0.02	0-01	0-01	-		[16]
1	0.09	0.40	0.43	0.015	<0.01	8.80	0.89	0.19	0.10	0.05	0.09	0.024	-	-	-		[17]
2	0.1	0.36	0.41	0.015	0.003	8.43	0.92	0.20	0.068	0.059	0.11	0.022	-	-	0.04		[18]
3	0.1	0.38	-	-	-	8.10	0.92	0.18	0.073	0.049	0.38	0.049	-	-	-		[19]
4	0.1	0.36	0.41	0.015	0.003	8.43	0.92	0.20	0.068	0.059	0.11	0.022	-	-	0.04		[20]
5	0.09	0.20	0.56	0.021	0.009	8.36	0.86	0.20	0.06	0.065	0.47	0.007	-	-	0.05		[21], [22]
6	0.104	0.27	0.46	0.014	0.003	8.17	0.90	0.194	0.064	0.055	0.16	-	-	-	-		[13]
7	0.091	0.40	0.46	-	-	8.76	0.94	0.19	0.07	0.064	0.11	0.35	-	-	-		[23]
8	0.075	0.422	0.431	0.015	0.001	7.39	0.866	0.153	0.009	0.116	0.370	-	0.001	-	0.072	0.498	[24]
9	n.s.	n.s	n.s	n.s	n.s	9	1	n.s	n.s	n.s	n.s	n.s	n.s	n.s	n.s	n.s	[25]
n.s. … not specified																	

Table 1) Chemical composition of Gr. 91 steels presented in literature review [15]

2.2.1) Subgrain Size

Table 2 gives an insight into subgrain sizes before and after creep. The table includes both base material and FGHAZ.

Literature is partly contradicting, since [19] reports no coarsening of subgrains whereas other sources do. [15]

Data for FGHAZ in general is rare. However, [13] observed a higher coarsening rate and larger subgrain size for FGHAZ compared to BM.

Steel No.	Temp. [°C]	Time [h]	Stress [MPa]	Size [µm]	Investigation method	Reference
3	AR	AR	-	0.40 ±0.06	TEM	[19]
3	600	1014	100	0.40 ±0.06	TEM	[19]
3	600	17500	145	0.40 ±0.06	TEM	[19]
5	600	9111	0	0.4-0.8	TEM	[21]
5	600	9111	125	0.4-1.2	TEM	[21]
6	AR	-	-	0.458	TEM	[13]
6	650	14379	40	0.597	TEM	[13]
6	FGHAZ, PWHT	-	-	0.718	TEM	[13]
6	FGHAZ, PWHT, 650	14379	40	1.230	TEM	[13]
5	600	AR	0	0.2-0.9	TEM	[22]
5	600	16650	110	0.3-1.1	TEM	[22]
5	600	9111	125	0.2-1.0	TEM	[22]
5	600	387	175	0.3-1.0	TEM	[22]
9	780	1	0	0.53	-	[25]

Table 2) Subgrain size in Gr. 91 steel according to literature

2.2.2) Dislocation Density

Table 3 shows literature data on dislocation densities. The table treats of as-received and creep-loaded states of as-received BM as well as in FGHAZ condition. It can be recognized that dislocation density decreases when exposed to thermal loads and stresses during creep. The range of values seems to be huge, especially for XRD measurements. [15]

Steel No.	Temp. [°C]	Time [h]	Stress [MPa]	Dislocation density [m^{-2} x 10^{14}]	Investigation method	Reference
3	AR	AR	-	7.52 ±0.8	TEM	[19]
4	AR	AR	-	4.50 ±1.9	TEM	[20]
3	600	1014	100	4.80 ±0.8	TEM	[19]
4	600	113,431	-	2.20 ±1.3	TEM	[20]
4	600	113,431	80	1.80 ±1.3	TEM	[20]
6	AR	-	-	1.57	TEM	[13]
6	650	14379	40	0.87	TEM	[13]
6	FGHAZ, PWHT	-	-	0.63	TEM	[13]
6	FGHAZ, PWHT, 650	14379	40	0.24	TEM	[13]
8	1100	1	0	4.2	XRD	[24]
8	750	0.25	0	0.79	XRD	[24]
8	750	1	0	0.60	XRD	[24]
8	750	100	0	0.06	XRD	[24]
9	780	1	0	1.7	-	[25]

Table 3) Dislocation density in Gr. 91 steel according to literature

2.2.3) Precipitates

2.2.3.1) Chromium carbide ($M_{23}C_6$)

Table 4 introduces literature data on quantitative measurements of $M_{23}C_6$ sizes (namely the diameters). The table this time covers as-received BM (base metal), creep-loaded BM, FGHAZ (fine grain heat-affected zone) after post-weld heat treatment and creep-loaded FGHAZ. [15]

Steel No.	Temp. [°C]	Time [h]	Stress [MPa]	Shape	Nucleation sites	Main chem. elements	Diameter [nm]	Investigation method	Reference
1	AR	AR	-	CO	GB, LB	Cr	GB=124 LB=102	LOM, SEM, TEM, EDX, SAD	[17]
2	AR	AR	-	IR	GB	Cr	50-300	SEM, TEM, EDX	[18]
3	AR	AR	-	-	-	-	86 ±17	TEM	[19]
2	600	113,431	80	IR	-	Cr	150-800	SEM, TEM, EDX	[18]
1	625	4292	98	CO	GB, LB	Cr	GB=255 LB=215	LOM, SEM, TEM, EDX, SAD	[17]
5	AR	AR	-	IR	-	-	90-115	TEM	[21]
5	600	0-16650	0-175	IR	-	-	80-130	TEM	[21]
5	AR	AR	-	-	-	-	30-200	TEM	[22]
5	600	0-16650	0-175	-	-	-	30-300	TEM	[22]
6	FGHAZ, PWHT	-	-	IR	-	Cr	158	TEM	[13]
6	FGHAZ, PWHT, 650	14379	40	IR	-	Cr	173	TEM	[13]
7	AR	AR	-	-	-	-	79	TEM	[23]
7	600	50	200	-	-	-	72	TEM	[23]
7	600	250	175	-	-	-	95	TEM	[23]
7	600	2500	130	-	-	-	114	TEM	[23]
7	600	504	130	-	-	-	70	TEM	[23]
7	650	UF	115	-	-	-	111	TEM	[23]
7	650	UF	85	-	-	-	156	TEM	[23]
7	575	UF	185	-	-	-	115	TEM	[23]

Table 4) Size of $M_{23}C_6$ precipitates in Gr. 91 steel

In addition to raw data, Panait et al. [18] indicate the time evolution of $M_{23}C_6$ diameters during long term creep at 600°C and 80MPa, which can be seen in figure 2. [15]

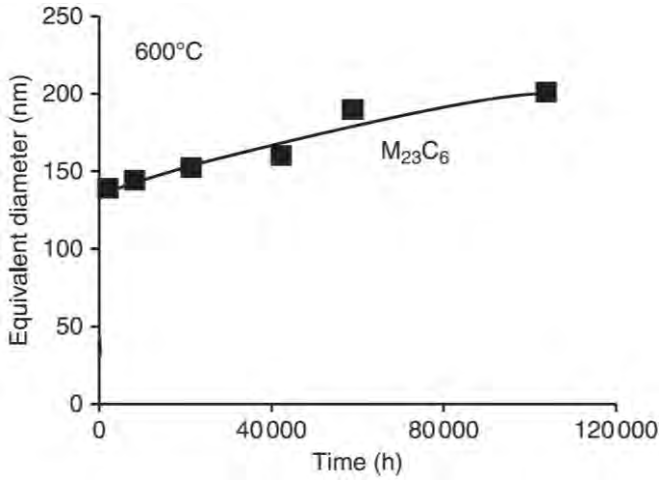

Figure 2) Evolution of equivalent diameter of M23C6 precipitates in P91 at 600°C [16]

2.2.3.2) MX precipitates (NbC and VN)

Table 5 gives an overview on literature data on quantitative measurements of MX diameters. The table shows as-received state of BM, creep-loaded BM, FGHAZ after post-weld heat treatment and creep-loaded FGHAZ. [15]

Steel No.	**Temp. [°C]**	**Time [h]**	**Stress [MPa]**	**Shape**	**Nucleation sites**	**Main chem. elements**	**Diameter [nm]**	**Investigation method**	**Reference**
2	AR	AR	-	-	LI	-	-	SEM	[18]
3	AR	AR	-	-	-	-	16 ±3	TEM	[19]
6	FGHAZ, PWHT	-	-	-	-	V	57	TEM	[13]
6	FGHAZ, PWHT	-	-	-	-	Nb	61	TEM	[13]
6	FGHAZ, PWHT, 650	14379	40	-	-	V	70	TEM	[13]
7	600	50	200	-	-	-	19	TEM	[23]
7	600	250	175	-	-	-	32	TEM	[23]
7	600	2500	130	-	-	-	33	TEM	[23]
7	600	504	130	-	-	-	22	TEM	[23]
7	650	UF	115	-	-	-	25	TEM	[23]
7	650	UF	85	-	-	-	27	TEM	[23]
7	575	UF	185	-	-	-	32	TEM	[23]

Table 5) MX precipitates in Gr. 91 steel

In addition to raw data, Abe and Panait et al. [16], [20] have demonstrated the time evolution of MX diameters during long-term creep at 600°C under a load of 80MPa (see figures 3 and 4). It can be seen that MX particles show comparably high stability against coarsening during creep at this temperature level. [15]

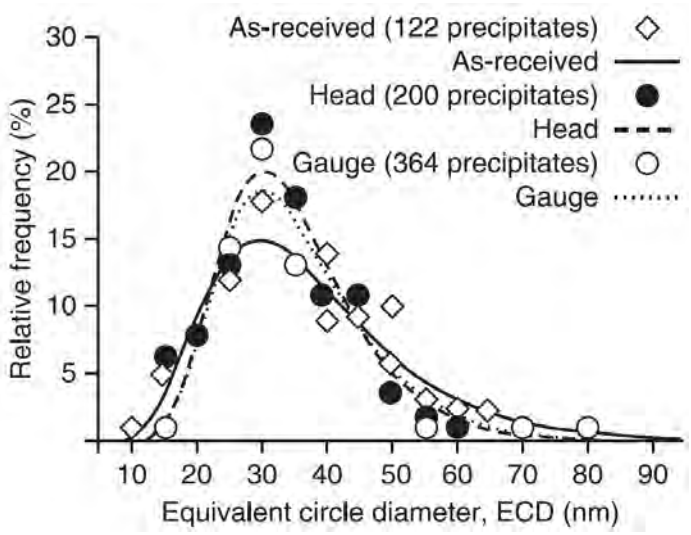

Figure 3) Size distribution of MX precipitates in as-received Gr. 91 steel and after creep rupture testing for 113,431h at 600°C and 80MPa [16], [20]

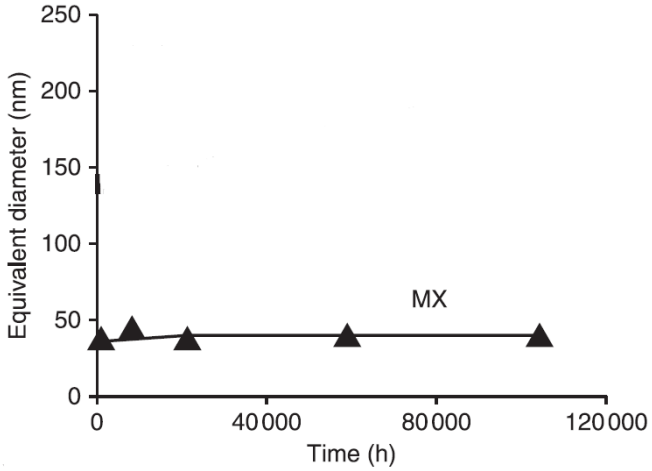

Figure 4) Evolution of diameter of MX precipitates in P91 at 600 °C [16]

2.2.3.3) Laves Phase

Table 6 contains literature data on Laves phase diameters after long-term creep in service. The table provides data on creep-loaded BM as well as creep-loaded FGHAZ. Basically, one has to distinguish between Laves phases formed with Mo and with W. It cannot be found in as-received condition, but starts to precipitate during service. Figure 5 presents the evolution of the equivalent Laves phase diameter at a service temperature of 600 °C. This Laves phase is based on Mo and shows a significant coarsening, reaching a maximum diameter of 450nm after 100 000 hours. [16] [15]

Steel No.	Temp. [°C]	Time [h]	Stress [MPa]	Shape	Nucleation sites	Main chem. elements	Diameter [nm]	Investigation Method	Reference
2	600	113,431	80	IR	GB	Mo	>1,000	SEM	[18]
2	600	113,431	-	IR	GB	Mo	>1,000	SEM	[18]
6	FGHAZ, PWHT 650	14379	40	-	-	-	775	TEM	[13]

Table 6) Laves phase precipitates of Gr. 91 steel according to literature

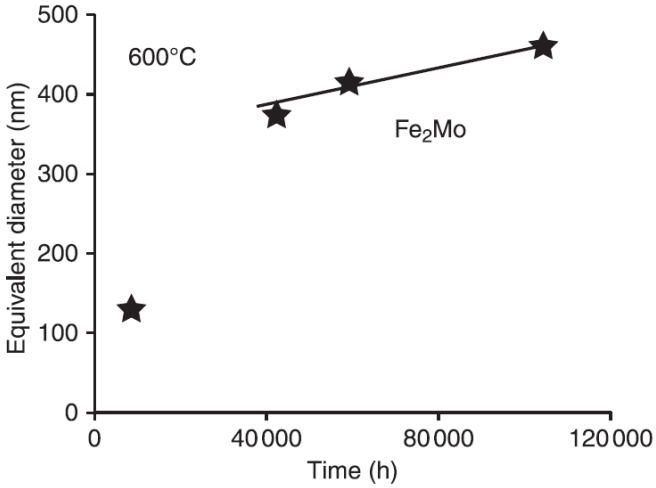

Figure 5) Evolution of equivalent diameter of Fe2Mo Laves precipitates in P91 at 600 °C [16]

2.2.3.4) Modified Z Phase

It is reported by Panait et al. [18] that only a small amount of modified Z phase could be found in Gr. 91 steel (41 precipitates out of 640 identified precipitates), which is confirmed by [16].

The results of investigation on the modified Z phase are summarized in table 7. Included are again data from creep-loaded BM such as creep-loaded FGHAZ. [15]

Steel No.	Temp. [°C]	Time [h]	Stress [MPa]	Shape	Nucleation Sites	Main chem. elements	Diameter [nm]	Investigation method	Reference
2	600	113,431	80	IR	MX	Cr, V, Nb, Fe	250-750	TEM, EDX	[18]
6	FGHAZ, PWHT, 650	14379	40	-	-	Cr, V, Fe, Nb	279	TEM	[13]

Table 7) Modified Z phase precipitates in the Gr. 91 steel

2.3) Thermodynamic Analysis of Microstructural Evolution

In order to model the microstructural evolution of complex alloys, the free Gibbs energy (in the text further denoted as G) is a very useful concept. As pointed out later (see equation 12), the energy of a complex alloy can be described by G: the minimum of G depicts the equilibrium state, whereas the evolution of the microstructure is strongly linked to the gradient of G with respect to the microstructural change (see equation 3.3.4). Therefor it is worth taking a closer look to the link between G and the microstructure.

2.3.1) Gibbs Free Energy and Thermodynamic Equilibrium

The fundamental thermodynamic relation (see equation 1) states that the internal energy U of a system can change because of 1.) transport of heat, 2.) pressure-volume work or 3.) due to change of the chemical composition. [26] [27] [28]

$$dU = \underbrace{T \cdot dS}_{1} \underbrace{-p \cdot dV}_{2} + \underbrace{\mu \cdot dn}_{3} \quad (1)$$

S stands for entropy, T for temperature, p for pressure, V for volume, μ for the chemical potential of a one component system and n for its amount.

With the definition of enthalpy H (equation 2) and introduction of a state function of G (equation 3), the original fundamental thermodynamic relation can be rewritten (equation 4).

$$H = U + p \cdot V \quad (2)$$

$$G = H - T \cdot S \quad (3)$$

$$dG = -S \cdot dT + V \cdot dp + \mu \cdot dn \quad (4)$$

Since most thermodynamic processes in material science are regarded to take place in isothermal condition (T=const.) under constant pressure (p=const.), the change of Gibbs energy becomes equal to the chemical potential times its amount (equation 5). [27] [28]

$$dG = \mu \cdot dn \quad (5)$$

Reaching a minimum value of Gibbs energy G is related to dH and dS, as can be seen in equation 6 (uniting equations 3 and 5). [27]

$$dG = \mu \cdot dn = dH - T \cdot dS = 0 \quad (6)$$

The entropy of a system S can be understood as its state of disorder and will always increase over time, following the second law of thermodynamics.
According to R. Clausius [29], „the entropy of the universe tends to a maximum“.

2.3.2) Nucleation, Growth and Coarsening of Precipitates

The following section explains under which conditions precipitates nucleate, grow and coarsen during heat treatments or in service and helps to identify the determining parameters. This is essential for the understanding of formation and dissolution of particles in the matrix and reflects both the microstructural changes during creep in reality and in the thermodynamic simulations.

2.3.2.1) Nucleation Theory

Nucleation rate can be expressed by equation 7 within the classical nucleation theory [30].

$$J = N_0 Z \beta^* exp\left(-\frac{\Delta G^*}{kT}\right) \qquad (7)$$

The nucleation rate J represents a product of the number of available nucleation sites N_0, the Zeldovich factor Z, the atomic attachment rate β^* and a term containing critical Gibbs energy ΔG^*. T stands for temperature and k for the Boltzmann constant.

The basic idea is that a nucleus has to surmount a critical radius so not to decompose again. [31] This threshold size of the nucleus is associated with a critical Gibbs energy ΔG^* (equ. 8).

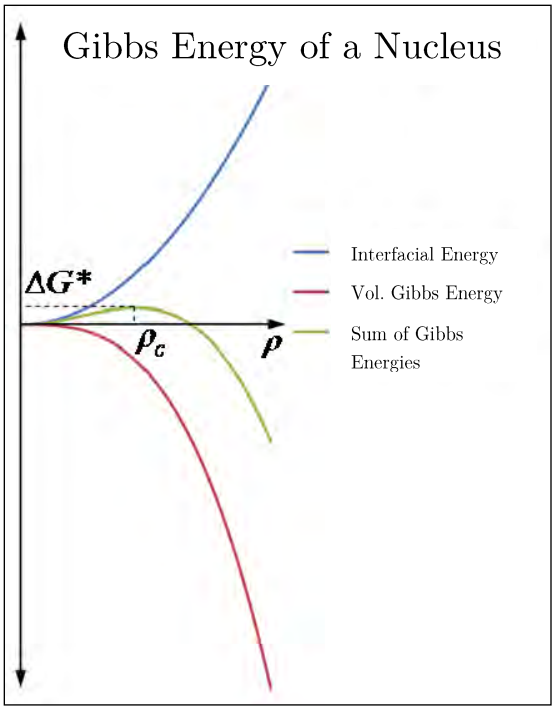

$$\Delta G^* = \frac{16\pi}{3} \cdot \frac{\gamma^3}{F^2} \qquad (8)$$

γ is the interfacial energy and F the driving force. The quantity of ΔG^* comes from a summation of Gibbs energy gains and losses during the nucleation process and the finding a maximum in the function (see figure 6).

The positive term of specific interfacial energy in figure 6 is marked in blue and the negative one for specific volumetric Gibbs energy is colored in red. The green line and its peak show the position of nucleation threshold value ΔG^* [32]

Figure 6) Gibbs energy of a nucleus [32]. *See text for explanation*

In general, the number of available nucleation sites N_0 is determined by the individual microstructure of the material. [31]

2.3.2.2) Precipitate Growth

Growth can be described in a simplified way by Fick's 2nd law, which is a differential equation for diffusion (see equation 9) [33].

$$\frac{\partial c}{\partial t} = \frac{\partial}{\partial x}\left(-D\,\frac{dc}{dx}\right) \qquad (9)$$

c here stands for the concentration of an element, D is the diffusion coefficient and x is the position of the diffusion length.

The physical meaning is that a concentration gradient acts as a driving force and will lead to a flow of atoms, until a balance is reestablished and local differences in the concentration of elements are compensated.

On basis of Fick's law, C. Zener in the year 1949 [34] succeeded in formulating a parabolic growth law for a two-component system with a moving interface in between (see equation 10.)

$$\rho = \sqrt{\rho_0 + \left(\frac{n_\infty - n_1}{n_0 - n_1}\right) \cdot Dt} \qquad (10)$$

Besides a diffusion constant D it contains a concentration term: n_∞ stands for the concentration in the matrix located far away from the particle, n_1 for the concentration in the matrix in equilibrium with the precipitate and n_0 is the concentration of solute atoms inside the precipitate.

2.3.2.3) Coarsening- Ostwald Ripening

Finally, **coarsening** is characterized by Ostwald's ripening and is also connected to diffusion (equation 11) [35].

$$r_1{}^3 - r_0{}^3 = \frac{8\gamma c_\infty v^2 D}{9R_g T}.t \qquad (11)$$

r_1 represents the end size of the precipitate after coarsening, r_0 the start value. γ is the surface energy of the particle and c_∞ stands for the precipitate's solubility. v names the phase fraction of the precipitate and D is the diffusion constant. R_g is the ideal gas constant (8,314 J/molK), T means temperature and t expresses the time under effect of coarsening.

2.3.3) Gibbs Free Energy of a Complex Alloy

Equation number 6 was defined for a one component system.

However, in a more complex alloy multi-component driving forces have to be considered. Consequently, the change of free energy G has to be expressed as the sum of chemical potential times the individual amount for each component (see equation 12). [28]

$$dG = \sum_i \mu_i \cdot dn_i = dH - T \cdot dS = 0 \quad (12)$$

This part of Gibbs energy will be included in the SFFK model as contribution from the matrix.

2.3.4) SFFK Model (MatCalc)

The SFFK (Svoboda, Fischer, Fratzl, Kozeschnik) model from [36], which involves growth and coarsening of particles, does not only consider the Gibbs energy of the system, but also its dissipation rate with respect to changes in the microstructure [14]. According to Lars Onsager [37] a complex thermodynamic system always evolves into the direction of the maximum energy dissipation, known as the thermodynamic extremum principle. Taking this concept into account and describing G according to equation 13, the SFFK model derives the dissipation rate due to all potential microstructural changes and finds the evolution with the maximum dissipation.

$$G = \underbrace{\sum_{i=1}^{n} N_{0i}\mu_{0i}}_{1} + \underbrace{\sum_{k=1}^{m} \frac{4\pi{\rho_k}^3}{3}\left(\lambda_k + \sum_{i=1}^{n} c_{ki}\mu_{ki}\right)}_{2} + \underbrace{\sum_{k=1}^{m} 4\pi{\rho_k}^2\gamma_k}_{3} \quad (13)$$

In general, index "i" in equation 13 is the component of the system and index "k" the particle.

Term 1 stands for the **Gibbs energy of the matrix** expressed as the sum of mole number N_{0i} times the chemical potential μ_{0i} for each component. [36] [38]

Term 2 can be interpreted as the **sum of bulk free energies for all precipitates**, consisting of one part considering a contribution of *mechanical free energy* λ_k (like volumetric misfit stresses e.g.) and another one taking into account the share of *chemical free energy* $\sum_{i=1}^{n} c_{ki}\mu_{ki}$, both of which are multiplied by the particle volume ($4\pi{\rho_k}^3/3$). [36] [38]

Term 3 represents the **energy of the interfaces between precipitates and matrix**, containing a specific interfacial energy γ_k times the individual particle surface $4\pi{\rho_k}^2$. [36] [38]

With every microstructural change happening in the simulation, Gibbs energy is dissipated [38]. As a result, SFFK model predicts rates of microstructural evolution considering

1.) moving interfaces (particle growth/ shrinkage)
2.) diffusion in the matrix and
3.) diffusion in the precipitates. [39] [38]

Since all governing equations are linear, they can be solved for very complex systems (e.g. 10 components, 1000+ particles). The concept is therefore ideal for industrially relevant complex alloys, such as martensitic chromium steels.

The SFFK model is implemented in the software tool MatCalc, which amongst other things allows to conduct equilibrium calculations and precipitation kinetic simulations in order to compute the microstructural evolution of materials.

2.4) IWS Status of Precipitation Modelling (Model 0)

The following section treats a previous project of IWS and MHI from the year 2015, where Gr. 91 microstructural investigations were made and a precipitation kinetic simulation was realized. The most important input data for MatCalc included the dislocation density and its reduction rate during creep, prior austenitic grain sizes for BM and FGHAZ as well as subgrain sizes. The measurement methods in 2015 comprised XRD for dislocation density and EBSD for grain sizes.
Unfortunately, there is discrepancy between the measurement results, the values found in the precipitation report and the input parameters actually used in the MatCalc script.

Table 8 gives a systematic overview about measured input parameters from 2015, provided ones from literature and adjusted ones that were finally used in S. Vujic's MatCalc script (later referred to as model 0) to receive good results for P91 Raccord (version TU Graz). Raccord is a special chemical composition of Gr. 91 steel, which will be described later in chapter 4.4.2.

However, the investigated kind of P91 steel in 2015 is identical to the 2016 material which the thes focuses on (both for simulation and measurements).

Overview about MHI project 2015	Experiments IWS institute	Values found in 2015 [40]		Prec. Report Values [41]		Script Values 2015 [42]	
		BM	FGHAZ	BM	FGHAZ	BM	FGHAZ
Dislocation density in martensite	Yes: X-Ray Diffract.	6,2.10^{15} m^{-2}	1,8.10^{15} m^{-2}	M: 1.10^{15} m^{-2} (A: 1.10^{11} m^{-2}) *		M: 1.10^{15} m^{-2} (A: 1.10^{11} m^{-2}) *	
Dislocation density reduction factor	No- values from [20]	-	-	25 % every 25 000 h		12,5 % every 25 000 h	
PAGS- mean grain size	Yes- EBSD	67,1 µm ±39,4 µm	11,9 µm ±7,7 µm	90 µm	30 µm	30 µm	30 µm
Martensitic block size	Yes- EBSD	14 µm ±7,6 µm	8,4 µm ±4,2 µm	14 µm	8,4 µm	14 µm as subgrain size= WRONG	8,4 µm as subgrain size= WRONG
		As-received	Creep-loaded			BM	FGHAZ
Martensitic lath size	No- values from [17]	540 nm	900 nm	-		Should be used as subgrain size instead	Should be used as subgrain size instead
Subgrain size (diameter)	No- values from [16]	250 nm	250-2000 nm (750-1250 nm) **	-		14 µm	8,4 µm

Table 8) Measured input parameters 2015, literature values + script values 2015 (model 0)
**A: dislocation density for austenite **mostly in this part of the distribution*

In MatCalc script of model 0 the dislocation density of 1.10^{15} m^{-2} for martensite was chosen lower compared to measurements (6,2.10^{15} m^{-2} in BM and 1,8.10^{15} m^{-2} in FGHAZ).

Instead of a 25 % reduction rate every 25 000 hours for dislocations suggested by Panait et al. [20], a decrease factor of 12,5 % every 25 000 hours was selected. [42]

For the subgrain diameter, estimated by literature to lie between 250 nm and 2000 nm [16], the measured martensitic block sizes were used (14 µm in BM and 8,4 µm in FGHAZ). [41] [42]

As the results of MatCalc simulation in the end did not completely meet the microstructural investigations, a variation of prior austenitic grain sizes was conducted, until calculated phase fraction and mean diameter of laves phase corresponded to measurements. In fact, the four parameters martensite and austenite grain size both in base metal and in FGHAZ were all adjusted to 30 µm [42].

The martensite lath elongation factor (known as the length-width ratio) was assumed to be 3 in BM and only 1 in the FGHAZ [42].

2.5) Strengthening Mechanisms and Backstress

One of the objectives in the 2016 project with MHI was the calculation of a total backstress on basis of MatCalc simulation results to predict the steel's potential creep resistance due to various strengthening mechanisms. In the following section, all relevant mechanisms of hardening will be explained, and the determination of a total backstress will be discussed.

As it is widely known from stress-strain curves, the yield strength is defined as the value where additional to a reversible elastic deformation an irreversible plastic deformation starts, once a force is imposed upon a specimen during tensile testing.

However, a "*backstress concept*" expresses, how strongly "*the inner stress reduces the effect of the external stress*". [43] So not the "*entire external load*" (which plays a major role for tensile testing in room temperature conditions) is relevant for creep processes. [43]

In case of high temperature applications under load conditions, it is important to be aware that creep even takes place, if the difference of external load σ_{ext} and inner backstress σ_i remains negative, since creep is a process strongly governed by diffusion. Only shortly before damage and going hand in hand with extreme plastic deformation and necking, the subtraction in equation 14 will become positive.

The **effective creep stress** $\boldsymbol{\sigma_{eff}}$ thus is the reduction of external stress by different contributions for the backstress, representing barriers or obstacles for dislocation movement [8], which can be seen in equation 14.

$$\sigma_{eff} = \sigma_{ext} - \sigma_i \qquad (14)$$

According to Dimmler [44] the **inner stress** (mostly called **backstress**) consists of shares of dislocations τ_ρ, precipitates τ_{Or} and subgrain boundaries τ_{sgb}, and he suggests to linearly sum them up (see equation 15).

Taylor factor M (usually chosen between 2 and 3) serves to convert τ into σ.

$$\sigma_i = M \cdot (\tau_\rho + \tau_{Or} + \tau_{sgb}) \qquad (15)$$

This equation 15 will later serve to estimate the material's backstress in room temperature conditions. When it comes to evaluating high temperature backstress at 650 °C, the inner stress is assumed to include mobile dislocation strengthening σ_{ρ_m}, immobile/ boundary dislocation strengthening $\sigma_{\rho_{im}}$ and a particle hardening on basis of climb phenomenon σ_{part} (equation 16).

$$\sigma_i = \sigma_{\rho_m} + \sigma_{\rho_{im}} + \sigma_{part} \qquad (16)$$

2.5.1) Mobile Dislocation Strengthening

Abe [45] provides an equation for **strengthening due to mobile dislocations** (equation 17) that contains a constant α for dislocation interaction, shear modulus G, Burger's vector b and the square root of mobile dislocation density ρ_m.

$$\sigma_{\rho_m} = \alpha \cdot M \cdot G \cdot b \cdot \sqrt{\rho_m} \qquad (17)$$

While Abe sets α=0,5 other sources, such as Basirat [46] argue to use a reduced value for high temperatures (between 600 and 700 °C) of α=0,02. Gupta and Was [47] agree that for dislocation networks regarded as weak barriers, α should be less than 0,1 (in their paper α=0,07).

The shear modulus is connected to Young's modulus, both of which depend on temperature. With an assumed Poisson's ratio of ϑ=0,3 shear modulus G can easily be calculated from the Young's modulus (equation 18).

$$G = \frac{E}{2 \cdot (1 + \vartheta)} \qquad (18)$$

The phenomenon of dislocation strengthening is often called work-hardening effect in literature. The basic idea is that dislocations hinder each other from movement due to their high density. According to [2] dislocation hardening is restricted to short-term creep, but will fail to offer high backstress in long-term conditions due to soon dislocation recovery.

2.5.2) Subgrain Strengthening

Subgrain strengthening provided by [48] and [45] is reflected by equation (19), including shear modulus G, Burger's vector b as well as subgrain width λ_{sg}.

$$\sigma_{sg} = \frac{10 \cdot G \cdot b}{\lambda_{sg}} \qquad (19)$$

It is regarded to be highly significant in P91 (at least in room temperature conditions).

However, the role of subgrain strengthening during creep at high temperatures is disputed. According to [48] equation 19 rather reveals a theoretical "athermal yield stress", but obviously it is not suitable to predict a real strength during creep.

Holzer [3] blames the drastic coarsening of precipitates located at subgrain boundaries and the reduction of their number density during service to decrease the effectiveness of subgrain strengthening as the available zone of subgrain boundaries will decrease.

As far as the choice of the subgrain width λ_{sg} is concerned, literature such as El-Azim and others [13] reports a faster subgrain coarsening for FGHAZ during creep compared to BM.

One has to be aware that this original concept intends to reflect subgrain strengthening in room temperature conditions.

2.5.3) Immobile Dislocation Strengthening/ Subgrain Strenghtening

Using the same formula as in chapter 3.5.1, Magnusson and Sandström for Gr. 91 advise to consider immobile dislocations, too [49], being denoted as boundary dislocations in this thesis (equ. 20). It is an alternative point of view by the authors for subgrain strengthening at high temperatures.

$$\sigma_{\rho_{im}} = \alpha \cdot M \cdot G \cdot b \cdot \sqrt{\rho_{im}} \qquad (20)$$

$\alpha \cdot M$ in their approach is unity (=1). However, the authors suggest to separately calculate immobile dislocation strengthening for subgrain interiors and subgrain walls and use weighting factors similar to composite materials. In this way it is possible to distinguish softer regions from harder areas in the microstructure, containing different immobile dislocation densities. [49]

2.5.4) Grain Boundary Strengthening

Grain boundary strengthening is based on the so-called Hall-Patch equation (number 20) (ref. [38]). It plays a minor role in case of P91 because of the large prior austenitic grain sizes and their low phase fraction in contrast to subgrain boundaries [8]. Thus it will not be considered.

Nevertheless, the formula (equation 20) will be stated:

$$\tau_{gr} = k_{gr} \cdot \frac{1}{\sqrt{d_{gr}}} \qquad (21)$$

While k_{gr} is the strengthening coefficient, d_{gr} stands for the diameter of the prior austenitic grains.

2.5.5) Precipitate Dislocation Interaction

In regard to the interaction between precipitates and the moving dislocations inside the glide planes, different mechanisms have to be distinguished according to McLean [50].

Whereas 1.) dislocations that cut precipitates are unlikely to be found, 2.) climbing of dislocations 3.) Orowan looping have been proven in 9- 12 % chromium steels [8].

This has to do with the fact that precipitates in case of Gr. 91 are semicoherent or incoherent. In general, stress level and temperature decide whether climbing or Orowan looping predominate: Orowan mechanism shows only little dependence on temperature, but correlates with high stresses. Climbing, on the other hand, is the preferred dislocation motion at elevated temperatures, but low stresses. [3]

2.5.5.1) Orowan Mechanism

According to [8], climbing in comparison to Orowan mechanism is neglectable in 9 % Cr steel, so that the focus will first of all lie on discussing Orowan looping as the largest contributor to the backstress originating from precipitates.

For Orowan stress, a new formulation was found by Ahmadi et al. [51], which can be automatically calculated in MatCalc version 5.62.

$$\tau_{Or} = \frac{J \cdot G \cdot b}{2 \cdot \pi \cdot \lambda \cdot (1 - \vartheta)} \cdot ln\left(\frac{2r_s}{r_i}\right) \qquad (22)$$

As can be seen in equation 22, apart from shear modulus G and Burger's vector b, a particle arrangement factor J (0,8 to 1) and Poisson's ratio ϑ of the matrix are contained. Whereas r_s stands for the equivalent particle radius, r_i is the inner cut-off distance of dislocations [15] [51]. λ is the so-called critical particle distance, marking a theoretical threshold for the start of plastic deformation [52].

Equation 23 offers a method to realistically evaluate a two-dimensional interparticle distance (ref. [52]) in the glide plane of the dislocation (from surface to surface) with the help of mean particle radius r and number density N_V. These values will later be provided by MatCalc results.

$$\lambda_{2D-SS} = \sqrt{\frac{\ln 3}{2 \cdot \pi \cdot N_v \cdot r} + 2.67 \cdot r^2} - 1.63 \cdot r \qquad (23)$$

In general, it has to be mentioned that Orowan process is only relevant for precipitates located at dislocations.

2.5.5.2) Effect of Dislocation Climb

In paper [53] Magnusson and Sandström argue that so far the effect of dislocation climb at elevated temperatures (such as 650 °C for instance) has been underestimated. They introduce a novel critical radius r_c which represents the largest precipitate size that allows climb, before Orowan looping starts for bigger particles. [53]

The main contributors to precipitation backstress according to Magnusson and Sandström are MX and $M_{23}C_6$ particles.

They suggest a Pythagorean addition (equation 24) for the interparticle distances of MX and $M_{23}C_6$ on basis of Martin [54] to calculate a total value λ_{tot}:

$$\frac{1}{{\lambda_{tot}}^2} = \frac{1}{{\lambda_{MX}}^2} + \frac{1}{{\lambda_{M23C6}}^2} \qquad (24)$$

Finally, the authors provide a slightly different Orowan equation (number 25) for particle hardening, containing dislocation line tension T_L, Taylor factor m=3, Burger's vector b and the interparticle distance λ_{tot} from above.

$$\sigma_{part} = \frac{2T_L m}{b\lambda_{tot}} \qquad (25)$$

A constant and particle-independent dislocation line tension T_L can be derived from the simplified equation 26 (reference [55]):

$$T_L = \frac{Gb^2}{2} \qquad (26)$$

G again stands for the shear modulus and b for the Burger's vector ($2{,}866.10^{-10}$ m).

A more complex equation for the dislocation line tension depending on varying radii r of precipitates (equation 27) can be written in the following way (reference [55]):

$$T_L = \frac{Gb^2}{4\pi K} \cdot ln\left[\frac{2\sqrt{\frac{2}{3}}r}{(1..4)b}\right] \qquad (27)$$

Actually the fraction inside the logarithm is the modified ratio of outer and inner cut-off radius. K is a factor between 0,7 and 1 and makes it possible to distinguish between edge and screw dislocations. However, in this thesis it was decided to use a mean value of 0,85.

2.5.6) Solid Solution Hardening

Finally, **solid solution hardening** effect has to be mentioned.

In a paper about long-term creep properties of 9- 12 % Cr steels, J. Hald comes to the conclusion, that the main elements responsible for solid solution strengthening are Mo and W (which is not relevant for Raccord Gr. 91 TU Graz version). However, their back stress is estimated to stay below 1 MPa so that the effect of solid solution hardening can be neglected [7]. Whereas the role of rapidly coarsening Laves phase for precipitation strengthening during service is disputed, there is agreement that it can be blamed for reducing the solid solution strengthening due to depletion of W or (in this case for Raccord Gr. 91) Mo in the matrix. [3]

As a result, strengthening due to subgrain boundaries and because of dislocations play a far more important role in Gr. 91 steel.

3.) Experimental

The following section focuses on the settings for precipitation kinetic simulations in MatCalc and shows how the discussed models differ from each other concerning input and output. Furthermore, the applied methods for microstructure investigations are introduced.

3.1) Overview on Thermodynamic Simulations

To avoid confusion when comparing different versions of MatCalc scripts, names are introduced for the discussed precipitation kinetic models in the following chapters and their basic differences are shown concerning stages of heat treatment and service temperatures.

An example for a typical 5 stage heat treatment taken from Vujic's MatCalc model 2015 (later named model 0) is depicted in figure 7. [41] The picture includes heating rates, cooling rates, holding temperatures and times. On the right side of the figure, martensite start temperature M_S and reaustenitization temperatures A_T for different kinds of Gr. 91 steel are indicated.

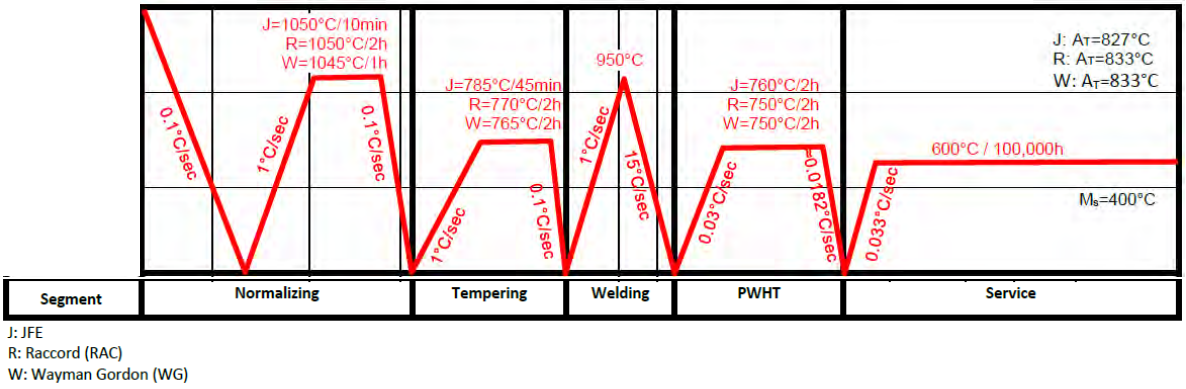

Figure 7) 5 stage heat treatment from Vujic's MatCalc script 2015 (model 0) [41]

3.1.1) Vujic's Model 0 (Year 2015)

The original 2015 model from S. Vujic is refered to as "model 0". The script name of model 0 was "kinetics_v24.mcs". It simulates a 5 stage heat treatment (normalizing, tempering, welding, PWHT and service) with an assumed operation of this FGHAZ material in a power plant for 100 000 hours at 600 °C. The incorporated heat treatment was already shown in figure number 7. For more information about heat treatment see chapter 4.4.3.4 and for further input data see chapter 3.4.

3.1.2) Model 1 on Basis of 2015 Experiments (Year 2016)

The 2016 model with realized adjustments on 2015 findings is named "model 1".
This model 1 was calculated on basis of the script file
"dbn_pn_ns_bf_ddm_fct_1.5e14_vmf_aln_NbC_dg_eie_z_vn_1_MX_vmc_heat_cool_npc50.mcs".

It includes a 3 stage heat treatment (normalizing, tempering, service) with a creep time for the base metal of 100 000 hours at 600 °C. For more details, see section 4.4.3.4 and 5.2.

3.1.3) Model 2 on Basis of 2016 Experiments (Year 2016)

"Model 2" includes an update of parameters derived from 2016 measurements. The script used for model 2 was "P91_76_9_0.5_ict_laves1452K_ agsfghaz950C_650C_100000h_mdef8.mcs".

Model 2 deals with both BM (using a 3 stage heat treatment) and FGHAZ (applying a 5 stage heat treatment). Time of creep once more is 100 000 hours, but service temperature is increased to 650 °C.

For details about heat treatment see section 4.4.3.4 and for other input data see chapter 5.3.3.

The following table 9 serves to summarize this first introduction to MatCalc models 0, 1 and 2. Further details about differences in regard to input parameters will be discussed later.

	Script Author	Heat Treatment Stages	Time of Creep	Service Temperature
Model 0	S. Vujic	5 (FGHAZ)	100 000 hours	600 °C
Model 1	F. Riedlsperger*	3 (BM)		600 °C
Model 2	F. Riedlsperger*	3 (BM) or 5 (FGHAZ)		650 °C

*Table 9) Comparison of models 0, 1 and 2; * 2016 on basis of S. Vujic's model 0 from 2015*

3.2) EBSD Microscopy and TEM (External Work)

Electron Backscatter Diffraction (EBSD) investigations were carried out at FELMI Institute, TU Graz. Analysis of obtained data was conducted at IWS by the author with help of TSL OIM software (Version 7.1.1/ 64 bit, EDAX company, released in 2015; available online at http://www.edax.com/Products/EBSD/OIM-Data-Analysis-Microstructure-Analysis.aspx).
The purpose was to measure prior austenitic grain sizes and subgrain sizes for P91 specimen sent to IWS from MHI. These values were important input parameters for MatCalc models 1 and 2.

Transmission Electron Microscopy (TEM) was used by FELMI Institute to get information about shape, form, number and size of precipitates. To distinguish the detected particles from each other by chemical composition, the techniques of EDX (energy despersive X-ray spectroscopy) and EELS (electron energy loss spectroscopy) were applied.

Processing and analysis of measurement data was predominantly done at FELMI Institute and then completed at IWS Institue by the author with help of the software Microsoft Excel. This information about precipitates later served to assess the quality of MatCalc results.

3.3) Overview on Specimen 2016 (IWS)

Table 10 provides a full project overview on FELMI investigation and IWS analysis of base metal and FGHAZ specimen from MHI in 2016 (status end of July). For the crept samples, stresses (in MPa) and creep rupture times (in hours) are stated. SEM and TEM served to determine shape, size and quantity of precipitates. EBSD analysis with TSL OIM software revealed prior austenitic grain sizes and subgrain sizes. XRD measurements and analysis were made in cooperation with the Institute of Solid State Physics, TU Graz, to find out the mobile dislocation density, whereas the boundary dislocation density could be derived and calculated by the author from EBSD data. Specimen 4 (load 70 MPa) led to a very small rupture time of 172 hours and had to be replaced by specimen 7 with a load of 45 MPa, resulting in a higher rupture time of 2181 hours.

Condition			Specimen Number	Precipitate Analysis		Subgrain Size	PAGS	Dislocation Density	
								Mobile	Bound.
				SEM	TEM	EBSD	EBSD	XRD	EBSD
BM	as-rec.	0 h	(1)	●	●	●	●	●	●
	crept	650 °C 100 MPa t_r=306 h	(3)	•		●		•	●
		650 °C 80 MPa t_r=2283 h	(5)	•	●	●		•	●
FGHAZ	as-rec.	0 h	(2)	●	•	●	●	●	●
	crept	650 °C 70 MPa t_r=172 h	(4)	(•)		(●)		(•)	(•)
		650 °C 55 MPa t_r=763 h	(6)	•	•	●		•	•
		650 °C 45 MPa t_r=2181 h	(7)	•		●		•	•

Table 10) Overview on experimental investigations in 2016

● *already investigated* ● *under investigation (status July 2016)* • *planned for investigation*

	Specimen condition	Specimen condition	Specimen condition	Specimen condition
BM	(1) As-received → EBSD + TEM	(3) σ=100 MPa T=650 °C → EBSD	(5) σ=80 MPa T=650 °C → EBSD	
FGHAZ	(2) As-received → EBSD	(4) σ=70 MPa T=650 °C	(6) σ=55 MPa T=650 °C	(7) σ=45 MPa T=650 °C

Table 11) Overview about specimens sent from MHI to IWS in 2016

So far (status end of July 2016), specimens 1, 2, 3 and 5 have been measured at FELMI Institute and analyzed by the author at IWS in regard to EBSD, which is marked in green colour. TEM results originating from FELMI were processed by the author only for specimen 1.

The individual results of EBSD as well as TEM measurements will be presented in chapter 5.

3.4) MatCalc Simulations

The following chapters will describe technical details about the realized MatCalc simulation. It starts with information about MatCalc version and computer types and continues with details about the maintained or adjusted input parameters on basis of 2015 findings (for model 1). Finally, 2016 measurements will be implemented (in model 2), and again the input parameters are modified.

3.4.1) MatCalc Version and Computer Types

Vujic's 2015 script ran on MatCalc version 5.60 with the databases "mc_fe_v2.039.tdb" as well as "mc_fe_v2.005.ddb".

The current 2016 scripts run on MatCalc version 5.62. New databases were introduced in the 2016 models: "mc_fe_v2.050.tdb" and "mc_fe_v2.008.ddb".

Two computers were used for the calculations in 2016, and the results were always cross-checked, in order to find out and minimize effects coming from different CPUs. The first computer had Windows 7 (64 bits) installed and contained four Intel Core i7-4500U @ 1,80 GHz processors. The second one had Windows 8 (64 bits) installed and contained four Intel Core 2 Quad Q9500 @ 2,83 GHz processors.

3.4.2) Chemical Composition of Investigated Gr. 91 Steel in 2016

	C	Si	Mn	P	S	Cu	Ni	Cr	Mo	V	Nb	Al	N
HiMAT	0,118	0,49	0,37	0,021	0,003	0,13	0,40	8,95	0,90	0,183	0,061	0,016	0,0488
TU Graz	0,112	0,48	0,37	0,022	0,003	0,13	0,37	8,98	0,87	0,199	0,063	0,016	0,0473

Table 12) Chemical composition for two versions of Gr. 91 steel in 2016

The chemical compositions of Gr. 91 steel in the version HiMAT and for TU Graz slightly differ in regard to carbon, nickel and vanadium content (see table 12). Further important to note is that none of them contains tungsten, but will develop a molybdenum-based Laves phase instead.

The focus of the present study will lie on the TU Graz version, which in 2015 reports was named Gr. 91 Raccord steel. [40] [41].

Sulphur and phosphorus were neglected both in stepped equilibrium calculations such as in precipitation kinetics (marked in red).

3.4.3) Adjustment of 2015 Findings (Model 1)

Since a major part of the 2015 measurements varied from the input parameters implemented in Vujic's MatCalc script (model 0) for precipitation kinetics, an attempt was made to reduce this discrepancy and to improve the agreement with available physical data without worsening results. Model 1 focused on incorporating all measurements and data from 2015 together with updates and extensions for numerous settings that will be presented in the next chapters. So the next sections will explain the most important changes in model 1 and justify them. Model 2 included basically the same changes, except for differences concerning grain sizes and heat treatments: New 2016 measurements were available, and FGHAZ (5 heat treatment stages) was modelled additionally to BM (3 h.t. stages). A first introduction about model 2 will already be given in the following section, but more information and details will follow in chapter 5.3.

3.4.3.1) Grain Sizes

The first step in model 1 was the correction of prior austenitic grain sizes in the MatCalc script (see table 13), based on the values of IWS measurements from 2015. Using the square mean value of grain size statistics from OIM software for EBSD data, PAGS for base metal was increased from 30 µm to 79 µm.

As far as FGHAZ is concerned, PAGS reduced from 30 µm to 14,3 µm (square mean value).

Subgrain sizes both for base metal and FGHAZ were set to 1 µm, as it seems to be an appropriate mean value according to literature, such as [16] and [4].

For the subgrain elongation factor in base metal the value became 5 instead of 3, based on optical interpretation of subgrains in EBSD pictures. In FGHAZ, the subgrain elongation factor of 1 was maintained due to the regular structure that predominates.

	Model 0 [41]	Model 1
Aust. grain size BM	30 µm	79 µm (SMV) a, [40]
Mart. grain size BM	30 µm	Not used
Aust. grain size FGHAZ	30 µm	14,3 µm (SMV) a, [40]
Mart. grain size FGHAZ	30 µm	Not used
Subgrain elongation BM	3	5
Subgrain elongation FGHAZ	1	1
Subgrain size BM	14 µm (MBS) b	1 µm [16], [4]
Subgrain size FGHAZ	8,4 µm (MBS) b	1 µm [16], [4]

Table 13) Change of major settings between model 0 and model 1;
a…SMV= square mean value of grain size distribution; b…MBS=martensitic block size

3.4.3.2) Nucleation Sites

As far as the nucleation sites is concerned, the original model was extended. B.S. Srinivas Prasad et al. [37] gave suggestions in their work how to create a more complex, but physically more accurate MatCalc precipitation kinetics model. Most of their recommendations were implemented in the updated 2016 MatCalc script used for models 1 and 2 (see an overview in table 14), except for Laves phase located at grain boundaries due to a dramatic overestimation of its mean diameter in service. Instead, Laves phase was restricted to form at subgrain boundaries only.

Another difference to B.S. Srinivas Prasad et al. has to be mentioned: Niobium carbide at austenitic dislocations NbC(aust,d) was also added as nucleation site- regardless of any literature source, as it showed high stability against coarsening during creep.

The term "**mart**" in table 14 refers to the precipitation domain of the precipitates, namely martensite functioning as surrounding matrix in the moment of nucleation, whereas "**aust**" stands for an austenitic matrix.

The spectrum of used nucleation sites involves grain boundaries, dislocations, subgrain boundaries as well as vanadium nitrides for modified Z phase.

Name of Precipitate	Model 0	Model 1 + 2
$M_{23}C_6$(mart)	s	g, s
Laves(mart)	g	(g), s
VN(mart)	d	g, d, s
VN(aust)	-	g
NbC(aust)	-	g, d
NbC(mart)	d	g, d, s
AlN(aust)	d	d
AlN(mart)	d	d
Cr_2N(aust)	d	d
Cr_2N(mart)	d	d
Cem(mart)	s	s
M_7C_3(mart)	s	s
Modified Z Phase	vn d	vn_i d

Table 14) Nucleation sites of precipitates in 2015 (model 0) and 2016 (models 1, 2);
aust: austenite (prec. domain); mart: martensite (prec. domain);
g=grain boundary; d=dislocation; s=subgrain boundary; vn=vanadium nitride(s)

3.4.3.3) Dislocation Densities

Testing the new input parameters from table 13 and 14, $M_{23}C_6$ turned out to coarsen too fast and to reach a too high diameter (around 800 nm after 100 000 hours of creep) during the service section of model 1 at 600 degrees Celsius.

Several attempts were made to decrease the size of chromium carbide, such as the use of an inactive radius factor for example, which led to numerical mistakes in the calculation and did not succeed. Considering diffuse interface correction [56] for $M_{23}C_6$ slightly improved the situation, but had too little effect (showing only a 5 % smaller diameter after 100 000 hours).

Finally, a deviating (mobile) dislocation density was identified as main cause of exaggerated $M_{23}C_6$ coarsening during service. Both the start value for dislocation density in martensite in Vujic's 2015 script (model 0) was chosen too high and the linear reduction rate did not meet the reality.

On the basis of experimental data on P92 from S. Yadav et al. [57], a reduction equation for non-linear mobile dislocation density could be derived. To obtain equation number 12, figure 3b out of [57] (containing the dislocation density) was used utilizing software Origin 8.6G (see figure 8).

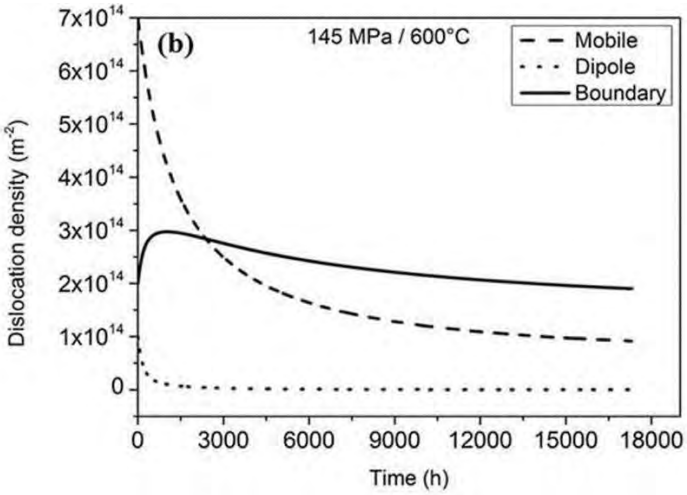

Figure 8) Original image for dislocation density evolution for P92 on basis of S. Yadav [57]

A graphical spline was inserted to fit the curve for mobile dislocation density. The software's tool box then automatically found the coefficients *a* and *b*.

As the start value of the function initially proved to be too high, literature was consulted, and a mobile dislocation density of $1{,}5.10^{14}$ m^{-2} from [13] was chosen for the beginning of creep. To incorporate this new start value, the original equation had to be adapted with the help of a time constant t_0, which was set 7000.

Indeed, this led to good results for the evolution of $M_{23}C_6$, keeping in mind data from literature (see chapter 3.2.3.1).

As a result, start and end values as well as the shape of the dislocation function changed significantly in comparison to model 0 (see table 15, equation 28 and figure 9). The new dislocation density equation was implemented in MatCalc as a step function with small time steps in the beginning (Δt=100 hours) and bigger ones at higher creep times (Δt=5000 to 10 000 hours), since the predicted drop in dislocation density is most extreme in the beginning. Boundary dislocations were not included in the MatCalc model to avoid a double definition, because subgrain boundaries rank amongst the nucleation sites.

	Model 0	Model 1 + 2
Dislocation density aust.	1.10^{11} m^{-2}	1.10^{11} m^{-2}
Dislocation density mart. (start value for service)	1.10^{15} m^{-2}	$1{,}5.10^{14}$ m^{-2}
Reduction rate for mart. dislocation density	- 12,5 % every 25000 h	Non-linear formula (28)

Table 15) Adjustment of dislocation density start and end values based on Yadav et al. [57] *and* [13]*, comparing model 0 and models 1, 2*

The found reduction function for mobile dislocation density has the following form:

$$\rho = a \cdot (t + 7000)^{-b} \qquad (28)$$

ρ = dislocation density in martensite during service
t = time of service at 600 °C (0< t≤100 000 h)
a = 2,39257. 10^{16} b = 0,57315

Figure 9 depicts a plot for the evolution of mobile dislocation density during creep, created with Microsoft Excel.

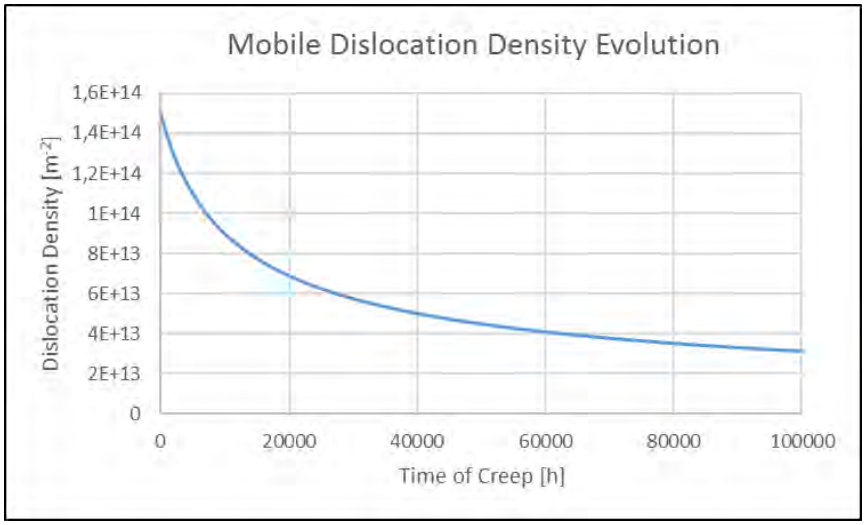

Figure 9) Plot of mobile dislocation density over time according to equation (26)

Table 16 presents precise dislocation density values for different creep times during service and it also reveals the used variable names for the step function used in MatCalc script models 1 and 2.

Segment	**Real Time**	**Virtual Time**	**Dislocation Density**	% of Start Value	Variable Name
1	0	7000	$1{,}50.10^{14}$ **m^{-2}**	100,00%	Ddm
2	100	7100	$1{,}48.10^{14}$ **m^{-2}**	99,19%	ddm_100h
3	200	7200	$1{,}47.10^{14}$ **m^{-2}**	98,40%	ddm_200h
4	300	7300	$1{,}46.10^{14}$ **m^{-2}**	97,62%	ddm_300h
5	400	7400	$1{,}45.10^{14}$ **m^{-2}**	96,86%	ddm_400h
6	500	7500	$1{,}44.10^{14}$ **m^{-2}**	96,12%	ddh_500h
7	600	7600	$1{,}43.10^{14}$ **m^{-2}**	95,40%	ddm_600h
8	700	7700	$1{,}42.10^{14}$ **m^{-2}**	94,68%	ddm_700h
9	800	7800	$1{,}41.10^{14}$ **m^{-2}**	93,99%	ddm_800h
10	900	7900	$1{,}40.10^{14}$ **m^{-2}**	93,30%	ddm_900h
11	1000	8000	$1{,}39.10^{14}$ **m^{-2}**	92,63%	ddm_1000h
12	1250	8250	$1{,}36.10^{14}$ **m^{-2}**	91,01%	ddm_1250h
13	1500	8500	$1{,}34.10^{14}$ **m^{-2}**	89,47%	ddm_1500h
14	2000	9000	$1{,}30.10^{14}$ **m^{-2}**	86,58%	ddm_2000h
15	2500	9500	$1{,}26.10^{14}$ **m^{-2}**	83,94%	ddm_2500h
16	3000	10000	$1{,}22.10^{14}$ **m^{-2}**	81,51%	ddm_3000h
17	3500	10500	$1{,}19.10^{14}$ **m^{-2}**	79,26%	ddm_3500h
18	4000	11000	$1{,}15.10^{14}$ **m^{-2}**	77,18%	ddm_4000h
19	4500	11500	$1{,}13.10^{14}$ **m^{-2}**	75,23%	ddm_4500h
20	5000	12000	$1{,}10.10^{14}$ **m^{-2}**	73,42%	ddm_5000h
21	6000	13000	$1{,}05.10^{14}$ **m^{-2}**	70,13%	ddm_6000h
22	9000	16000	$9{,}31.10^{13}$ **m^{-2}**	62,26%	ddm_9000h
23	12000	19000	$8{,}44.10^{13}$ **m^{-2}**	56,42%	ddm_12000h
24	15000	22000	$7{,}76.10^{13}$ **m^{-2}**	51,87%	ddm_15000h
25	20000	27000	$6{,}90.10^{13}$ **m^{-2}**	46,13%	ddm_20000h
26	25000	32000	$6{,}26.10^{13}$ **m^{-2}**	41,85%	ddm_25000h
27	30000	37000	$5{,}76.10^{13}$ **m^{-2}**	38,50%	ddm_30000h
28	40000	47000	$5{,}02.10^{13}$ **m^{-2}**	33,57%	ddm_40000h
29	50000	57000	$4{,}50.10^{13}$ **m^{-2}**	30,06%	ddm_50000h
30	60000	67000	$4{,}10.10^{13}$ **m^{-2}**	27,40%	ddm_60000h
31	70000	77000	$3{,}78.10^{13}$ **m^{-2}**	25,30%	ddm_70000h
32	80000	87000	$3{,}53.10^{13}$ **m^{-2}**	23,59%	ddm_80000h
33	90000	97000	$3{,}31.10^{13}$ **m^{-2}**	22,16%	ddm_90000h
34	100000	107000	$3{,}13.10^{13}$ **m^{-2}**	20,95%	ddm_100000h

Table 16) Decrease of mobile dislocation density over time based on Yadav's formula (start and end values for the simulation are marked in green)

3.4.3.4) Heat Treatment

Heating and cooling rates were updated according to MHI data sent to IWS in January 2016.

Basically, one has to distinguish between BM, consisting of a 3 stage heat treatment (normalizing, tempering and service) and FGHAZ which is exposed to 5 stages (normalizing, tempering, welding, PWHT and service).

First of all, in model 1 code a service temperature of 600 °C was incorporated, treating only BM. Later, the advanced model 2 code comprised both a working FGHAZ and a BM part in the script with an increased service temperature of 650 °C (in agreement with 2016's MHI specimen). When starting the script for precipitation kinetic simulation, the user may actually select one of two different kinds of Gr. 91 steels (TU Graz version and HiMAT) as well as either a BM 3 stage or a FGHAZ 5 stage simulation.

Please note that this thesis focuses on TU Graz version of Raccord steel and that the chemical composition of HiMAT has not been tested so far.

For a better visualization of all holding temperatures and times of models 1 and 2 see figure 10.

To simplify the readability and avoid mistakes during programming if-loops, the MatCalc script structure of model 2 was finally divided into a base metal and a FGHAZ part, each of which has to be stored with a different name.

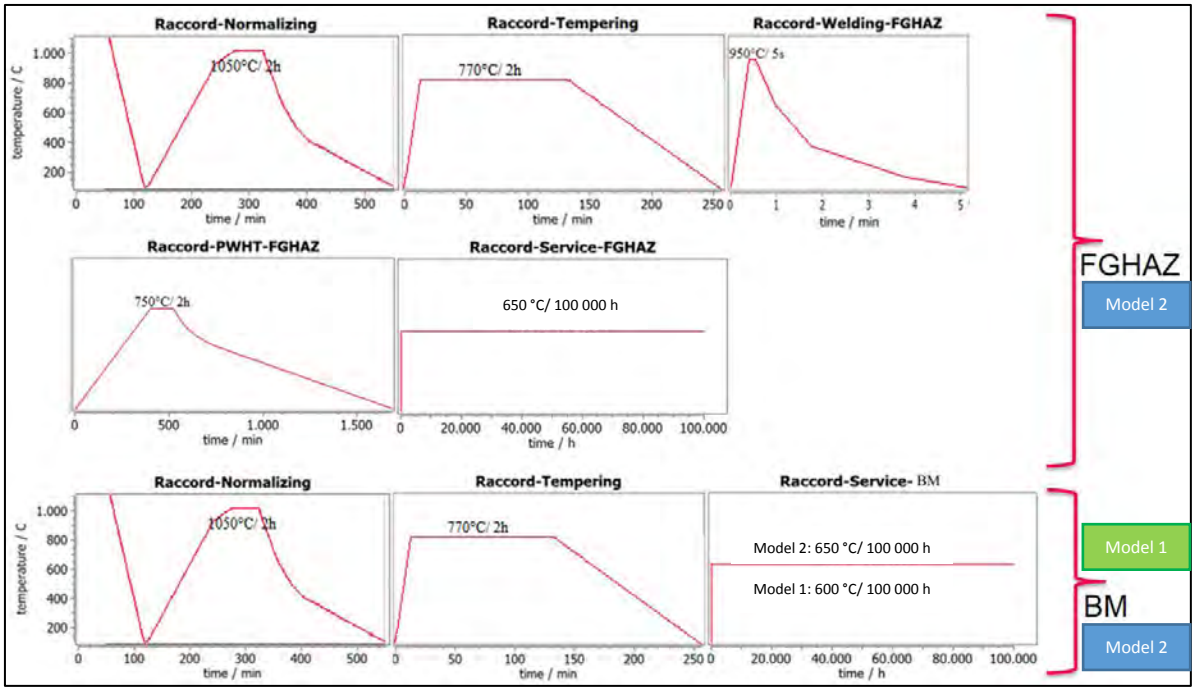

Figure 10) Heat treatments for BM and FGHAZ: holding times and temperatures

To improve the quality and accuracy of the MatCalc simulation, the heating and cooling rates for normalizing, tempering and welding were adjusted.

Formerly, 1 °C/s as heating rate and 0,1 °C/s as cooling rate was assumed for normalizing and tempering due to missing data (see figure 7 as well as tables 17 and 18). The manual analysis of T-t-diagrams (temperature vs. time) from MHI showed that both heating and cooling rates had been overestimated in Vujic's MatCalc model 0 (tables 17 and 18). The welding cycle was updated also and became more realistic (table 19). At the local peak temperature of 950 °C a holding time of 5 seconds was introduced. Welding and PWHT (table 20- without changes) of course are not relevant for base metal, but for FGHAZ.

Eventually, the adjusted heating and cooling rates resulted in numerical inaccuracies on the weaker computer and demanded a higher number of precipitation classes. 50 instead of 15 size classes (default value= 25) were needed in 2016's model 1 to solve the problem and avoid errors, especially for MX precipitates. In model 2 the size classes were even increased to 100 for Lave phase and $M_{23}C_6$. Further details about size classes for other particles see in chapter 5.3.3.

In general, it seems recommendable not to go below the default value of 25 with the size classes and increase them in case of obvious calculation inaccuracies or singularities. It can at least be one of the reasons for deviating MatCalc results, again depending on interaction with the individual CPU architecture.

The heating and cooling rates of all models (1 and 2 incorporated by the author) in overview:

Normalizing	Model 0	Model 1 + 2
Heating rate	1 °C/s	0,0083 °C/s 0,0444 °C/s
Peak time	2 h; 1050 °C	2 h; 1050 °C
Cooling rate	0,1 °C/s	0,0694 °C/s 0,0556 °C/s 0,0389 °C/s 0,0278 °C/s 0,0111 °C/s 0,0167 °C/s

Table 17) Heating + cooling rates for normalizing

Tempering	Model 0	Models 1 + 2
Heating rate	1 °C/s	0,0306 °C/s 0,0295 °C/s
Peak time	2 h; 770 °C	2 h; 770 °C
Cooling rate	0,1 °C/s	0,0244 °C/s 0,0181 °C/s 0,0111 °C/s 0,0134 °C/s

Table 18) Heating + cooling rates for tempering

Welding	Model 0	Model 1 + 2
Heating rate	1 °C/s	37,85 °C/s
Peak time	0 s; 950 °C	5 s; 950 °C
Cooling rate	15 °C/s	11,25 °C/s 6,19° C/s 1,84 °C/s

Table 19) Heating + cooling rates for welding cycle

PWHT	Models 0 + 1 + 2
Heating rate	0,0272 °C/s
Peak time	2 h; 750 °C
Cooling rate	0,0272 °C/s 0,0242 °C/s 0,0293 °C/s 0,0118 °C/s

Table 20) Same heating + cooling rates for PWHT

3.4.3.5) Modified Z Phase Settings

Unfortunately, the current MatCalc version 5.62 does not yet offer a physically accurate simulation of modified Z phase evolution during long-term creep. At the moment the user has to handle an empirical model, involving an equivalent interface energy and defining all sorts of vanadium nitrides as possible nucleation sites. The second possibility to control the modified Z phase is via nucleation constant in case nucleation at dislocations is intended.

For both model 1 and model 2 simulations in year 2016, equivalent interface energies for modified Z phase were chosen as 1 (formerly 0,45 in Vujic's model 0), whereas the nucleation constant remained unchanged (a value of 1.10^{-12}).

An explanation about the determination of these values and consequences for the Z phase behavior will be given in chapter 6.2.1.4.

3.4.3.6) Diffuse Interface Correction Temperature of Laves Phase

Diffuse interface correction temperature plays an important role for Laves phase and makes it possible to handle interfaces that are not sharp, but rather show a concentration gradient. [56] In general, choosing the right interface temperature in MatCalc offers a good compromise between dramatical coarsening and suppressed Laves phase formation during service, which both is not realistic and desirable.

Whereas in model 1 the originally determined value from S. Vujic of 1700 K (in model 0) was kept, in model 2 a method was found to calculate this quantity in a more accurate way on a physical basis. Details will be discussed in chapter 5.3.3

3.4.3.7) Volumetric Misfit for Aluminium Nitride

Although the amount of the chemical element aluminium and the phase fraction of aluminium nitride AlN precipitates is low in Raccord P91 steel, it is suggested to consider stress fields caused by these particles in a current 9 % Cr steel template script included in MatCalc version 5.62. The so-called volumetric misfit as the ratio of matrix phase molar volume and precipitate molar volume for aluminium nitride is defined as 0,27. It is only relevant for particles located at dislocations. MatCalc documentary [58] on basis of paper [59] states that this quantity will increase the nucleation barrier ΔG^* from equation 8. Source [59] emphasizes not to neglect strong modifications of the theoretical misfit due to lattice defects (such as dislocations or grain boundaries), leading to a proposed effective volumetric misfit of only 0,19 (=19 %) in this paper. However, in model 1 and 2 simulations, a factor of 0,27 (=27 %) originating from the template recommendations was implemented.

3.5) Backstress Calculation

Backstress calculations were conducted using Microsoft Excel as well as a pocket calculator. For details about results and the inserted parameters see chapter 5.3.4

4.) Results

The following chapter covers all MatCalc simulation results.

After presenting an equilibrium calculation and a precipitation kinetic simulation on basis of 2015 measurements (model 1), new 2016 measurements (EBSD and TEM) will be shown. This new data will contribute to advanced MatCalc model 2 and lead to an update of results. Finally, on basis of model 2 the total backstress will be calculated, applying two different methods based 1.) on room temperature situation and 2.) on evaluating the effect of elevated temperatures.

4.1) Equilibrium Calculation

With the chemical composition of Gr. 91 steel (Raccord in the version TU Graz) from table 10, a stepped equilibrium calculation between 400 °C and 1600 °C has been conducted (figure 11), showing which precipitates to expect and their phase fraction depending on temperature.

Beside chromium carbide ($M_{23}C_6$), laves phase and MX precipitates (NbC and VN) aluminium nitride (AlN) and copper (Cu) were revealed by the simulation.

In the thermodynamic equilibrium also a modified Z phase was observed.

The temperature range for stability of these precipitates is once more summarized in table 21. Please note that copper was excluded in the following precipitation kinetic simulations. Furthermore, one should be aware that according to simulation niobium carbide at 600 °C (relevant for precipitation kinetic model 1) is stable, but not at 650 °C (relevant for precipitation kinetic model 2).

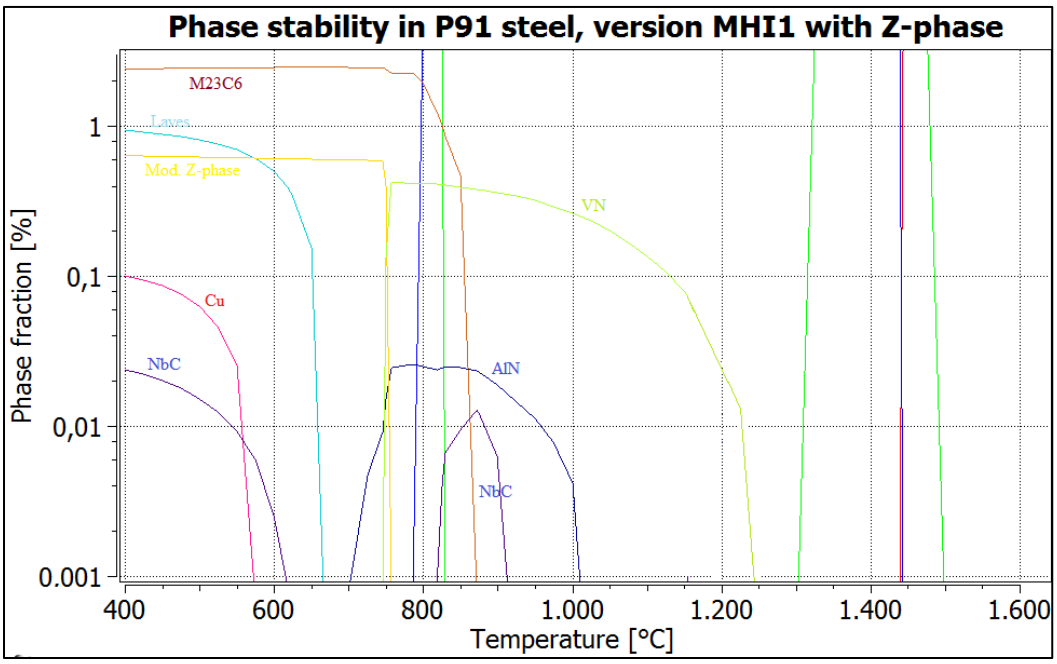

Figure 11) Equilibrium calculation with MatCalc for Raccord Gr. 91 between 400 and 1600 °C

Phase Stability of Precipitates	Temperature	Stability at 600 °C (Model 1)	Stability at 650 °C (Model 2)
$M_{23}C_6$	<400 °C - 871 °C	Yes	Yes
NbC	<400 °C - 617 °C 819 °C - 978 °C	Yes	No
VN	745 °C - 1245 °C	No	No
Laves Phase	<400 °C - 665 °C	Yes	Yes
AlN	700 °C - 1010 °C	No	No
Modified Z Phase	<400 °C - 758 °C	Yes	Yes
Cu	<400 °C - 573 °C	No	No

Table 21) Phase stability of precipitates for Raccord Gr. 91 (TU Graz version)

4.2) Microstructure Evolution: Model 1- BM Creep at 600 °C

The results for improved MatCalc model 1 were achieved from the script file with the name "dbn_pn_ns_bf_ddm_fct_1.5e14_vmf_aln_NbC_dg_eie_z_vn_1_MX_vmc_heat_cool_npc50" and made use of the settings in table 22 (summarizing tables 13 to 15).

MatCalc version	5.62	Subgrain size BM + FGHAZ	1 µm
Databases used	mc_fe_v2.050.tdb mc_fe_v2.008.ddb	Dislocation density in aust.	1.10^{11} m^{-2}
Service temperature	600° C	Dislocation density in mart. (start value before service)	$1{,}5.10^{14}$ m^{-2}
Aust. grain size BM	79 µm	Dislocation density in mart. (end value after service)	$3{,}1.10^{13}$ m^{-2}
Aust. grain size FGHAZ	14,3 µm		
Subgrain elongation BM	5	Diffuse interface correction temperature for Laves phase	1700 K
Subgrain elongation FGHAZ	1	Number of size classes for precipitates	50

Table 22) Major settings for MatCalc model 1 (Gr. 91 Raccord steel)

Model 1 only served to simulate the behavior of as-received base metal under creep conditions. This means that only a 3 stage heat treatment was incorporated, focusing on adapted heat treatments, grain and subgrain sizes as well as changed mobile dislocation density.

In contrast to dislocation density in martensite, that follows a non-linear reduction function derived from S. Yadav et al. [57], the constant dislocation density in austenite was not modified and still amounts to 1.10^{11} m^{-2} as in Vujic's model 0 and also in Yadav's model for paper [57] .

In 2016's model 1 a service temperature of 600 °C is assumed.

First of all, the diffuse interface correction temperature of 1700 K from model 0 was maintained for model 1. Later, validation with a new calculation method for diffuse interface correction in model 2 (see chapter 5.3.3) showed that this 1700 K deviated from the physically correct value. Nevertheless, at a temperature level for service of 600 °C the negative effect of using this slightly imperfect quantity was small and did not significantly worsen the model 1 results.

Modified Z phase in MatCalc so far is controlled by a nucleation constant for the formation at dislocations (set to 10^{-12}) as well as by determining an equivalent interface energy (currently a factor of 1) for nucleation on vanadium nitride precipitates. Important to know is that at the moment Z phase nucleation is based on an empirical model and the chosen parameters in fact are not completely reflecting the physical reality.

4.2.1) As-received Condition of Base Metal (BM)

After normalizing (which includes austenization as well as quenching) and tempering the so-called as-received condition of base metal (BM) is reached.

The simulation results therefore are summarized in figures 12 and 13 as well as in table 23.

Raccord Gr. 91 steel then contains a high amount of 2,273 % chromium carbide at martensitic subgrain boundaries **$M_{23}C_6$(mart,s)** with a diameter of around 96 nm. It forms during heating in the tempering stage.

Nucleation of vanadium nitride at martensitic subgrain boundaries **VN(mart,s)** also takes place during heating in the tempering section and finally shows a phase fraction of 0,379 % with a diameter of 45 nm.

Niobium carbide at martensitic subgrain boundaries **NbC(mart,s)** exists in the end with a phase fraction of 0,065 % and a size (mean diameter) of 31 nm. It evolves during heating in normalizing stage and stays stable during tempering.

Aluminium nitride at martensitic dislocations **AlN(mart,d)** occurs with a phase fraction of 0,026 % and a mean diameter of 44 nm, nucleating during heating in tempering stage.

Niobium carbide at austenitic dislocations **NbC(aust,d)** comes from heating in the normalizing section and stays stable during tempering with a phase fraction of 0,012 % and a size of 34 nm.

Vanadium nitride at martensitic grain boundaries **VN(mart,g**)- which grows during heating in tempering stage- has a low phase fraction of 0,0065 %, which makes the big diameter of 109 nm acceptable, even though it has not been found in any microscopic investigation.

All other precipitates with a phase fraction of lower than 0,01 % are not discussed here in detail, but can be seen in table 23. They are marked with yellow colour.

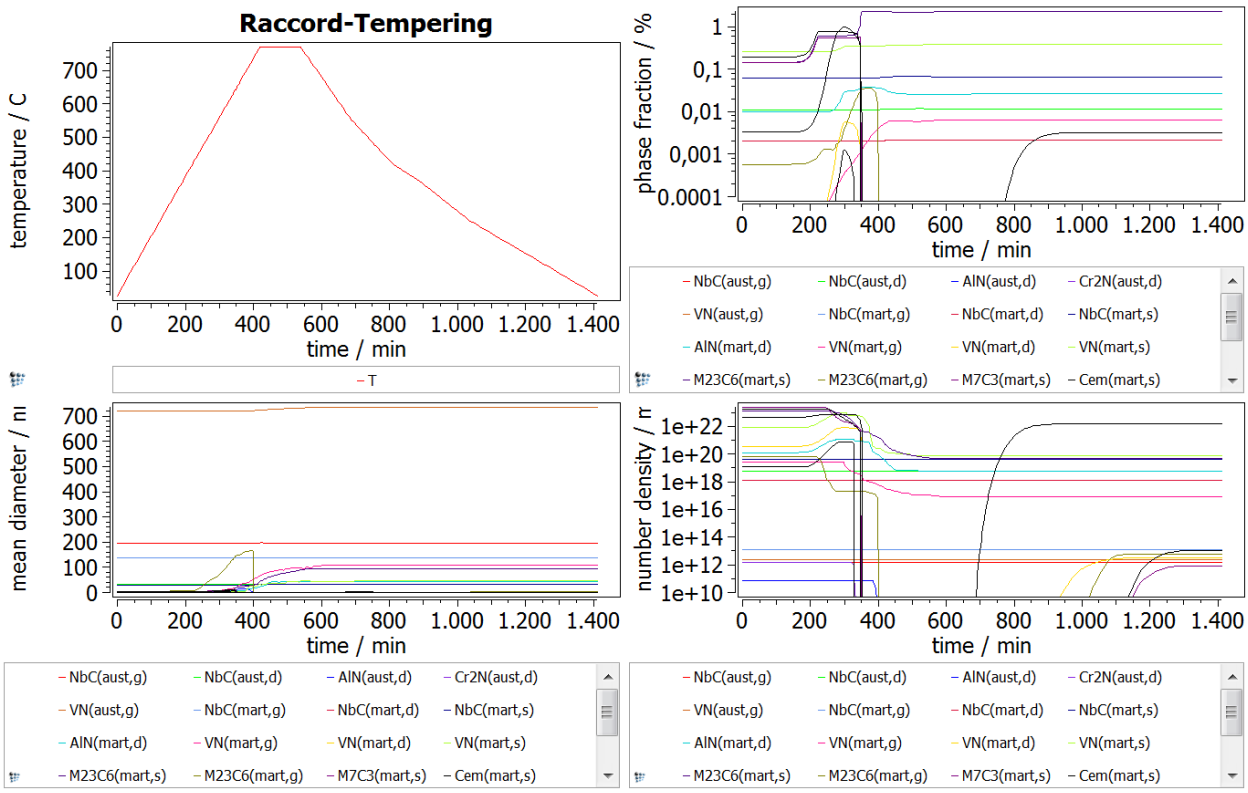

Figure 12) As-received condition BM (model 1); phase fraction, diameter + number density

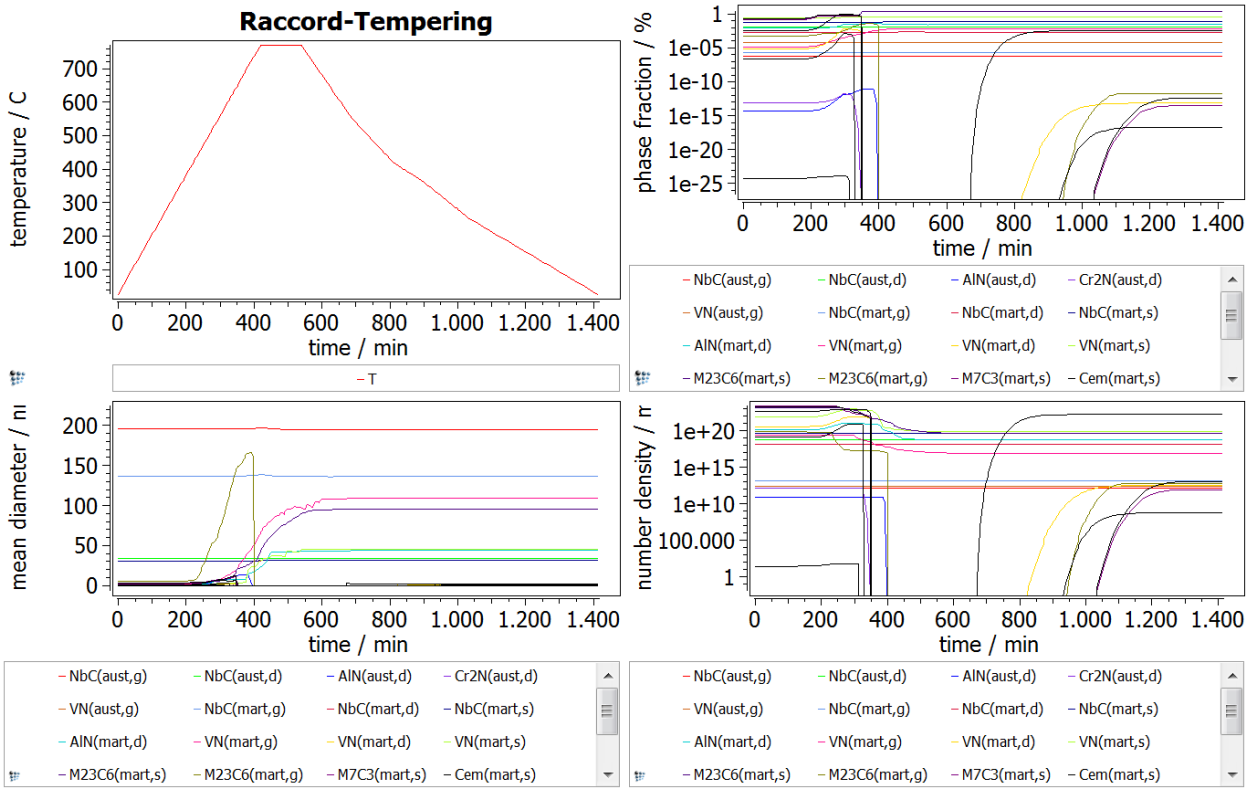

Figure 13) Zoom of BM as-received (model 1); phase fraction, diameter + number fraction

AR, BM	Phase Fraction	Mean Diameter	Number Density
$M_{23}C_6$(mart,s)	2,273 %	95,6 nm	$4{,}68.10^{19}$ m^{-3}
VN(mart,s)	0,379 %	45,3 nm	$7{,}08.10^{19}$ m^{-3}
NbC(mart,s)	0,065 %	31,1 nm	$4{,}14.10^{19}$ m^{-3}
AlN(mart,d)	0,026 %	43,7 nm	$5{,}65.10^{18}$ m^{-3}
NbC(aust,d)	0,012 %	33,9 nm	$5{,}6.10^{18}$ m^{-3}
VN(mart,g)	$6{,}47.10^{-3}$ %	108,7 nm	$8{,}09.10^{16}$ m^{-3}
Laves(mart,s)	$3{,}21.10^{-3}$ %	1,4 nm	$1{,}58.10^{22}$ m^{-3}
NbC(mart,d)	$2{,}09.10^{-3}$ %	31 nm	$1{,}34.10^{18}$ m^{-3}
VN(aust,g)	$5{,}51.10^{-5}$ %	734,8 nm	$2{,}51.10^{12}$ m^{-3}
NbC(mart,g)	$1{,}86.10^{-6}$ %	136 nm	$1{,}22.10^{13}$ m^{-3}
NbC(aust,g)	$6{,}19.10^{-7}$ %	194,8 nm	$1{,}51.10^{12}$ m^{-3}
$M_{23}C_6$(mart,g)	$1{,}93.10^{-12}$ %	1,8 nm	$5{,}88.10^{12}$ m^{-3}
Cem(mart,s)	$3{,}95.10^{-13}$ %	0,9 nm	$1{,}12.10^{13}$ m^{-3}
VN(mart,d)	$7{,}34.10^{-14}$ %	0,7 nm	$3{,}28.10^{12}$ m^{-3}
M_7C_3(mart,s)	$3{,}09.10^{-14}$ %	0,9 nm	$8{,}52.10^{11}$ m^{-3}
Cr2N(mart,d)	$2{,}06.10^{-17}$ %	0,9 nm	$6{,}02.10^{8}$ m^{-3}

Table 23) Model 1 results of as-received condition BM

4.2.2) BM creep-loaded for 100 000 hours at 600 °C

The results of BM creep-loaded for 100 000 hours at 600 °C are depicted in figures 14 and 15. Table 24 gives detailed data (phase fraction, diameter and number fraction) about the individual precipitates.

Chromium carbide at martensitic subgrain boundaries maintains a high phase fraction of 2,24 % **$M_{23}C_6$(mart,s)** and coarsens up to a diameter of 426 nm at the end of 100 000 hours service.

Laves phase at martensitic subgrain boundaries **Laves(mart,s)**- which was already present in as-received condition, but with minor phase fraction and diameter- increases its phase fraction to 0,447 % at the beginning of service and starts to grow rapidly immediately. Laves phase finally reaches a diameter of 193 nm after 100 000 hours of creep.

Vanadium nitride at martensitic subgrain boundaries **VN(mart,s)** develops a higher phase fraction of 0,404 % compared to as-received condition and slightly raises its mean diameter to 62 nm.

Niobium carbide at austenitic dislocations **NbC(aust,d)** also increases its phase fraction and diameter, reaching 0,04 % and 51 nm after 100 000 hours.

Niobium carbide at martensitic subgrain boundaries **NbC(mart,s)** in contrast reduces its phase fraction to 0,025 % and shrinks to 23 nm after 100 000 hours.

The phase fraction of aluminium nitride at martensitic dislocations **AlN(mart,d)** decreases a little to 0,021 %, while the mean diameter grows to around 148 nm after 100 000 hours.

Vanadium nitride located at martensitic grain boundaries **VN(mart,g)** dissolves completely in the beginning of service.

The rest of precipitates with minor phase fractions lower than 0,01 % (mainly niobium carbides) are listed again in table 24.

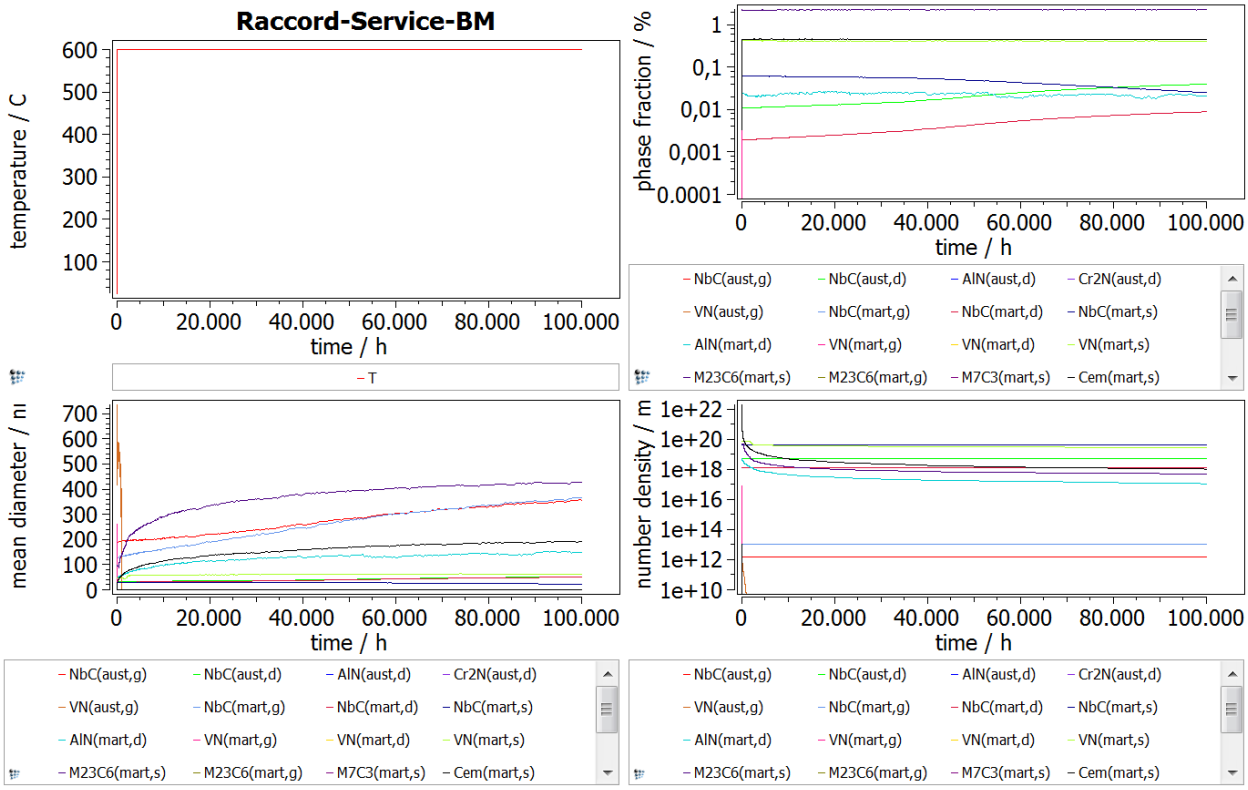

Figure 14) Service section in model 1 (BM creep loaded for 100 000 hours at 600 °C)

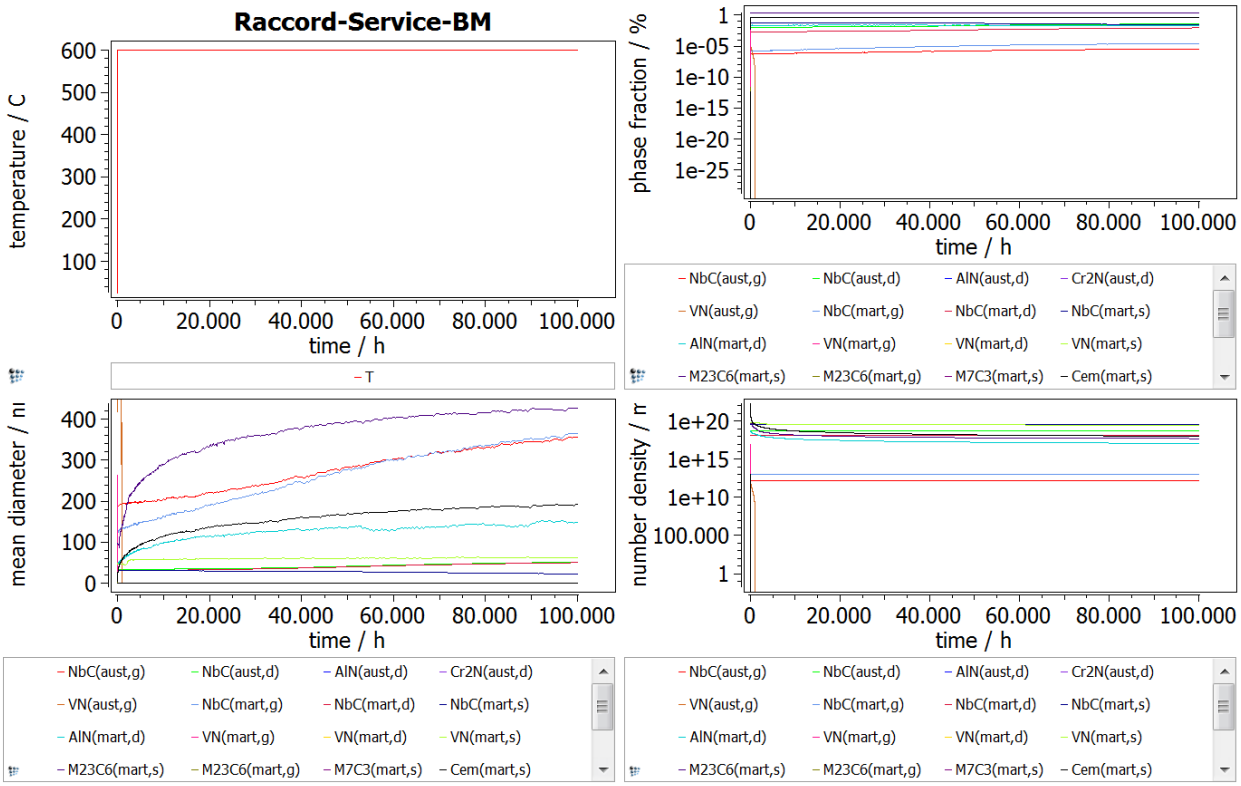

Figure 15) Zoom of service section in model 1 (BM creep loaded for 100 000)

100 000 h service, 600°C	Phase Fraction	Mean Diameter	Number Density
$M_{23}C_6$(mart,s)	2,24 %	426 nm	$5{,}18.10^{17}$ m^{-3}
Laves(mart,s)	0,447 %	192,6 nm	$1{,}05.10^{18}$ m^{-3}
VN(mart,s)	0,404 %	61,9 nm	$2{,}66.10^{19}$ m^{-3}
NbC(aust,d)	0,040 %	51,3 nm	$5{,}6.10^{18}$ m^{-3}
NbC(mart,s)	0,025 %	22,5 nm	$4{,}16.10^{19}$ m^{-3}
AlN(mart,d)	0,021 %	148 nm	$1{,}13.10^{17}$ m^{-3}
NbC(mart,d)	$8{,}85.10^{-3}$ %	50,2 nm	$1{,}34.10^{18}$ m^{-3}
NbC(mart,g)	$2{,}69.10^{-5}$ %	365,8 nm	$1{,}04.10^{13}$ m^{-3}
NbC(aust,g)	$3{,}59.10^{-6}$ %	356 nm	$1{,}51.10^{12}$ m^{-3}

Table 24) Model 1 results of service BM (100 000 hours at 600 °C)

4.3) Microstructure Evolution: Model 2- BM and FGHAZ Creep at 650 °C

4.3.1) EBSD Results 2016

4.3.1.1) EBSD Analysis 2016 of PAGS in BM (as-received condition)

New EBSD measurements from as-received condition of base metal (specimen 1) were analyzed with help of TSL OIM Analysis Software package (OIM = Orienting Imaging). The first IPF map (figure 16) depicts a step size of 1,5 µm and a field of view of 1000 x 1000 µm.

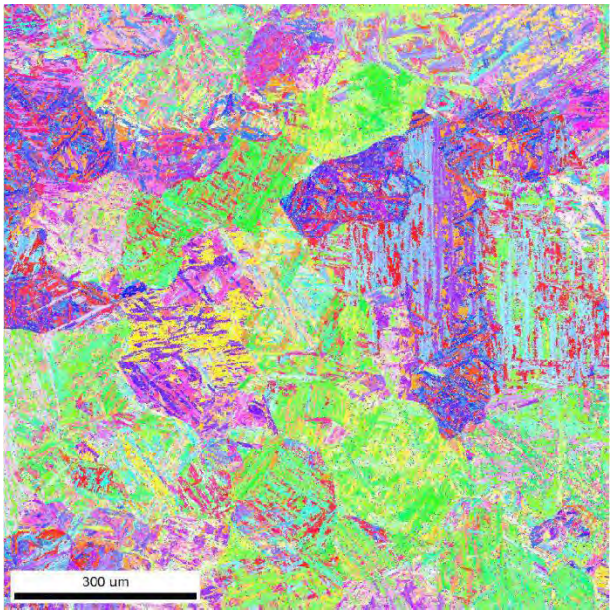

Figure 16) IPF map of BM in as-received condition

A range of the misorientation angle between 18 and 50 degrees was found to reveal the prior austenitic grains most effectively [60](figure 17).

Unfortunately, the quality of data was not good enough to automatically calculate the prior austenitic grain size as the grains were not completely visible or had an open form (figure 16). The software misinterpreted martensitic block boundaries as PAGS and gave far too low values.

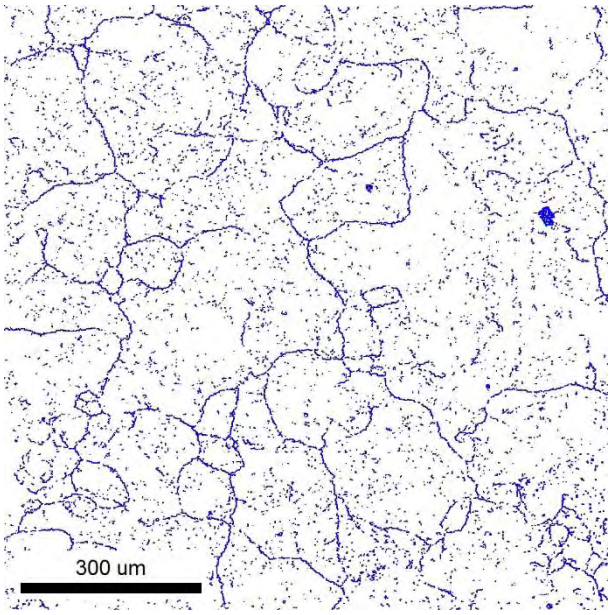

Figure 17) PAGS with misorientation 18- 50 °

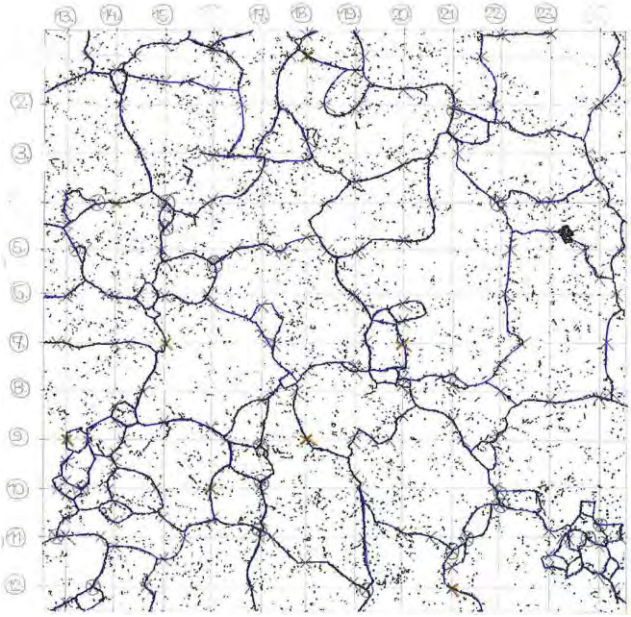

Figure 18) Manually completed grain bound.
+ use of 24 intersection lines for AGI meth.

As a result, the mean linear intercept method was chosen to manually detect the right PAGS for base metal (figure 18), consisting of the following steps:

- Marking grain boundaries on printout by hand and completing them, if not fully visible
- Drawing a sufficient number of lines with same length on the picture

- Sum up certain values for each point:
  - 0,5 for start and end point of the line, if located in centre of a grain
  - 1 if start and end point are located on a grain boundary
  - 1 for each intersection of line and grain boundary
  - 1,5 for each intersection of line and grain boundary triple point
- Subtract value of 1 per line (because there is always 1 point of intersection more than the actual number of grains)
- Calculate the length of lines (consider the scale!)
- Division of each line‘s length by the number of counted points

To account for the grains that were not fully visible, a correction factor based on a generalized Mackenzie distribution for disorientation angles in unique cubic crystals without texture [61] was introduced.

The calculated function for the distribution has to be separated in 4 equations, whose last one does not have an analytical solution and will not be stated (more important: equations 29 to 31). As the contribution of the fourth part of the function can be neglected, it is replaced by a lengthened equation w(x).

The minor difference in the distribution function shape is marked in figures 18 and 19. The 3 functions u(x), v(x) and w(x)- with x standing for misorientation angle- are defined:

$$u(x) = \frac{24}{\pi}[1 - \cos(x_1)] \qquad (29)$$

$$0 \leq x_1 \leq 0{,}7854\, rad$$

$$v(x) = \frac{24}{\pi}[1 - \cos(x_2)] \cdot \left[3\left(\sqrt{2} - 1\right)\cot\left(\frac{x_2}{2}\right) - 2\right] \qquad (30)$$

$$0{,}7854\, rad < x_2 \leq 1{,}0472\, rad$$

$$w(x) = \frac{24}{\pi}[1 - \cos(x_3)] \cdot \left\{\left[3\left(\sqrt{2} - 1\right) + \frac{4}{\sqrt{3}}\right] \cdot \cot\left(\frac{x_3}{2}\right) - 6\right\} \qquad (31)$$

$$1{,}0472\, rad < x_3 \leq 1{,}0685\, rad$$

The correction factor K (equation 32) can now be calculated as the ratio of the integral between 0 and 61 degrees, which represents the whole distribution (from 0 to 1,0685 rad), and the integral between 18 and 50 degrees (from 0,3142 to 0,8727 rad).

Calculations were realized with software package Mathematica.

$$K = \frac{\int_0^{1,0685} f(x)dx}{\int_{0,3142}^{0,8727} f(x)dx} = \frac{0,998671}{0,736622} = 1,35575 \qquad (32)$$

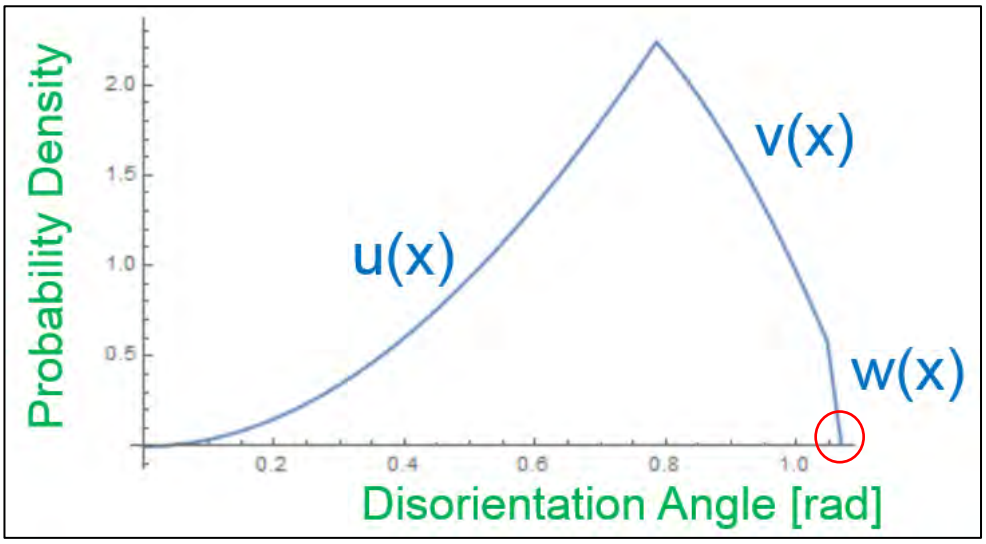

Figure 19) Slightly modified disorientation angle distribution of unique cubic crystals by C. A. Schuh et al. [61]*; plot created with Wolfram Mathematica software (student version)*

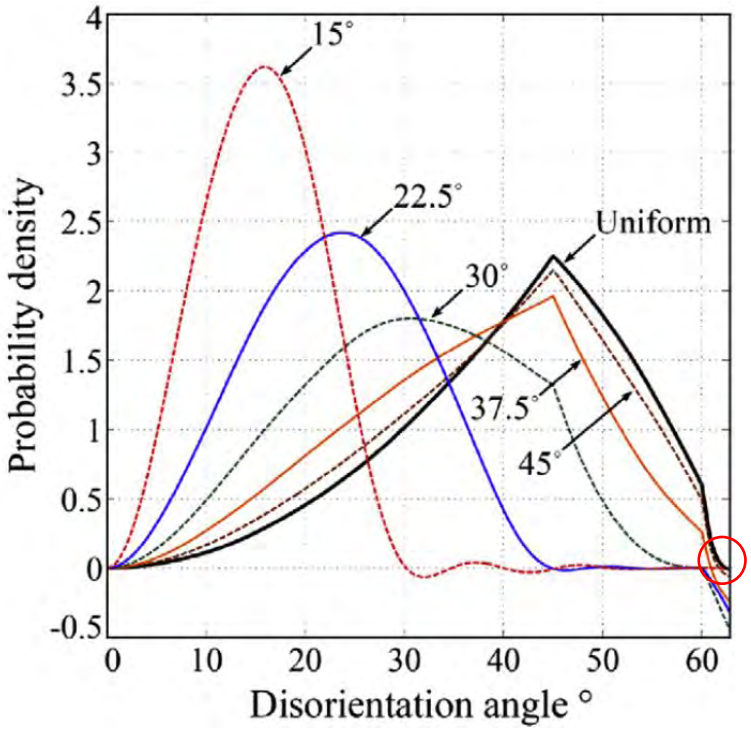

Figure 20) Original solution for disorientation angle distribution functions for textures of varying degrees of sharpness by C. A. Schuh et. al [61]

Table 25 shows the results for the mean linear intercept method (counts of intersections). Equations 33 to 36 describe two possible ways how to involve the calculated correction factor K from the Mackenzie distribution and find the corrected, real PAGS.

Line Numb.	1	2	3	4	5	6	7	8	9	10	11	12
S+E	1	1	1	1	1	1	1,5	1	1	1	1	1
POI	8	8	8	7	10	8	9	6	11	7	10	4
POIT	0	0	0	3x1,5	1x1,5	0	0	0	0	1x1,5	3x1,5	2x1,5
Sum	9	9	9	12,5	12,5	9	10,5	7	12	9,5	15,5	8
$PAGS_1$	124,88	124,88	124,88	86,87	86,87	124,88	105,16	166,5	90,18	117,53	68,90	142,71
$PAGS_2$	89,16	89,16	89,16	62,63	62,63	89,16	75,46	117,64	65,41	84,08	49,91	101,44

Line Numb.	13	14	15	16	17	18	19	20	21	22	23	24
S+E	1	1	1	1	1	1	1	1	1	1	1	1
POI	14	13	10	9	8	8	11	11	7	7	8	6
POIT	0	0	0	1x1,5	3x1,5	0	0	0	2x1,5	2x1,5	0	1x1,5
Sum	15	14	11	11,5	13,5	9	12	12	11	11	9	8,5
$PAGS_1$	71,36	76,85	99,9	95,14	79,92	124,88	90,82	90,82	99,9	99,9	124,88	133,2
$PAGS_2$	51,65	55,55	71,79	68,45	57,73	89,16	65,41	65,41	71,79	71,79	89,16	94,91

Table 25) Number of intersections with PAGS (mean linear intercept meth.)

*Legend: S+E … Start and end point of line POI … Point of intersection between line and grain boundary POIT… Point of intersection between line and grain boundary triple point	Scale: 1mm=6 µm Line length: 166,5 mm=999 µm Correction factor K=1,356

$$PAGS_1 = \frac{Length}{Sum - 1} = \frac{999\ \mu m}{Sum - 1} \quad (33)$$

$$\overline{PAGS}_{BM1} = \frac{1}{K} \cdot \frac{\sum PAGS_1}{\sum Lines} = \frac{1}{1{,}356} \cdot \frac{124{,}88 + \cdots + 133{,}2}{24} = \frac{106{,}33\ \mu m}{1{,}356} = 78{,}43\ \mu m \quad (34)$$

$$PAGS_2 = \frac{Length}{K \cdot Sum - 1} = \frac{999\ \mu m}{1{,}356 \cdot Sum - 1} \quad (35)$$

$$\overline{PAGS}_{BM2} = \frac{\sum PAGS_2}{\sum Lines} = \frac{89{,}31 + \cdots + 95{,}06}{24} = 76{,}19\ \mu m \quad (36)$$

Whereas in method 1 (equ. 33 and 34) the sum of PAGS is corrected, in method 2 (equ. 35 and 36) this correction is conducted for the PAGS of each intersection line. It can be said that method 2 artificially increases the number of intersection points, which leads to a reduction of the PAGS. Finally, the PAGS was estimated to be between 78,4 µm and 76,2 µm instead of 106,3 µm, applying these two models based on Mackenzie distribution. This is close to the used value of 79 µm for MatCalc model from April 2016.

4.3.1.2) EBSD Analysis 2016 of Subgrain Size in BM (as-received condition)

In similar manner, TSL OIM software was used to analyze the EBSD data and find out the subgrain size for specimen 1.

Therefore, a misorientation angle between 1 and 4 degrees was applied to reveal subgrains (see the red low-angle boundary areas in figure 22).

In this case, data quality for the picture (figure 21) with a step size of 0,05 µm and a field of view of 40 x 40 µm turned out to be excellent, so that automatic calculation of the subgrain size immediately succeeded (figure 21).

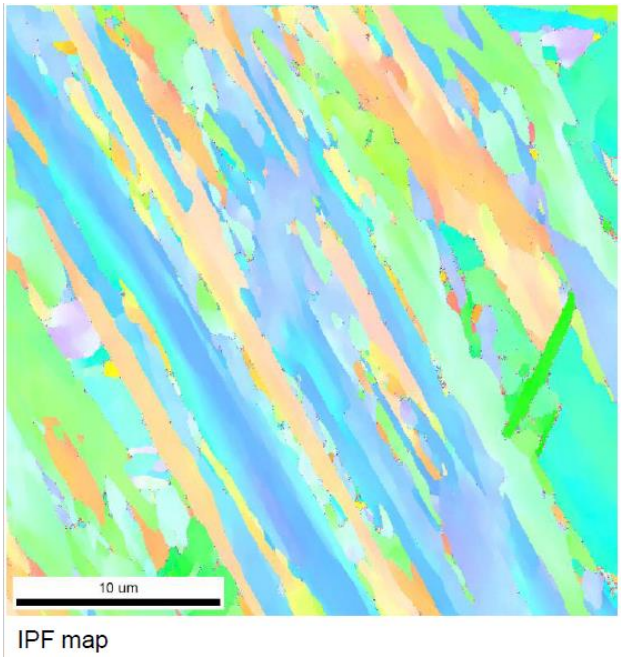

Figure 21) IPF map of Gr. 91 BM as-received with higher resolution

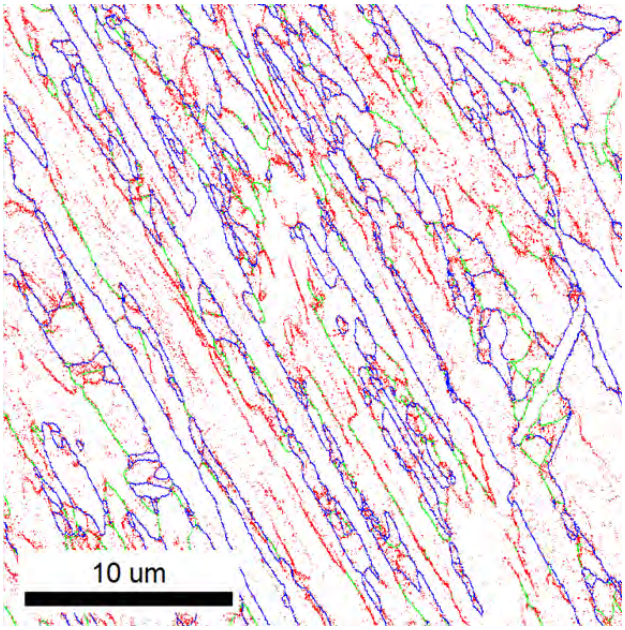

Figure 22) Blank map of Gr. 91 BM as-received (subgrain boundaries in red)

LEGEND

Red: 1°-4° M.A.* (Subgrain Boundaries)

Green: 4°-15° M.A.*

Blue: 15°-180 ° M.A.* (PAGB+Martensite Laths=HAGB**)

*M.A. = Misorientation Angle; **HAGB = High Angle Grain Boundaries

Based on evaluating statistics, a mean subgrain size of 0,56 µm in as-received condition of BM was estimated (figure 23), which seems in good agreement with literature data [16] [4].

OIM software also served to calculate the mean misorientation angle of the distribution between 1 and 4 degrees. For BM a value of 1,40281°=0,02448 rad was found, which combined with Burgers vector and subgrain size helped to determine a boundary dislocation density of around $4{,}58.10^{14}$ m^{-2} [62].

The way of calculating the boundary dislocation density can be seen in equation 37. $\boldsymbol{\theta_i f_i}$ stands for the mean misorientation angle (here 0,02448 rad), **b** for the Burgers vector of around 2,866 Å= $2{,}866.10^{-10}$ m and **sgs** denotes the subgrain size, using 0,56 µm=$0{,}56.10^{-6}$ m.

$$\rho_{bi} = \frac{\theta_i f_i}{2b} \cdot \frac{3}{sgs} \qquad (37)$$

This value was not used in MatCalc precipitation kinetics, but instead ranks amongst important input parameters for Yadav's creep model in MatLab and was used by Bernhard Krenmayr in his creep-curve simulation part.

S. Yadav who is PhD graduate at IWS, TU Graz, developed a novel hybrid model for creep of martensitic steel, combining a physical background with continuum damage theory. [57] The found equations were implemented and numerically solved in MatLab code for P92 steel. B. Krenmayr, another PhD student at IWS, in the 2016 project for MHI focused on adjusting Yadav's code to P91 parameters and simulating creep curves on basis of experimental data.

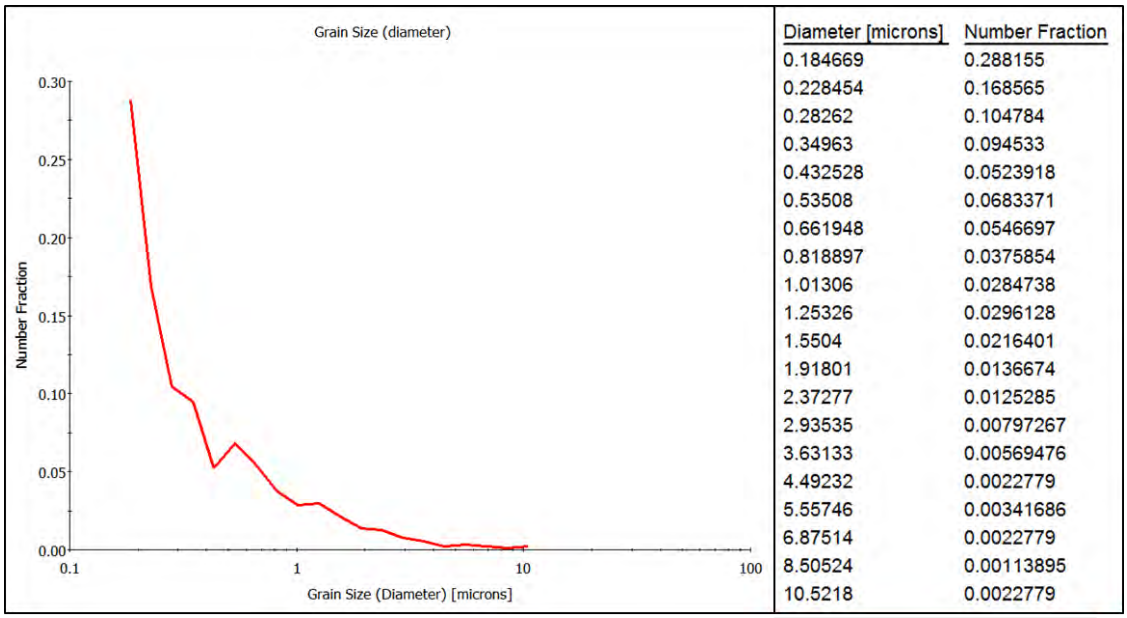

Diameter [microns]	Number Fraction
0.184669	0.288155
0.228454	0.168565
0.28262	0.104784
0.34963	0.094533
0.432528	0.0523918
0.53508	0.0683371
0.661948	0.0546697
0.818897	0.0375854
1.01306	0.0284738
1.25326	0.0296128
1.5504	0.0216401
1.91801	0.0136674
2.37277	0.0125285
2.93535	0.00797267
3.63133	0.00569476
4.49232	0.0022779
5.55746	0.00341686
6.87514	0.0022779
8.50524	0.00113895
10.5218	0.0022779

Average	
Number	0.557278
Area	5.4444
Standard Deviation	
Number	0.89765
Area	3.85915

SGS_{BM}=0,56 µm

Figure 23) Number fraction of subgrain size in OIM TSL software + calculation of mean value

4.3.1.3) EBSD Analysis 2016 of PAGS in FGHAZ (as-received condition)

New EBSD measurements from as-received condition of FGHAZ (specimen number 2) were again analyzed with the help of TSL OIM Analysis Software package.

The IPF map in figure 24 depicts a step size of 0,4 µm and a field of view of 300 x 300 µm.

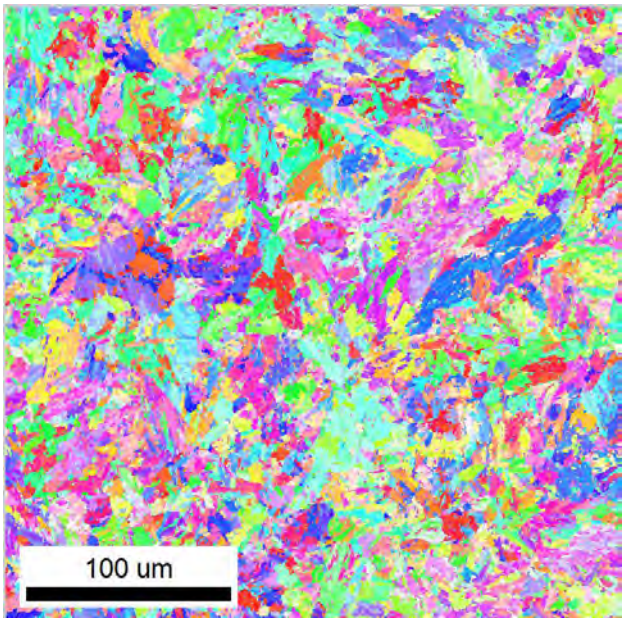

Figure 24) IPF map of FGHAZ in as-received condition

For revealing the PAGS most effectively, a blank map (figure 25) with a range of the misorientation angle between 18 and 50 degrees was created.

The visibility of grain boundaries turned out to be good enough for an automatic calculation of the grain size (figure 27), giving a value of 7,75 µm.

The reliability of the automatic result was checked manually with help of the mean linear intercept method on a print-out (figure 26).

Table 26 shows the number of intersection points.

The individual prior austenitic grain sizes are then calculated as the division of each line‘s length by the number of counted points (see equation 36). To find a mean value, all PAGS results are added and divided by the number of lines, which is 24 in this case.

Equation 38 then leads to a mean PAGS value for the FGHAZ of 8,98 µm.

As a result, the automatic calculation (7,75 µm) and the manual result (8,98 µm) lie close to each other and a Mackenzie-based correction factor like for base metal is not regarded necessary for the FGHAZ data.

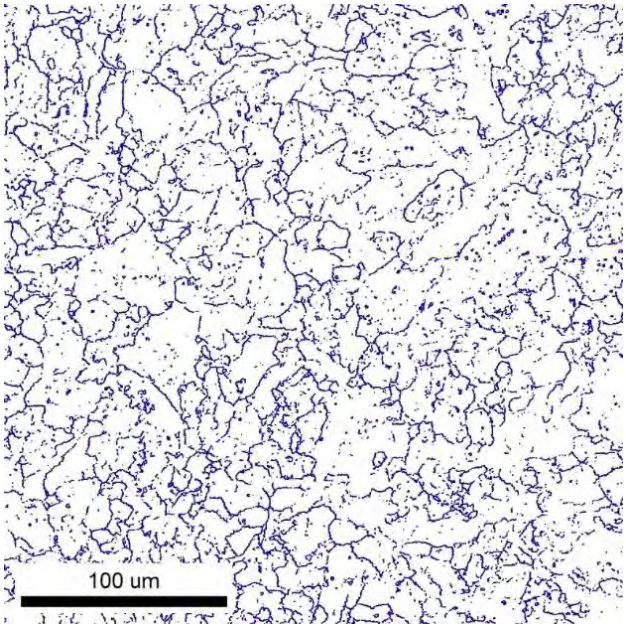

Figure 25) PAGS (misorientation 18- 50 °)

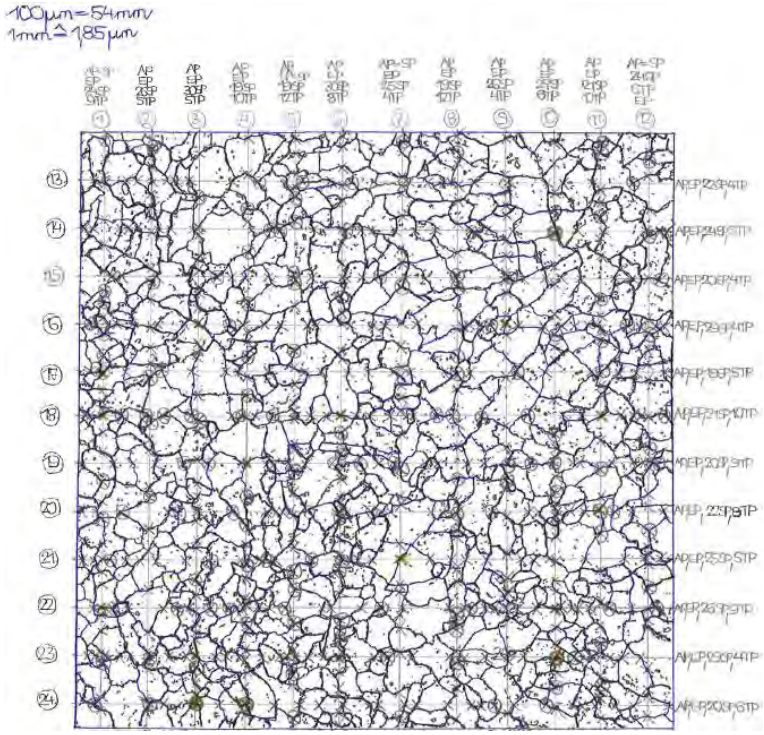

Figure 26) Manually completed grain bound. and use of 24 intersection lines for AGI meth.

Line Numb.	1	2	3	4	5	6	7	8	9	10	11	12	13	14	15	16	17	18	19	20	21	22	23	24
S+E	1,5	1	1	1	1,5	1	1,5	1	1	1	1	1,5	1	1	1	1	1	1	1	1	1	1	1	1
POI	24	26	30	19	19	30	25	19	26	27	21	24	22	24	20	29	19	21	20	22	25	26	29	20
POIT	9x 1,5	5x 1,5	5x 1,5	10x 1,5	12x 1,5	8x 1,5	4x 1,5	12x 1,5	4x 1,5	6x 1,5	10x 1,5	6x 1,5	4x 1,5	5x 1,5	4x 1,5	4x 1,5	5x 1,5	10x 1,5	9x 1,5	8x 1,5	5x 1,5	9x 1,5	4x 1,5	6x 1,5
Sum	39	34,5	38,5	35	38,5	43	32,5	38	33	37	37	34,5	29	32,5	27	36	27,5	37	34,5	35	33,5	40,5	36	30
PAGS	7,91	8,97	8,02	8,84	8,02	7,16	9,54	8,13	9,39	8,35	8,35	8,97	10,74	9,54	11,56	8,59	11,34	8,35	8,97	8,84	9,25	7,61	8,59	10,37

Table 26) Number of intersections with PAGS (mean linear intercept meth.)

*Legend:
S+E ... Start and end point of line
POI ... Point of intersection between line and grain boundary
POIT... Point of intersection between line and grain boundary triple point

Scale: 1mm=6,45 µm
Line length: 156 mm=1006,2 µm

$$\overline{PAGS}_{FGHAZ} = \frac{\sum PAGS}{\sum Lines} = \frac{7{,}91 + \cdots + 10{,}37}{24} = 8{,}98\ \mu m \quad (38)$$

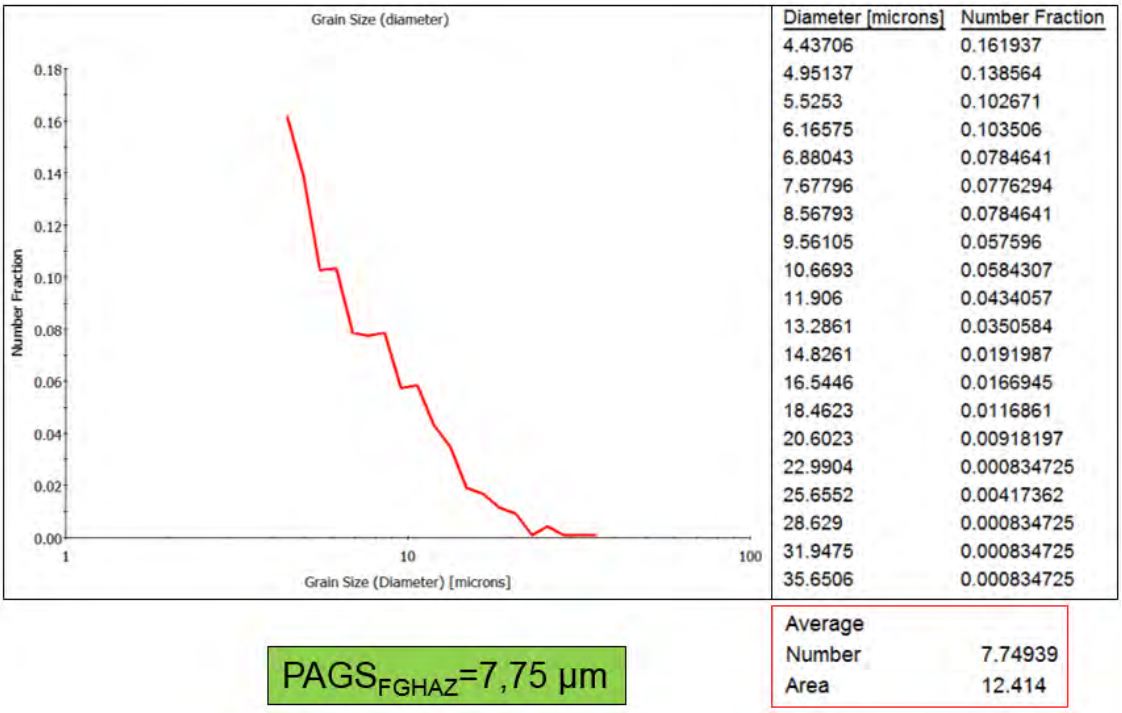

Diameter [microns]	Number Fraction
4.43706	0.161937
4.95137	0.138564
5.5253	0.102671
6.16575	0.103506
6.88043	0.0784641
7.67796	0.0776294
8.56793	0.0784641
9.56105	0.057596
10.6693	0.0584307
11.906	0.0434057
13.2861	0.0350584
14.8261	0.0191987
16.5446	0.0166945
18.4623	0.0116861
20.6023	0.00918197
22.9904	0.000834725
25.6552	0.00417362
28.629	0.000834725
31.9475	0.000834725
35.6506	0.000834725

Average	
Number	7.74939
Area	12.414

Figure 27) Number fraction of PAGS in OIM TSL software + calculation of mean value

4.3.1.4) EBSD Analysis 2016 of Subgrain Size in FGHAZ (as-received condition)

Once more, a misorientation angle between 1 and 4 degrees was applied to reveal subgrains of specimen number 2 within TSL OIM Analysis Software (see red lines in figure 29). Data quality for the picture (figure 28) with a step size of 0,05 µm and a field of view of 40 x 40 µm turned out to be excellent again, so that automatic calculation of the subgrain size was successful (figure 30).

The mean misorientation angle of the distribution between 1 and 4 degrees in the case of FGHAZ was 1,5286° = 0,026679 rad. This allowed to determine a boundary dislocation density of $5{,}48.10^{14}$ m^{-2} [62] based on equation 37, using a Burgers vector of 2,866 Å = $2{,}866.10^{-10}$ m and a subgrain size of 0,51 µm = $0{,}51.10^{-6}$ m.

This input parameter for Yadav's creep model in MatLab was used by Bernhard Krenmayr in his creep-curve simulation part.

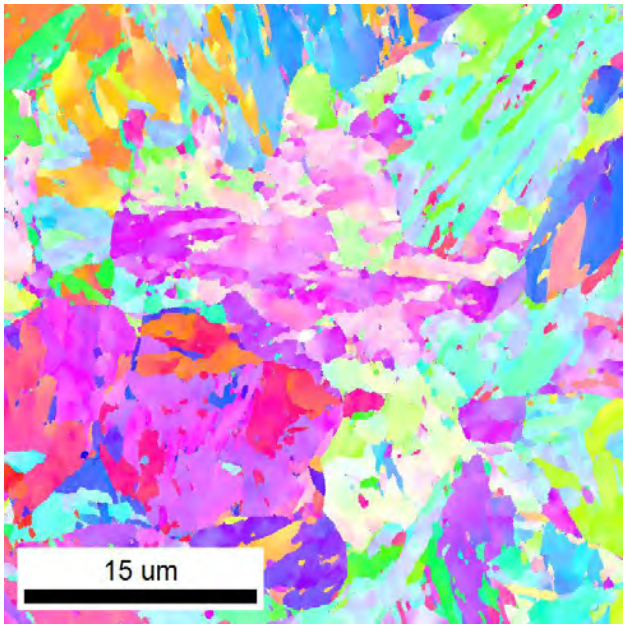

Figure 28) IPF map of Gr. 91 FGHAZ as-received with higher resolution

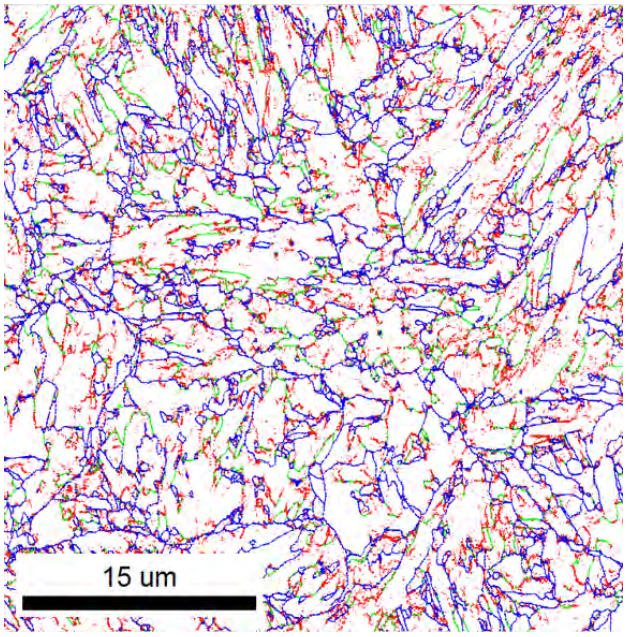

Figure 29) Blank map of Gr. 91 FGHAZ as-received (subgrain boundaries in red)

LEGEND

Red: 1°-4° M.A.* (Subgrain Boundaries)

Green: 4°-15° M.A.*

Blue: 15°-180 ° M.A.* (PAGB+Martensite Laths=HAGB**)

*M.A. = Misorientation Angle; **HAGB = High Angle Grain Boundaries

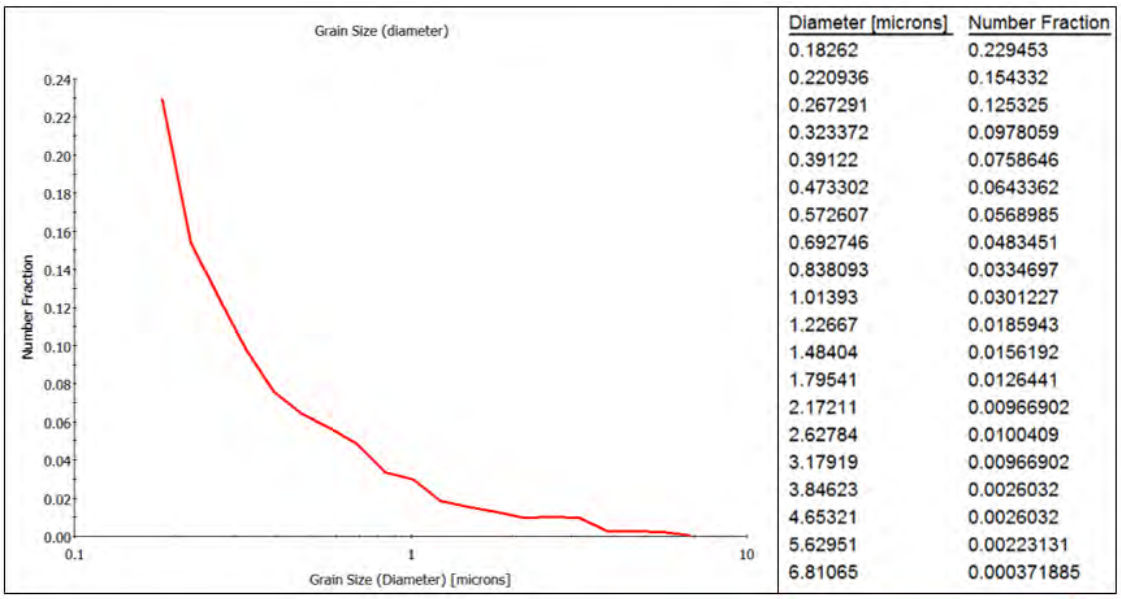

Diameter [microns]	Number Fraction
0.18262	0.229453
0.220936	0.154332
0.267291	0.125325
0.323372	0.0978059
0.39122	0.0758646
0.473302	0.0643362
0.572607	0.0568985
0.692746	0.0483451
0.838093	0.0334697
1.01393	0.0301227
1.22667	0.0185943
1.48404	0.0156192
1.79541	0.0126441
2.17211	0.00966902
2.62784	0.0100409
3.17919	0.00966902
3.84623	0.0026032
4.65321	0.0026032
5.62951	0.00223131
6.81065	0.000371885

Average	
Number	0.507425
Area	2.69761
Standard Deviation	
Number	0.626393
Area	1.79064

SGS_{FGHAZ}=0,51 µm

Figure 30) Number fraction of subgrain size in OIM TSL software + calculation of mean value

4.3.1.5) EBSD Analysis 2016 of Subgrain Sizes in BM creep-loaded (100 MPa and 80 MPa)

Analysis of specimen 3 (100 MPa load) and 5 (80 MPa load) was not carried out to gain further input parameters for MatCalc precipitation kinetics models, but rather to achieve control values for the MatLab creep-curve simulation of B. Krenmayr on basis of S. Yadav's findings.

After analyzing the subgrain sizes from EBSD data with the help of TSL OIM Analysis Software, a high number fraction of grains turned out to be smaller than 0,15 µm.

However, this size is close to the detection limit of the EBSD investigations. Generally, when dealing with digitized data, it is assumed good practice to ignore signals smaller than 3 digits. With a stepsize of 50 nm, this limit equals 0,15 µm.

All subgrains below this value were finally excluded, which led to a corrected subgrain size for specimen 5 (80 MPa) of 1,50 µm (table 27) instead of the automatically calculated 1,05 µm (see figure 31). This procedure was done with Microsoft Excel.

The same subgrain size correction was conducted for specimen 3 (100 MPa), achieving a result of 1,94 µm (table 28) instead of 1,47 µm (see figure 32).

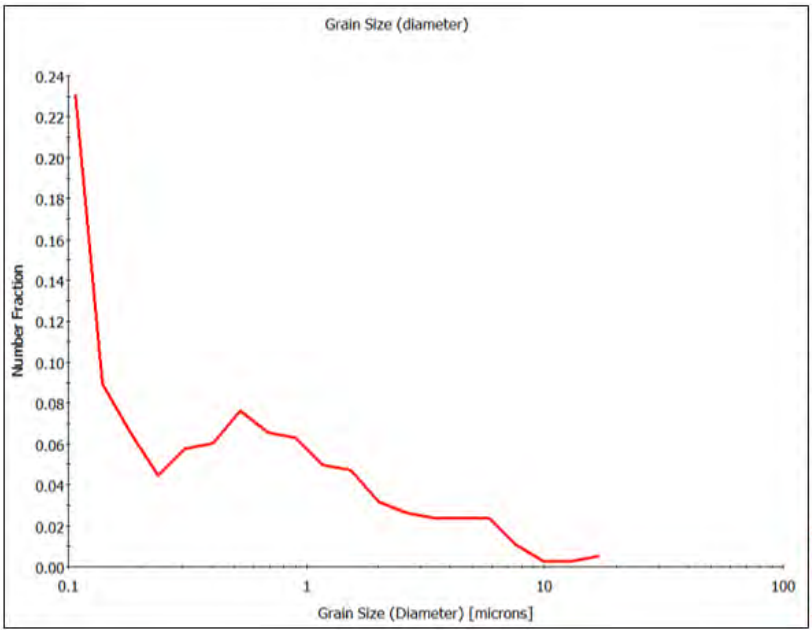

Diameter [microns]	Number Fraction
0.106841	0.230971
0.139478	0.0892388
0.182086	0.0656168
0.23771	0.0446194
0.310326	0.0577428
0.405125	0.0603675
0.528883	0.0761155
0.690446	0.0656168
0.901365	0.0629921
1.17671	0.0498688
1.53618	0.0472441
2.00545	0.0314961
2.61808	0.0262467
3.41785	0.023622
4.46194	0.023622
5.82497	0.023622
7.60439	0.0104987
9.92738	0.00262467
12.96	0.00262467
16.919	0.00524934

Average	
Number	1.05083
Area	9.87388

Figure 31) Number fraction of subgrain size in OIM TSL software + calculation of mean value for specimen 5 (base metal creep-loaded with 80 MPa)

SGS in BM 80 MPa	Number Fraction	Number Fraction NEW	Multiplied	Multiplied NEW
0,106841	0,230971		0,024677173	
0,139478	0,0892388		0,012446849	
0,182086	0,0656168	0,096525106	0,011947901	0,01757587
0,23771	0,0446194	0,065637037	0,010606478	0,01560258
0,310326	0,0577428	0,084942117	0,017919092	0,026359747
0,405152	0,0603675	0,088803162	0,024458013	0,035978779
0,528883	0,0761155	0,111969141	0,040256194	0,059218575
0,690446	0,0656168	0,096525106	0,045304857	0,066645373
0,901365	0,0629921	0,092664061	0,056778874	0,083524141
1,17671	0,0498688	0,073359128	0,058681116	0,086322419
1,53618	0,0472441	0,069498082	0,072575442	0,106761564
2,00545	0,0314961	0,046332104	0,063163854	0,092916718
2,61808	0,0262467	0,038610013	0,06871596	0,101084103
3,41785	0,023622	0,034748968	0,080736453	0,118766759
4,46194	0,023622	0,034748968	0,105399947	0,155047809
5,82497	0,023622	0,034748968	0,137597441	0,202411694
7,60439	0,0104987	0,015444035	0,079836209	0,117442463
9,92738	0,00262467	0,003861001	0,026056096	0,038329627
12,96	0,00262467	0,003861001	0,034015723	0,050038577
16,919	0,00524934	0,007722003	0,088813583	0,130648562
	0,67978998		≈1,06 µm	≈1,50 µm

Table 27) Distribution of subgrain sizes (SGS) in BM creep-loaded with 80 MPa; Multiplication of subgrain sizes times number fractions and calculation of mean grain sizes after adding up

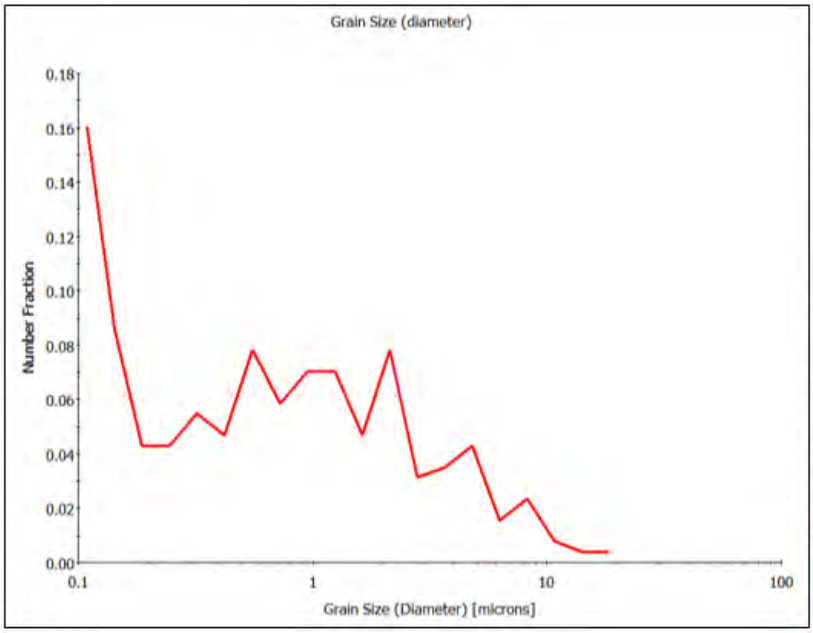

Diameter [microns]	Number Fraction
0.109209	0.160156
0.143096	0.0859375
0.187498	0.0429688
0.245676	0.0429688
0.321907	0.0546875
0.421792	0.046875
0.55267	0.078125
0.724158	0.0585938
0.948857	0.0703125
1.24328	0.0703125
1.62906	0.046875
2.13454	0.078125
2.79686	0.03125
3.6647	0.0351563
4.80183	0.0429688
6.29179	0.015625
8.24407	0.0234375
10.8021	0.0078125
14.1539	0.00390625
18.5457	0.00390625

Average	
Number	1.47385
Area	10.1847

Figure 32) Number fraction of subgrain size in OIM TSL software + calculation of mean value for specimen 3 (base metal creep-loaded with 100 MPa)

SGS in BM 100 MPa	Number Fraction	Number Fraction NEW	Multiplied	Multiplied NEW
0,109209	0,160156		0,017490477	
0,143096	0,0859375		0,012297313	
0,187498	0,0429688	0,056994866	0,008056564	0,010686423
0,245676	0,0429688	0,056994866	0,010556403	0,014002271
0,321907	0,0546875	0,072538836	0,017604289	0,023350759
0,421792	0,046875	0,062176145	0,0197715	0,026225401
0,55267	0,078125	0,103626909	0,043177344	0,057271484
0,724158	0,0585938	0,077720248	0,042431169	0,056281739
0,948857	0,0703125	0,093264218	0,066716508	0,088494406
1,24328	0,0703125	0,093264218	0,087418125	0,115953537
1,62906	0,046875	0,062176145	0,076362188	0,101288671
2,13454	0,078125	0,103626909	0,166760938	0,221195782
2,79686	0,03125	0,041450763	0,087401875	0,115931982
3,6647	0,0351563	0,046632175	0,128837293	0,170892932
4,80183	0,0429688	0,056994866	0,206328873	0,273679658
6,29179	0,015625	0,020725382	0,098309219	0,13039975
8,24407	0,0234375	0,031088073	0,193220391	0,256292247
10,8021	0,0078125	0,010362691	0,084391406	0,111938823
14,1539	0,00390625	0,005181345	0,055288672	0,073336245
18,5457	0,00390625	0,005181345	0,072444141	0,096091678
	0,7539065		≈1,49 µm	≈1,94 µm

Table 28) Distribution of subgrain sizes (SGS) in BM creep-loaded with 100 MPa; Multiplication of subgrain sizes times number fractions and calculation of mean grain sizes after adding up

4.3.2) TEM Results 2016

The following investigations serve to validate the correctness of MatCalc precipitation kinetic outputs from models 1 and 2, in addition to sources from literature.

4.3.2.1) TEM Investigations of Base Metal in As-Received Condition

EFTEM- a special technique of transmission electron microscopy- was used to visualize different locations in the specimen of Gr. 91 base metal in as-received condition (figure 33). The discovered precipitates were classified depending on their chemical composition with the help of EELS (electron energy loss spectroscopy) and EDX (energy despersive X-ray spectroscopy).

As can be seen in figure 34, chromium carbide $M_{23}C_6$ (position 1 and 2) as well as MX particles (position 3) were identified.

The precipitate in position 1 of the EFTEM location revealed 41 at. % of Cr and 43 at. % of C by EELS method (figure 35), which was confirmed by EDX (figure 33). Similar results were found for position 2, whereas position 3 turned out to be MX, having around 29 at. % of V and 34 at. % of N with the rest being matrix (figure 36).

Afterwards, the number of pixels for the diameter of these species of precipitates was measured. The unit of pixels was then converted into nanometers by a factor of 3,835 because each pixel was equal to 3,835 nm.

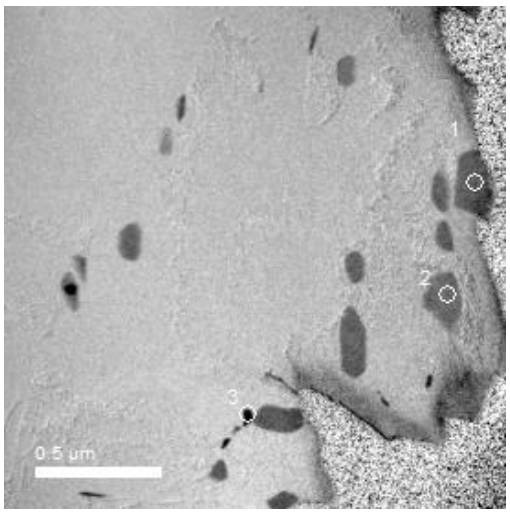

Figure 33) EFTEM analysis of Gr. 91 BM as-received

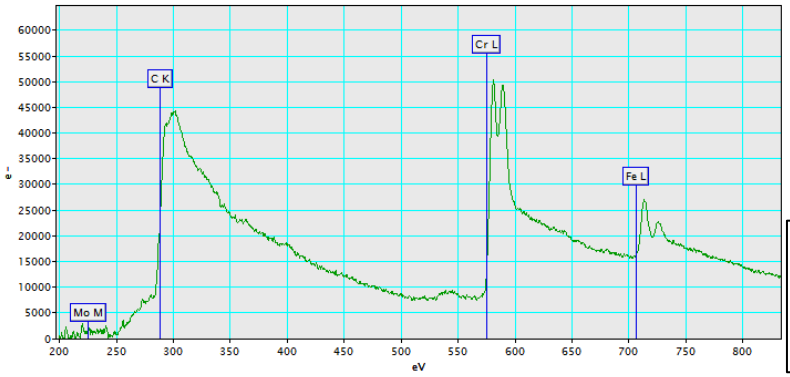

Element	Shell	Signal (e-)	Comp. (at.%)
Mo	M	1333985.5 ± 2122.7	2.0
C	K	3191594.9 ± 1992.4	43.0
Cr	L	4128456.4 ± 2352.5	40.9
Fe	L	983128.7 ± 2129.8	14.2

Figure 34) EELS peaks and analysis of chemical composition in point 1 of figure 34

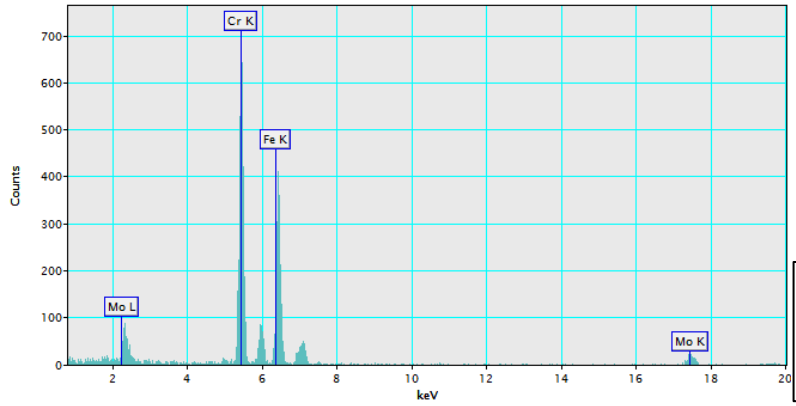

Element	Shell	Signal (Counts)	Comp. (at.%)
Cr	K	4854.4 ± 71.5	57.9
Fe	K	3068.0 ± 56.2	37.1
Mo	K	224.6 ± 14.4	5.0

Figure 35) Counts for EDX spectrum and analysis of chemical comp. of point 2 in figure 34

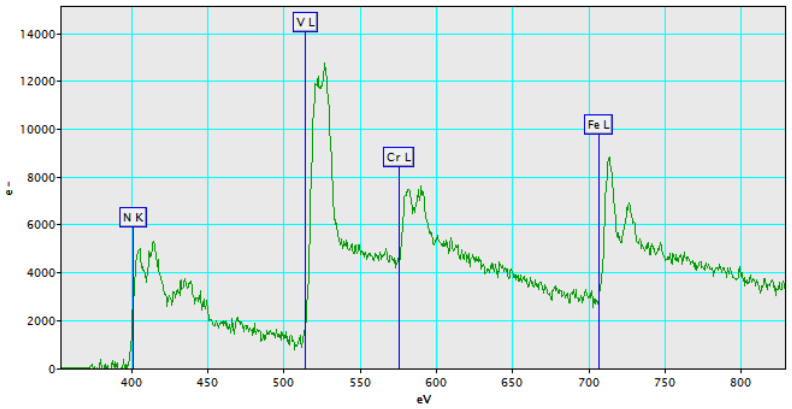

Element	Shell	Signal (e-)	Comp. (at.%)
N	K	475493.1 ± 681.3	34.1
V	L	1475147.0 ± 1353.1	29.3
Cr	L	163021.6 ± 1024.9	5.4
Fe	L	648231.5 ± 1119.1	31.2

Figure 36) EELS peaks and analysis of chemical composition in point 3 of figure 34

As far as the calculation of the mean diameters for $M_{23}C_6$ and MX is concerned, a graphical distribution with 10 size classes (figures 37 and 38) was created with the software Microsoft Excel. The mean value for $M_{23}C_6$ in the investigated specimen is 134 nm, whereas for MX approximately 54 nm were found (table 29 with additional maximum and minimum values).

BM as-received	Mean Diameter	Min. Diameter	Max. Diameter
$M_{23}C_6$	134 nm	24 nm	328 nm
MX	54 nm	10 nm	150 nm

Table 29) Mean values, maxima and minima for diameters of $M_{23}C_6$ and MX from TEM

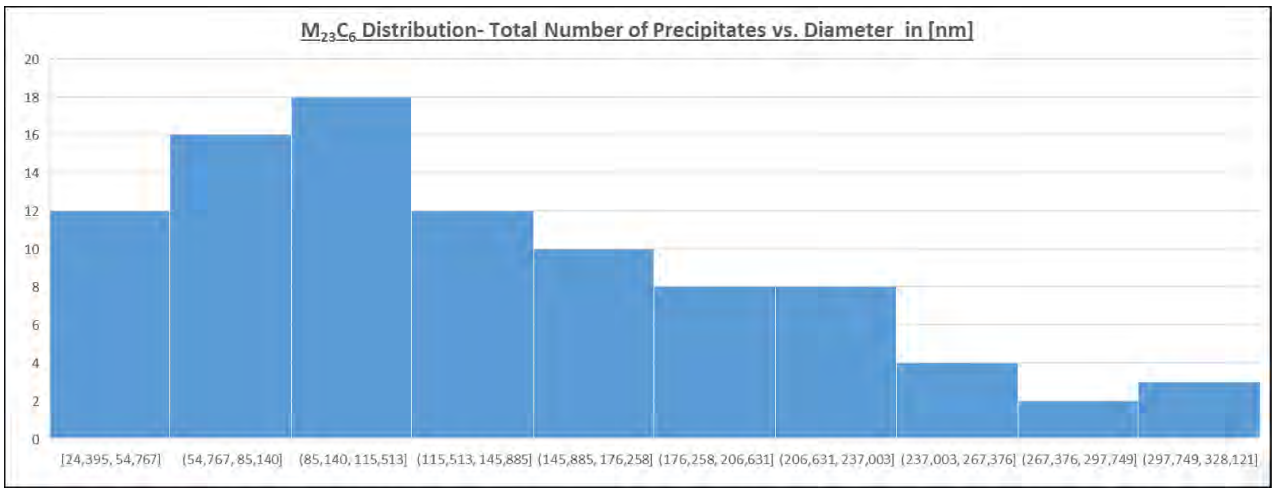

Figure 37) Total number of $M_{23}C_6$ precipitates sorted by size classes for the diameter

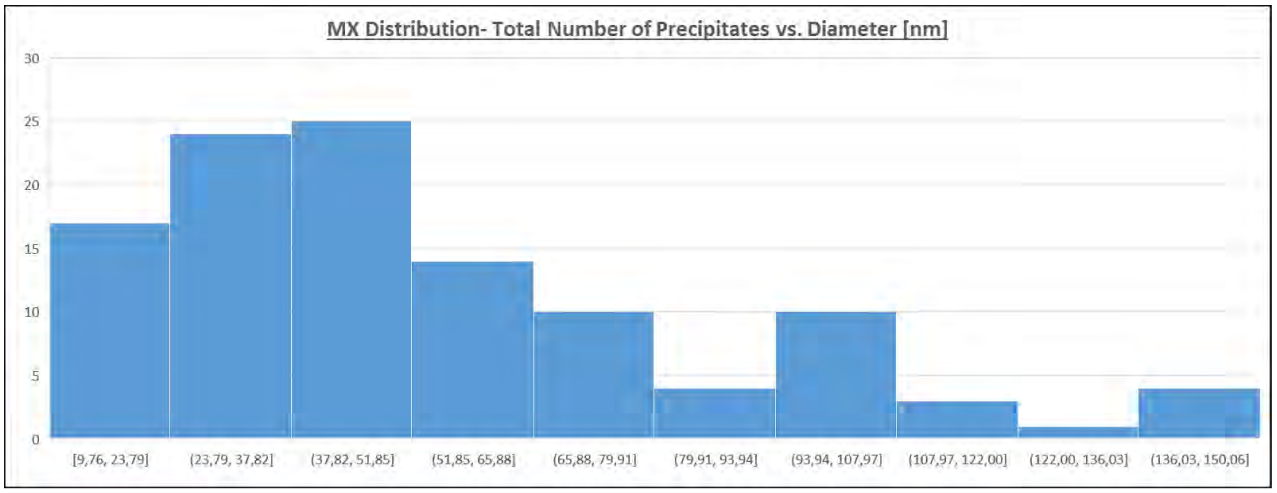

Figure 38) Total number of MX precipitates sorted by size classes for the diameter

The calculation of number density was conducted on the basis of source [63] with equation 41, uniting equations 39 and 40.

The total number of precipitates N_{tot} can be expressed as the number density n_V times the possible volume V containing a particle (equation 39). This volume V can also be defined as the area of the concerning specimen A (in this case 4 µm²) multiplied by the diameter d=2.r of the precipitate. The number of particles per area is then defined as the total number of precipitates per image devided by the area (equation 40). Together with equation 39 the number of precipitates per area n_A simplifies to the diameter d=2.r times the number density n_V.

The number density n_V finally can be gained from equation 41, using the total number of precipitates per image N_{tot} devided by the are of investigation A and the particle diameter d=2.r. From using equation number 42, the phase fraction of the precipitate in the investigated specimen can be obtained by multiplication with the particle volume.

$$N_{tot} = n_V \cdot V = n_V \cdot A \cdot 2r \quad (39)$$

$$n_A = \frac{N_{tot}}{A} = 2r \cdot n_V \quad (40)$$

$$n_V = \frac{n_A}{2r} = \frac{N_{tot}}{2Ar} \quad (41)$$

$$\rho = n_V \cdot \frac{4\pi}{3} \cdot r^3 \quad (42)$$

Inserting a total number of particles per image for $M_{23}C_6$ of 9,3 and using an area of 4µm² with a mean precipitate radius of 67 nm, a number density of $1{,}73.10^{19}$ m^{-3} could be derived and a phase fraction of around 2,193 %.

For MX a total number of precipitates per image of 11,2 and a mean radius of 27 nm led to a number density of $5{,}17.10^{19}$ m^{-3} and a phase fraction of 0,435 %.

Table 30 once more summarizes these results.

AR, BM TEM	Mean Diameter	Number Density	Phase Fraction
$M_{23}C_6$	134 nm	$1{,}73.10^{19}$ m^{-3}	2,193 %
MX	54 nm	$5{,}17.10^{19}$ m^{-3}	0,435 %

Table 30) Mean values, maxima and minima for diameters of $M_{23}C_6$ and MX from TEM

4.3.3) Model 2 Results (BM and FGHAZ)

All the new input values for BM and FGHAZ that were achieved with help of OIM software evaluation were implemented in MatCalc model 2.
This includes a prior austenitic grain size of 76 µm as well as a subgrain size of 0,56 µm for base metal and 0,51 µm for FGHAZ.

Moreover, the temperature in service stage was increased from 600 to 650 °C.
Both measures had the effect that evolution of the Laves phase turned unrealistic: In service section fast coarsening of Laves phase to 1800 nm within only 10 000 hours of creep was observed. To solve this problem, the interface correction temperature for Laves phase was varied in test calculations to a value suitable for both 600 °C and 650 °C service temperature. The new maximum solution temperature decreased from initially 1700 K (model 0 and 1) to 1452 K (model 2).

To validate this value, the maximum dissolution temperature of Laves phase in ferrite (bcc) within a Fe-Mo binary system was calculated (figure 39).
Therefore, the stepped equilibrium tool of MatCalc helped to vary the Fe and Mo content (in weight %), while the composition of all other chemical elements was fixed.
This led to a detected diffuse interface correction temperature of 1477 K for Laves phase, which lies close to the 1452 K (1,7 % away) that were identified as benefitial for Laves evolution during service section in the precipitation kinetic simulation.

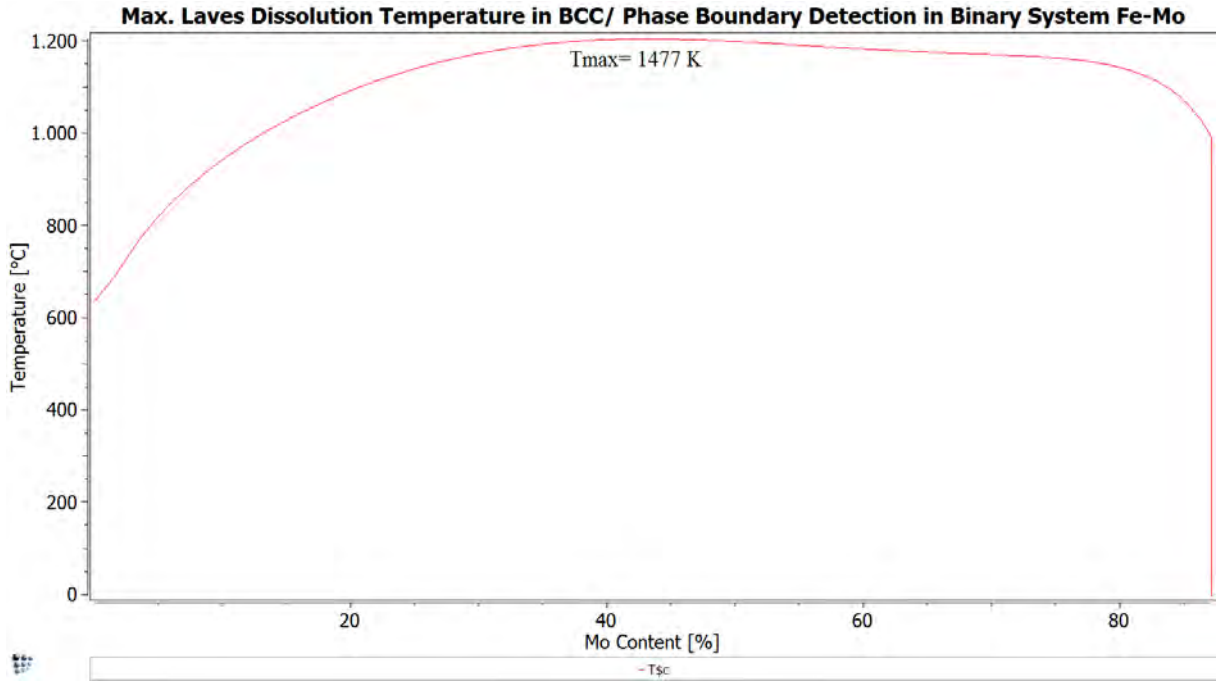

Figure 39) Diffuse interface correction temperature for Laves phase from Fe-Mo binary system

An update of dislocation density to a start value of $4{,}7.10^{13}$ m^{-2} according to new Rietveld refinement data on basis of XRD measurements 2016 at TU Graz (IWS in cooperation with the Institue of Solid State Physics) proved to be too low in the simulation to produce promising results. In the service section of MatCalc precipitation kinetic model, Laves(mart,s) phase and AlN(mart,d) coarsened dramatically after only 1000 hours, using $4{,}7.10^{13}$ m^{-2}.

However, internal MHI measurement results (Rietveld refinement as well) sent to TU Graz in July 2016 revealed a dislocation density in as-received condition of $1{,}9.10^{14}$ m^{-2}, which confirms the assumption of $1{,}5.10^{14}$ m^{-2}.
So in the MatCalc script for model 2 the start value for mobile dislocation density of $1{,}5.10^{14}$ m^{-2} (based on literature source [13]) was maintained, leading to an end value of $3{,}1.10^{13}$ m^{-2}.

The number of precipitation size classes was optimized in the new model, using 100 classes for Laves phase and $M_{23}C_6$, 75 for MX precipitates and 50 for all other precipitates. This had a negative effect on calculation time which became around 34 hours for simulation of base metal, but improved the shape and accuracy of Laves phase and $M_{23}C_6$ results.

The settings for MatCalc model 2 of BM and FGHAZ in Gr. 91 steel are summarized in table 31, referring either to measurements or to literature sources for the chosen parameters. Fixed changes are marked in green, temporary values (namely for the mobile dislocation densities) are coloured in orange.

MatCalc version	5.62	Number of size classes for precipitates	• $M_{23}C_6$: 100 • Laves: 100 • VN, NbC: 75 • All other: 50
Databases used	mc_fe_v2.050.tdb mc_fe_v2.008.ddb	Martensite start temperature	400 °C [g]
Service temperature	650 °C [a]	Martensite to austenite transformation temperature	833 °C [g]
Austenitic grain size BM	76 µm [b]	Equivalent interface energy for modified Z phase	1 [h]
Austenitic grain size FGHAZ	9 µm [b]	Nucleation constant for modified Z phase	1e-12 [i]
Subgrain elongation BM	5 [c]	Matrix diffusion enhancement factor for FGHAZ (mdef)	8
Subgrain elongation FGHAZ	1 [c]	Precipitates under regime of mdef during service section	• $M_{23}C_6$ • Laves • AlN
Subgrain size BM	0,56 µm [b]	Volumetric misfit for AlN	0,27 [j]
Subgrain size FGHAZ	0,51 µm [b]	Setting „nucleate only with valid major constituents“	• NbC • VN
Dislocation density in aust.	1.10^{11} m^{-2} [d]		
Dislocation density in mart. (start value before service)	$1,5.10^{14}$ m^{-2} [e1]		
Dislocation density in mart. (end value after service)	$3,1.10^{13}$ m^{-2} [e2]		
Diffuse interface correction temperature for laves phase	1452 K * [f]		

Table 31) Major settings for MatCalc model 2 of BM in Gr. 91 steel

[a] In accordance with temperature level of MHI creep specimen 2016

[b] TU Graz FELMI EBSD Measurements 2016; Analysis at IWS Institute with TSL OIM Software

[c] TU Graz FELMI EBSD Measurements 2016; Analysis at IWS Institute with TSL OIM Software

[d] Maintained from S. Vujic's MatCalc model 0 (year 2015); I. Holzer uses same value for 9 % Cr steel simulation in MatCalc script 2010; E. Kozeschnik's template also includes it

[e] M. A. El-Azim, O. Ibrahim und O. El-Desoky, „Long term creep behaviour of welded joints of P91 steel at 650 C," Materials Science and Engineering: A, Bd. 560, pp. 678-684, 2013.

[f] Maximum dissolution temperature of Laves phase in a Fe-Mo binary system on basis of MatCalc stepped equilibrium calculation. *See comments in section 5.3.3 and 5.3.3.1

[g] Data from MHI in 2015; Calculation acc. to chemical composition would also be possible

[h] Experimentally found in 2016's MatCalc model 1; maintained for model 2

[i] Estimation by Sonderegger/Danielsen/Kozeschnik, 2005, unpublished

[j] Value from 9 % Cr steel MatCalc template by E. Kozeschnik; included in version 5.62

4.3.3.1) As-received Condition of Base Metal (BM)

The results for as-received condition of base metal (BM) are summarized in figure 40 and in table number 32.

Results of model 2 in as-received condition strongly resemble model 1 with two exceptions: Laves phase nucleated in martensite at subgrain boundaries **Laves(mart,s)** reaches an unnaturally high phase fraction of 0,255 % (formerly 0,003 %) with a size of about 3,4 nm. Moreover, one might take note of smaller mean diameters for martensitic niobium carbide at subgrain boundaries **NbC(mart,s)** with 20,8 nm (formerly 31 nm) and also for martensitic aluminium nitride at dislocations **AlN(mart,d)** with 31,4 nm (formerly 44 nm).

Martensitic vanadium nitride at subgrain boundaries **VN(mart,s)** develops a diameter of 42,6 nm and a phase fraction of 0,416 %.

Martensitic chromium carbide at subgrain boundaries **$M_{23}C_6$(mart,s)** at the end of tempering has a diameter of 102,8 nm with a phase fraction of 2,219 %.

A deviating value for diffuse interface correction temperature of Laves phase represents a possible cause of the imperfection for Laves phase fraction in as-received condition. Nevertheless, 1452 K seems to be a recommendable value, assessing the service stage at 650 °C.

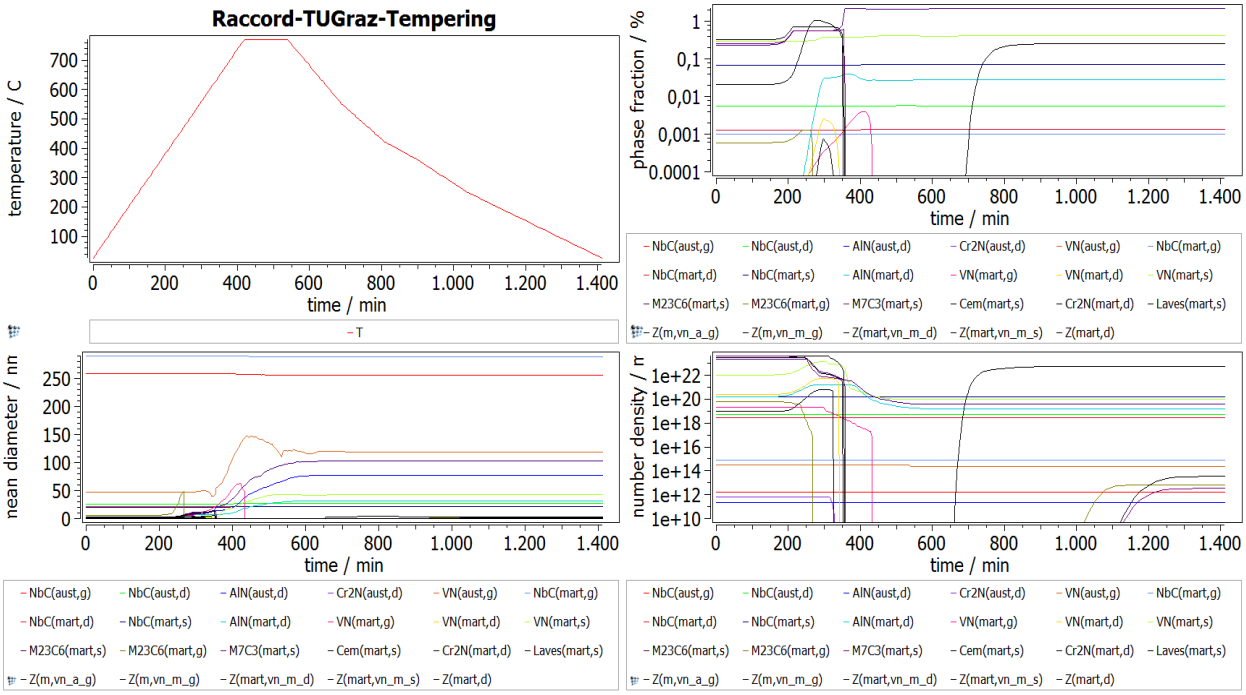

Figure 40) As-received condition BM (model 2); phase fraction, diameter + number density

AR, BM	Phase Fraction	Mean Diameter	Number Density
$M_{23}C_6$(mart,s)	2,219 %	102,8 nm	$3{,}63.10^{19}$ m^{-3}
VN(mart,s)	0,416 %	42,6 nm	$9{,}55.10^{19}$ m^{-3}
Laves(mart,s)	0,255 %	3,4 nm	$5{,}34.10^{22}$ m^{-3}
NbC(mart,s)	0,070 %	20,8 nm	$1{,}46.10^{20}$ m^{-3}
AlN(mart,d)	0,028 %	31,4 nm	$1{,}59.10^{19}$ m^{-3}
NbC(aust,d)	$5{,}61.10^{-3}$ %	26,5 nm	$5{,}55.10^{18}$ m^{-3}
NbC(mart,d)	$1{,}32.10^{-3}$ %	21 nm	$2{,}70.10^{18}$ m^{-3}
NbC(mart,g)	$9{,}91.10^{-4}$ %	288,7 nm	$7{,}70.10^{14}$ m^{-3}
VN(aust,g)	$2{,}28.10^{-5}$ %	119,4 nm	$2{,}21.10^{14}$ m^{-3}
NbC(aust,g)	$1{,}40.10^{-6}$ %	256,2 nm	$1{,}57.10^{12}$ m^{-3}
AlN(aust,d)	$5{,}28.10^{-9}$ %	77 nm	$2{,}21.10^{11}$ m^{-3}
$M_{23}C_6$(mart,g)	$2{,}26.10^{-12}$ %	1,9 nm	$6{,}23.10^{12}$ m^{-3}
Cem(mart,s)	$1{,}17.10^{-12}$ %	0,9 nm	$3{,}34.10^{13}$ m^{-3}
M_7C_3(mart,s)	$1{,}20.10^{-13}$ %	0,9 nm	$3{,}29.10^{12}$ m^{-3}
VN(mart,g)	$4{,}91.10^{-16}$ %	1,2 nm	$4{,}96.10^{9}$ m^{-3}
VN(mart,d)	$6{,}78.10^{-17}$ %	0,7 nm	$3{,}20.10^{9}$ m^{-3}
Cr_2N(mart,d)	$3{,}89.10^{-21}$ %	0,9 nm	$1{,}04.10^{5}$ m^{-3}

Table 32) Model 2 results of as-received condition BM

4.3.3.2) BM creep-loaded for 100 000 hours at 650 °C

The result of BM creep-loaded for 100 000 hours at 650 °C is shown in figure 41. Table 33 goes more into detail for each precipitate.

Martensitic chromium carbide **$M_{23}C_6$(mart,s)** reaches 696 nm after 100 000 hours of creep with a phase fraction of around 2,25 %.

Vanadium nitride at martensitic subgrain boundaries **VN(mart,s)** triples its diameter from 42,6 nm in the beginning of creep to 126,6 nm at the end of service with a phase fraction of 0,382 %.

Laves phase nucleated in martensite at subgrain boundaries **Laves(mart,s)** reduces its phase fraction to about 0,153 % at 650 °C of creep, which is in accordance with the stepped equilibrium calculation in figure 11.
Mean diameter grows to about 392 nm after 100 000 hours.

Niobium carbide at martensitic subgrain boundaries **NbC(mart,s)** develops a phase fraction of 0,041 %, having a mean diameter of 24,4 nm.
Aluminium nitride at martensitic dislocations **AlN(mart,d)** is estimated to coarsen to 211 nm after 100 000 hours, having a phase fraction of 0,033 %.

Niobium carbide at austenitic dislocations **NbC(aust,d)** must not be forgotten with a phase fraction of 0,025 %. A mean diameter of 43,6 nm can be observed after 100 000 hours of service.

For further details of precipitates with a phase fraction lower than 0,01 % that are difficult to detect in microscopes, see table 33.

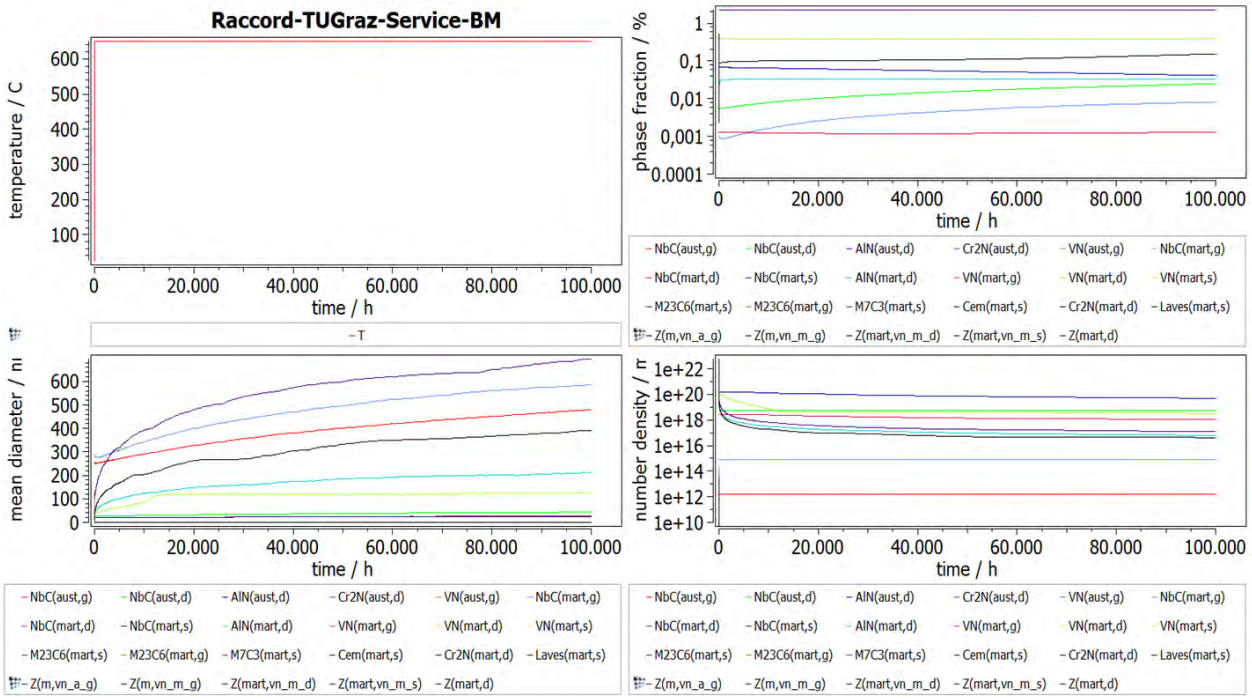

Figure 41) Model 2 results of service BM (100 000 hours at 650 °C)

100 000 h service, 650°C	Phase Fraction	Mean Diameter	Number Density
$M_{23}C_6$(mart,s)	2,249 %	695,9 nm	$1{,}19.10^{17}$ m^{-3}
VN(mart,s)	0,382 %	126,6 nm	$3{,}15.10^{18}$ m^{-3}
Laves(mart,s)	0,153 %	392,4 nm	$4{,}23.10^{16}$ m^{-3}
NbC(mart,s)	0,041 %	24,4 nm	$4{,}94.10^{19}$ m^{-3}
AlN(mart,d)	0,033 %	211,4 nm	$6{,}17.10^{16}$ m^{-3}
NbC(aust,d)	0,025 %	43,6 nm	$5{,}55.10^{18}$ m^{-3}
NbC(mart,g)	$8{,}12.10^{-3}$ %	586,4 nm	$7{,}69.10^{14}$ m^{-3}
NbC(mart,d)	$1{,}28.10^{-3}$ %	27,5 nm	$1{,}09.10^{18}$ m^{-3}
NbC(aust,g)	$9{,}07.10^{-6}$ %	479,4 nm	$1{,}57.10^{12}$ m^{-3}

Table 33) Model 2 results of service BM; 100 000 hours at 650 °C

4.3.3.3) Welded Condition (FGHAZ)

To model the welding process on basis of data from MHI, the grain sizes in precipitation domain austenite were changed after 5 seconds at a temperature level of 950 °C (see figure 42), those for precipitation domain martensite were changed when reaching martensite start temperature during cooling down (at a level of 400 °C).

So before cooling down, prior austenitic grain size was decreased in the precipitation domain austenite from 76 µm to 9 µm in order to transform the base metal into a fine-grain heat affected zone (FGHAZ).
After martensite formation at 400 °C (martensite start temperature), the same was implemented for the precipitation domain of martensite.
Subgrain size was adjusted in both cases from 0,56 µm in BM to 0,51 µm in FGHAZ.

The results after a finished singlepass welding cycle are presented in figure 42.
Table 34 goes more into detail.

According to MatCalc, most precipitates (such as MX and AlN) are not affected by welding. They keep relatively stable and show only a minor change of their size and phase fraction.

Martensitic chromium carbide at subgrain boundaries **$M_{23}C_6$(mart,s)** represents an exception: Its mean diameter falls from 103 nm in as-received condition of the base metal to only 3 nm in welded condition (FGHAZ). Phase fraction reduces from 2,219 % in BM to 1,367 % in FGHAZ.

Martensitic laves phase at subgrain boundaries **Laves(mart,s)** nearly dissolves completely, reaching a phase fraction of 4,42e-5 % (formerly 0,255 % in as-received condition of BM) with a size of less than 1 nm.

The rest of precipitates is presented in table 34.

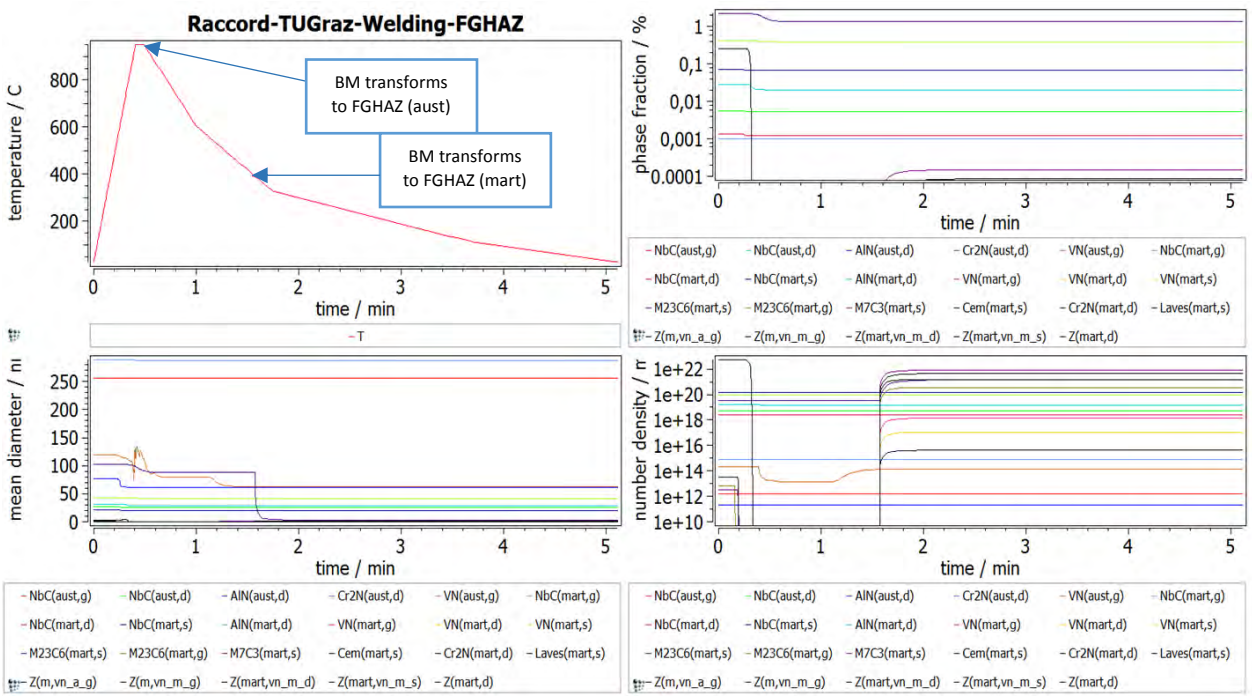

Figure 42) Model 2 results of welded condition (FGHAZ) and points of transformation

Welded, FGHAZ	Phase Fraction	Mean Diameter	Number Density
$M_{23}C_6$(mart,s)	1,367 %	2,8 nm	$1{,}44.10^{21}$ m^{-3}
VN(mart,s)	0,389 %	40,6 nm	$9{,}77.10^{19}$ m^{-3}
NbC(mart,s)	0,067 %	20,5 nm	$1{,}46.10^{20}$ m^{-3}
AlN(mart,d)	0,020 %	28,2 nm	$1{,}53.10^{19}$ m^{-3}
NbC(aust,d)	$5{,}38.10^{-3}$ %	26,2 nm	$5{,}55.10^{18}$ m^{-3}
NbC(mart,d)	$1{,}24.10^{-3}$ %	20,5 nm	$2{,}70.10^{18}$ m^{-3}
NbC(mart,g)	$9{,}82.10^{-4}$ %	287,7 nm	$7{,}70.10^{14}$ m^{-3}
M_7C_3(mart,s)	$1{,}49.10^{-4}$ %	0,7 nm	$8{,}18.10^{21}$ m^{-3}
Cem(mart,s)	$8{,}51.10^{-5}$ %	0,7 nm	$4{,}63.10^{21}$ m^{-3}
$M_{23}C_6$(mart,g)	$6{,}02.10^{-5}$ %	1,4 nm	$3{,}67.10^{20}$ m^{-3}
Laves(mart,s)	$4{,}42.10^{-5}$ %	0,8 nm	$1{,}53.10^{21}$ m^{-3}
VN(aust,g)	$2{,}01.10^{-6}$ %	62,2 nm	$1{,}34.10^{14}$ m^{-3}
NbC(aust,g)	$1{,}39.10^{-6}$ %	255,3 nm	$1{,}57.10^{12}$ m^{-3}
VN(mart,g)	$2{,}74.10^{-8}$ %	0,7 nm	$1{,}47.10^{18}$ m^{-3}
AlN(aust,d)	$2{,}57.10^{-9}$ %	60,6 nm	$2{,}21.10^{11}$ m^{-3}
VN(mart,d)	$2{,}01.10^{-9}$ %	0,7 nm	$1{,}12.10^{17}$ m^{-3}
Cr_2N(mart,d)	$7{,}63.10^{-11}$ %	0,7 nm	$4{,}22.10^{15}$ m^{-3}
Cr_2N(aust,d)	$1{,}81.10^{-20}$ %	0,9 nm	$4{,}31.10^{5}$ m^{-3}

Table 34) Model 2 results of welded condition (FGHAZ)

4.3.3.4) As-received Condition of FGHAZ (after PWHT)

To consider a higher diffusion rate for the FGHAZ than for the base metal, grain sizes were already adjusted before, as it was explained in chapter 9.3 about welding.
Additionally, at the beginning of post-weld heat treatment a matrix diffusion enhancement factor of 8 was introduced for Laves phase, $M_{23}C_6$ and AlN.
The target was to double the FGHAZ diameters of these 3 precipitates during service section compared to the BM results.
The meaning of matrix diffusion enhancement factor will be further explained in chapter 5.3.3.5.

The results for the as-received condition of FGHAZ are depicted in figure 43 and in table 35.

The PWHT section is characterized by growth of the **$M_{23}C_6$(mart,s)** diameter from 3 nm to about 187 nm in the end with a phase fraction of 2,22 %.

Martensitic Laves phase at subgrain boundaries **Laves(mart,s)** returns with a diameter of 6 nm and an unnaturally high phase fraction of around 0,6 %.

Martensitic vanadium nitride at subgrain boundaries **VN(mart,s)** increases its size from around 40 nm after welding to about 43 nm after PWHT, showing a nearly unchanged phase fraction (0,41 %).

Martensitic niobium carbide at subgrain boundaries **NbC(mart,s)** is extremely stable and maintains 21 nm in size and 0,07 % in phase fraction.

Martensitic aluminium nitride at dislocations **AlN(mart,d)** develops a mean diameter of 54 nm after PWHT (28 nm in the beginning) and a phase fraction of 0,032 % (formerly 0,02 %).

All other precipitates with a phase fraction of lower than 0,01 % are not discussed in here, but can be seen in table 35.

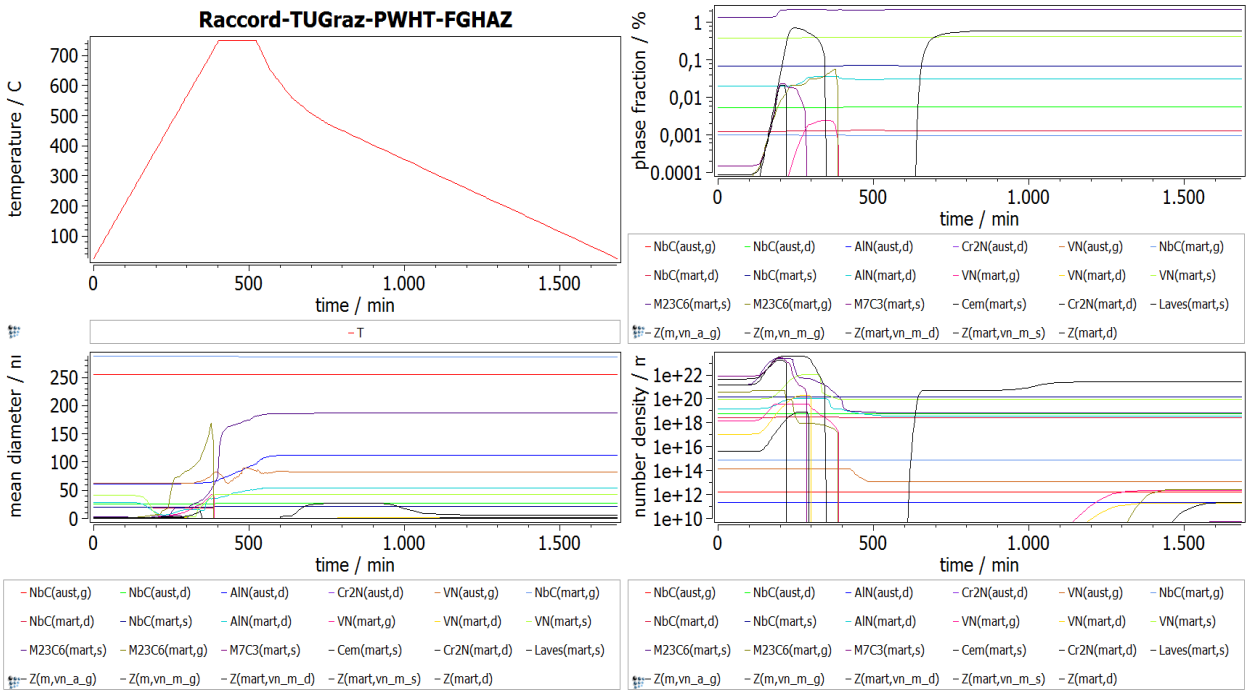

Figure 43) Model 2 results of as-received condition FGHAZ (PWHT)

PWHT, FGHAZ	Phase Fraction	Mean Diameter	Number Density
$M_{23}C_6$(mart,s)	2,223 %	186,6 nm	6,23.10^{18} m^{-3}
Laves(mart,s)	0,598 %	6,1 nm	2,70.10^{21} m^{-3}
VN(mart,s)	0,411 %	42,6 nm	9,36.10^{19} m^{-3}
NbC(mart,s)	0,070 %	20,8 nm	1,46.10^{20} m^{-3}
AlN(mart,d)	0,031 %	54,2 nm	3,50.10^{18} m^{-3}
NbC(aust,d)	5,50.10^{-3} %	26,4 nm	5,55.10^{18} m^{-3}
NbC(mart,d)	1,30.10^{-3} %	20,9 nm	2,70.10^{18} m^{-3}
NbC(mart,g)	9,70.10^{-4} %	286 nm	7,70.10^{14} m^{-3}
NbC(aust,g)	1,38.10^{-6} %	254,7 nm	1,57.10^{12} m^{-3}
VN(aust,g)	4,38.10^{-7} %	81,7 nm	1,12.10^{13} m^{-3}
AlN(aust,d)	1,61.10^{-8} %	111,7 nm	2,21.10^{11} m^{-3}
$M_{23}C_6$(mart,g)	5,32.10^{-13} %	1,6 nm	2,68.10^{12} m^{-3}
VN(mart,g)	2,95.10^{-13} %	1,3 nm	2,35.10^{12} m^{-3}
Cem(mart,s)	7,51.10^{-15} %	0,9 nm	2,15.10^{11} m^{-3}
VN(mart,d)	4,07.10^{-15} %	0,7 nm	1,87.10^{11} m^{-3}
M_7C_3(mart,s)	1,94.10^{-16} %	0,9 nm	5,44.10^{9} m^{-3}
Cr_2N(mart,d)	8,02.10^{-19} %	0,9 nm	2,28.10^{5} m^{-3}

Table 35) Model 2 results of as-received condition FGHAZ (PWHT)

4.3.3.5) FGHAZ creep-loaded for 100 000 hours at 650 °C

Before stating the results for creep-loaded FGHAZ at 650 degrees Celsius, a justification for the introduction of a matrix diffusion enhancement factor in PWHT and service section will be argued.

MatCalc tutorials in theory claim a strong influence of the grain sizes not only on nucleation, but also on the coarsening rate and thus the involved diffusion coefficient. To find out the status of implementation in MatCalc, a test calculation was conducted with the help of Laptop and a reduced number of size classes (50 for Laves and $M_{23}C_6$, 25 for the rest): Starting with the same base material in as-received condition, service section was simulated one time with settings for BM (PAGS=76 µm and SGS=0,56 µm with elongation=5) and one time with FGHAZ parameters (PAGS=9 µm and SGS=0,51 µm with elongation=1).

Unfortunately, it had to be concluded that the acceleration of diffusion processes related to FGHAZ is currently underestimated in MatCalc (see table 36), showing only minor differences when comparing BM and FGHAZ.

Martensitic vanadium nitride at subgrain boundaries **VN(mart,s)** represents the only remarkable precipitate that grows to a larger end diameter in FGHAZ (143 nm) compared to BM (127 nm) after 100 000 hours of service.

Martensitic chromium carbide at subgrain boundaries even develops a smaller diameter in FGHAZ (707,6 nm) than in BM (712,8 nm).

Martensitic Laves phase at subgrain boundaries in the experiment has a nearly identical size (406,5/ 405,4 nm), just as martensitic aluminium nitride at dislocations (212,5/ 211,6 nm) and austenitic niobum carbide at dislocations (both 39,5 nm).

BM 100 000 h service, 650°C	Phase Fraction	Mean Diameter	Number Density	FGHAZ 100 000 h service, 650°C	Phase Fraction	Mean Diameter	Number Density
$M_{23}C_6$(mart,s)	2,25 %	712,8 nm	$1,10.10^{17}$ m^{-3}	$M_{23}C_6$(mart,s)	2,25 %	707,6 nm	$1,13.10^{17}$ m^{-3}
VN(mart,s)	0,381 %	127 nm	$2,72.10^{18}$ m^{-3}	VN(mart,s)	0,381 %	143,2 nm	$2,38.10^{18}$ m^{-3}
Laves(mart,s)	0,162 %	406,5 nm	4.10^{16} m^{-3}	Laves(mart,s)	0,162 %	405,4 nm	4.10^{16} m^{-3}
NbC(mart,d)	0,057 %	30,7 nm	$3,70.10^{19}$ m^{-3}	NbC(mart,d)	0,057 %	30,8 nm	$3,70.10^{19}$ m^{-3}
AlN(mart,d)	0,034 %	212,5 nm	$6,16.10^{16}$ m^{-3}	AlN(mart,d)	0,033 %	211,6 nm	$6,16.10^{16}$ m^{-3}
NbC(aust,d)	0,018 %	39,8 nm	$5,48.10^{18}$ m^{-3}	NbC(aust,d)	0,018 %	39,6 nm	$5,48.10^{18}$ m^{-3}
NbC(aust,g)	$4,96.10^{-6}$ %	392 nm	$1,57.10^{12}$ m^{-3}	NbC(mart,d)	$4,52.10^{-6}$ %	23,2 nm	$1,57.10^{12}$ m^{-3}
NbC(mart,d)	$4,19.10^{-6}$ %	22,2 nm	$6,14.10^{15}$ m^{-3}	NbC(aust,g)	$4,44.10^{-6}$ %	377,8 nm	$6,14.10^{15}$ m^{-3}
NbC(mart,g)	$2,67.10^{-6}$ %	371,6 nm	$9,93.10^{11}$ m^{-3}	NbC(mart,g)	$2,29.10^{-6}$ %	353 nm	$9,93.10^{11}$ m^{-3}

Table 36) BM settings for 100 000 h in as-received condition at 650 °C (left) + FGHAZ settings for 100 000 h in as-received condition at 650 °C (right)= test calculation

As a result, it became obligatory to introduce a matrix diffusion enhancement factor for the FGHAZ, and the aim was to find a reasonable value for doubling the diameters of $M_{23}C_6$, Laves phase and AlN in comparison to BM.

VN and NbC were excluded from this intended acceleration of diffusion, because their size would then be out of range according to literature (see chapter 4.3 for details).

Ostwald ripening had to be defined both for BM (equation 44) and for FGHAZ (equation 43).

The matrix diffusion enhancement factor could then be expressed as the ratio of diffusion constants, so that for doubling a diameter from 700 nm to 1400 nm (for $M_{23}C_6$) a value of 8 is needed (equation 45). This means, the diffusion constant for FGHAZ exceeds 8 times the one for BM to make coarsening to 1400 nm instead of 700 nm possible for chromium carbide.

$$r_{1,FG}^3 - r_{0,FG}^3 = K_{FG}(D_{FG}) \cdot t_{FG} \qquad (43)$$

$$r_{1,BM}^3 - r_{0,BM}^3 = K_{BM}(D_{BM}) \cdot t_{BM} \qquad (44)$$

$$\frac{K_{FG}}{K_{BM}} = \frac{D_{FG}}{D_{BM}} = MDEF = \frac{r_{1,FG}^3 - r_{0,FG}^3}{r_{1,BM}^3 - r_{0,BM}^3} \cdot \frac{t_{BM}}{t_{FG}} = \frac{(700 \cdot 10^{-9})^3 - (50 \cdot 10^{-9})^3}{(350 \cdot 10^{-9})^3 - (50 \cdot 10^{-9})^3} = 8{,}02 \qquad (45)$$

$$\boxed{t_{BM} = t_{FG}}$$

MDEF was finally defined and switched on in model 2 after the end of welding and before the start of PWHT.

The results for service section of FGHAZ after 100 000 hours at 650 °C are presented in figure 44 and more detailed in table 37.

$M_{23}C_6$(mart,s) finally reaches a diameter of 1451 nm under the successful effect of MDEF with a phase fraction of around 2,25 %. Base metal size was less than half of it with 696 nm.

Vanadium nitride at martensitic subgrain boundaries **VN(mart,s)** grows to 126,1 nm (same in BM) at the end of service stage with a phase fraction of 0,381 % (nearly no difference to BM).
Laves phase located at martensitic subgrain boundaries **Laves(mart,s)** develops a phase fraction of 0,188 % in FGHAZ at 650 °C compared to 0,153 % in BM.
Its mean diameter under influence of MDEF coarsens to about 640 nm after 100 000 hours (in BM about 392 nm).

Niobium carbide at martensitic subgrain boundaries **NbC(mart,s)** shows a phase fraction of 0,044 %, having a mean diameter of 25 nm without modification through MDEF (nearly the same in BM with 24,4 nm).

Aluminium nitride at martensitic dislocations **AlN(mart,d)**, whose diffusion is accelerated by MDEF, is estimated to reach 421 nm in FGHAZ (compared to 211 nm in BM), having an unchanged phase fraction of 0,034 %.

Niobium carbide at austenitic dislocations **NbC(aust,d)** has a phase fration of 0,023 % in FGHAZ with a mean diameter of 42,6 nm (43,6 nm in base metal).

Seldom precipitates with a phase fraction lower than 0,01 % will not be discussed here, but can be seen in table 37. They are marked in yellow. Green colour indicates the fact that a precipitate was influenced by matrix diffusion enhancement factor of 8.

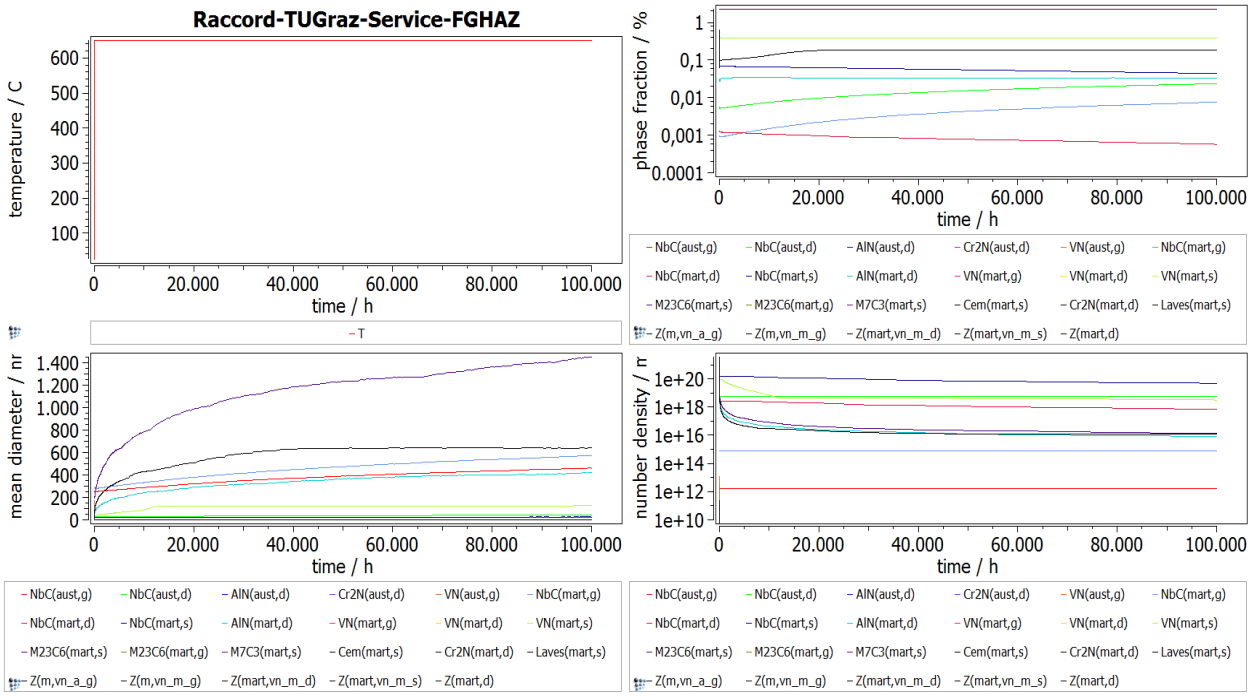

Figure 44) Model 2 results of service FGHAZ (100 000 hours at 650 °C)

FGHAZ 100 000 h service, 650°C	Phase Fraction	Mean Diameter	Number Density
$M_{23}C_6$(mart,s)	2,249 %	1451,3 nm	1,31e16 m^{-3}
VN(mart,s)	0,381 %	126,1 nm	3,17e18 m^{-3}
Laves(mart,s)	0,188 %	640,1 nm	1,18e16 m^{-3}
NbC(mart,s)	0,044 %	25 nm	4,85e19 m^{-3}
AlN(mart,d)	0,034 %	420,7 nm	7,97e15 m^{-3}
NbC(aust,d)	0,023 %	42,6 nm	5,55e18 m^{-3}
NbC(mart,g)	$7{,}62.10^{-3}$ %	574 nm	7,69e14 m^{-3}
NbC(mart,d)	$5{,}69.10^{-4}$ %	23,5 nm	7,36e17 m^{-3}
NbC(aust,g)	$8{,}05.10^{-6}$ %	460,7 nm	1,57e12 m^{-3}

BM 100 000 h service, 650°C	Phase Fraction	Mean Diameter	Number Density
$M_{23}C_6$(mart,s)	2,249 %	695,9 nm	1,19e17 m^{-3}
VN(mart,s)	0,382 %	126,6 nm	3,15e18 m^{-3}
Laves(mart,s)	0,153 %	392,4 nm	4,23e16 m^{-3}
NbC(mart,s)	0,041 %	24,4 nm	4,94e19 m^{-3}
AlN(mart,d)	0,033 %	211,4 nm	6,17e16 m^{-3}
NbC(aust,d)	0,025 %	43,6 nm	5,55e18 m^{-3}
NbC(mart,g)	$8{,}12.10^{-3}$ %	586,4 nm	7,69e14 m^{-3}
NbC(mart,d)	$1{,}28.10^{-3}$ %	27,5 nm	1,09e18 m^{-3}
NbC(aust,g)	$9{,}07.10^{-6}$ %	479,4 nm	1,57e12 m^{-3}

Table 37) Model 2 results of service FGHAZ (left) and BM (right); 100 000 hours at 650 °C

4.3.4) Backstress Calculation on Basis of Model 2 (BM + FGHAZ)

It was decided to calculate room temperature backstress as well as high temperature backstress for both BM and FGHAZ after 10 hours and after 14 379 hours of creep at 650 °C, using MatCalc results from model 2 simulation combined with literature data from [13].

4.3.4.1) Mobile Dislocation Strengthening

Abe [45] provides equation 46 for **strengthening due to mobile dislocations** (see also equation 17 in chapter 3.5.1 of the literature study) that contains a constant α for dislocation interaction with precipitates, shear modulus G, Burger's vector b and the square root of mobile dislocation density ρ_m.

$$\sigma_{\rho_m} = \alpha \cdot M \cdot G \cdot b \cdot \sqrt{\rho_m} \qquad (46)$$

In here the dislocation interaction for room temperature conditions was chosen according to Abe with [45] α=0,5. To reflect temperature influence, the suggestion of Basirat for 600 °C to 700 °C of service [46] was followed by applying factor α=0,02. MatCalc calculated a Young's modulus at 650 °C of E=161 250 MPa, which is similar to literature values for P92 at 650 °C [64]. With an assumed Poisson's ratio of ϑ=0,3 shear modulus G was calculated (equation 45), leading to around 62 019 MPa.

$$G = \frac{E}{2 \cdot (1 + \vartheta)} \qquad (47)$$

When inserting Abe's dislocation interaction value of α=0,5, a Taylor factor of M=3, a shear modulus of G=62 019 MPa, a Burger's vector of $2{,}866.10^{-10}$ m and a start dislocation density of $1{,}5.10^{14}$ m^{-2}, this leads to a start backstress for BM/ FGHAZ in the service section of 326,1 MPa originating from mobile dislocations.

After 14 379 hours of creep in BM/ FGHAZ, mobile dislocation density reaches a value of around $7{,}76.10^{13}$ m^{-2} and the room temperature backstress consequently is reduced to around 234,9 MPa.

When using Basirat's dislocation interaction value of α=0,02 from [46] to reflect conditions at elevated temperatures (between 600 and 700 °C) [46], this instead leads to a start backstress of only 13 MPa and the predicted value after 14 379 hours of service would reduce to app. 9,4 MPa.

Mobile Dislocation Strengthening P91@ 650 °C	BM/ FGHAZ 10 h	BM/ FGHAZ 14 379 h
Room Temperature (Abe)	326,1 MPa	234,9 MPa
High Temperature (Basirat)	13,0 MPa	9,4 MPa

Table 38) Backstress originating from mobile dislocations for 10 h+ 14 379 h of creep at 650 °C

4.3.4.2) Subgrain Strengthening at Room Temperature

Subgrain strengthening provided by [48] and [45] is expressed by equation 48 (see also equation 19 in chapter 3.5.2 of literature study), including shear modulus G, Burger's vector as well as subgrain width λ_{sg}.

$$\sigma_{sg} = \frac{10 \cdot G \cdot b}{\lambda_{sg}} \qquad (48)$$

It is regarded to be highly significant in P91 (at least in room temperature condition). Using the same values for G and b as in chapter 5.3.4.1 and a subgrain size of 0,56 µm after 10 hours of creep, a start backstress for BM in service section of around 317,4 MPa originating from subgrains can be obtained.

After 14 379 hours of service, the subgrain size in BM is assumed to coarsen to 2,5 µm, taking into account the measurement results of specimen 3 (2 µm after 306 h with 100 MPa load) and specimen 5 (1,5 µm after 2283 h with 80 MPa load) for 650 °C of creep (see chapter 5.3.1.5). This causes an estimated drop of the BM backstress after 14 379 hours to about 71,1 MPa.

Subgrain size in FGHAZ before the start creep was analyzed by IWS to be 0,51 µm. This leads to a higher subgrain strengthening effect after 10 hours of service for FGHAZ of around 348,5 MPa.

As already mentioned in the literature part, measurements by [13] showed a faster coarsening of subgrains in the FGHAZ after 14 379 hours (1,23 µm size/ diameter) compared to BM (0,597 µm). When applying this factor 2 to the assumed BM subgrain size of 2,5 µm, subgrain size in FGHAZ after 14 379 hours would become 5 µm. This value is used for the calculation of FGHAZ backstress.

As a result, after 14 379 hours of service, backstress for FGHAZ originating from subgrains turned out to be only 35,5 MPa and almost half of the BM value.

These results can be interpreted as "*athermal yield stress*" according to [48].

4.3.4.3) Immobile Dislocation Strengthening/ Subgrain Strengthening at High Temperature

Using the same formula as in chapter 5.3.4.1, Magnusson and Sandström for P91 advise to consider immobile dislocations for high temperatures [49], being denoted as boundary dislocations in this thesis (eq. 49 or eq. 20 in chapter 3.5.3 of the literature study). It is important to note that for 650 °C, the original subgrain strengthening model for room temperature (see chapter 5.3.4.2) was replaced in the thesis by a concept of immobile/ boundary dislocation strengthening.

$$\sigma_{\rho_{im}} = \alpha \cdot M \cdot G \cdot b \cdot \sqrt{\rho_{im}} \qquad (49)$$

$\alpha \cdot M$ in their approach is unity (=1). However, the authors suggest to separately calculate immobile dislocation strengthening for subgrain interiors and subgrain walls and use weighting

factors similar to composite materials. In this way it is possible to distinguish softer regions from harder areas in the microstructure, containing different immobile dislocation densities.

However, since therefor no literature data or measurement results were available, it was decided to homogenously calculate strengthening due to immobile dislocations that were detected in EBSD. Boundary dislocation density in as-received condition of BM was $4{,}58.10^{14}$ m^{-2}, in as-received condition of FGHAZ it turned out to be slightly higher with $5{,}48.10^{14}$.

The number of dislocations is indirectly proportional to the length of subgrain boundaries under the precondition of constant misorientation angles (which is usually the case). This concept enabled the calculation of boundary dislocation densities after 14 379 hours on basis of subgrain sizes from literature source [13] and boundary dislocation densities in as-received condition from IWS EBSD measurements (see equation 50). The inserted subgrain sizes were 0,458 µm for BM as-received and 0,597 µm for BM after 14 379 hours [13]. For FGHAZ in as-received condition 0,718 µm was used, and the subgrain size after 14 379 hours of service was 1,23 µm [13].

$$\frac{\lambda_{sg\_14379h}}{\lambda_{sg\_0h}} = \frac{\rho_{im\_0h}}{\rho_{im\_14379h}} \qquad (50)$$

In this way, immobile (or boundary) dislocation densities after 14 379 hours of creep at 650 °C for BM of $3{,}51.10^{14}$ m^{-2} and for FGHAZ of $3{,}19.10^{14}$ m^{-2} were derived.

Because the target lay in the calculation of high temperature backstress, the provided dislocation interaction factor of α=0,33 for immobile dislocation strengthening had to be critically questioned. Although it is basically unknown and not discussed anywhere in literature, if dislocation interaction factors α for mobile and boundary dislocations differ from each other, Basirat's high temperature factor (suitable for 650 °C of service) was regarded more reasonable also for immobile dislocation densities to avoid a possible overestimation of the inner stress.

So α=0,02 was inserted in equation 50 together with a Taylor factor M=3 and the already indicated values of shear modulus G=62019 MPa and Burger's vector b=$2{,}866.10^{-10}$ m.

This led to the following results (table 39):

Immobile Dislocation Strengthening P91@ 650 °C	BM 10 h	BM 14 379 h	FGHAZ 10 h	FGHAZ 14 379 h
High Temperature (Sandström + Basirat)	22,8 MPa	20,0 MPa	25,0 MPa	19,0 MPa

Table 39) Backstress due to immobile dislocations for 10 h + 14 379 h of creep at 650 °C

4.3.4.4) Grain Boundary Strengthening

Grain boundary strengthening plays a minor role in case of P91 because of the large prior austenitic grain sizes and their low phase fraction in contrast to subgrain boundaries [8]. Thus it is not considered.

4.3.4.5) Precipitate Dislocation Interaction

4.3.4.5.1) Orowan Mechanism

For Orowan stress, a new formulation was found by Ahmadi et al. [51], which can be automatically calculated in MatCalc version 5.62.

$$\tau_{Or} = \frac{J \cdot G \cdot b}{2 \cdot \pi \cdot \lambda \cdot (1 - \vartheta)} \cdot ln\left(\frac{2r_s}{r_i}\right) \qquad (51)$$

As can be seen in equation 51 (equal to equation 22 in chapter 3.5.5.1 of the literature study), apart from shear modulus G and Burger's vector b, a particle arrangement factor J (lying between 0,8 and 1) and Poisson's ratio ϑ of the matrix are contained. Whereas r_s stands for the equivalent particle radius, r_i represents the inner cut-off distance of dislocations [15] [51].

λ is the so-called critical particle distance, marking a theoretical threshold for the start of plastic deformation [52]. Equation 52 from reference [52] offers a method to realistically evaluate a two dimensional interparticle distance in the glide plane of the dislocation (from surface to surface) with the help of mean particle radius r and number density N_V from MatCalc results.

$$\lambda_{2D-SS} = \sqrt{\frac{\ln 3}{2 \cdot \pi \cdot N_v \cdot r} + 2.67 \cdot r^2} - 1.63 \cdot r \qquad (52)$$

A MatCalc diagram with the evolution of Ashby-Orowan shear stress over time during creep of FGHAZ at 650 °C (based on model 2) is shown in figure 43.

Only the precipitates located at dislocations- except for vanadium nitrid which occurs at subgrain boundaries according to simulation- were included in the automatic calculation. $M_{23}C_6$ nucleates at subgrain boundaries and was therefore not considered for the backstress calculation.

Table 40 summarizes the FGHAZ shear stress results from service stage for the invidual precipitates from figure 45 and transforms τ into σ with the help of Tayler factor M=3. This gives a total value for the precipitate backstress in FGHAZ of 396,6 MPa after 10 hours and 204,3 MPa after 14 379 hours of creep.

The same is done with the results for Ashby-Orowan shear stress of BM during creep (see figure 46 and table 41). Precipitate backstress in both cases is higher than for FGHAZ with a value of 422,7 MPa in the start of creep and 215,1 MPa after 14 379 hours of service.

Obviously, the results for the backstress originating from precipitates seem to represent a room temperature value instead of reflecting the real conditions for elevated temperature of 650 °C.

This leads to the situation that the internal stress, which should impede dislocation movement, exceeds the applied external stress (between 45 MPa and 100 MPa in the experiments), even though the important impact of $M_{23}C_6$ was neglected.

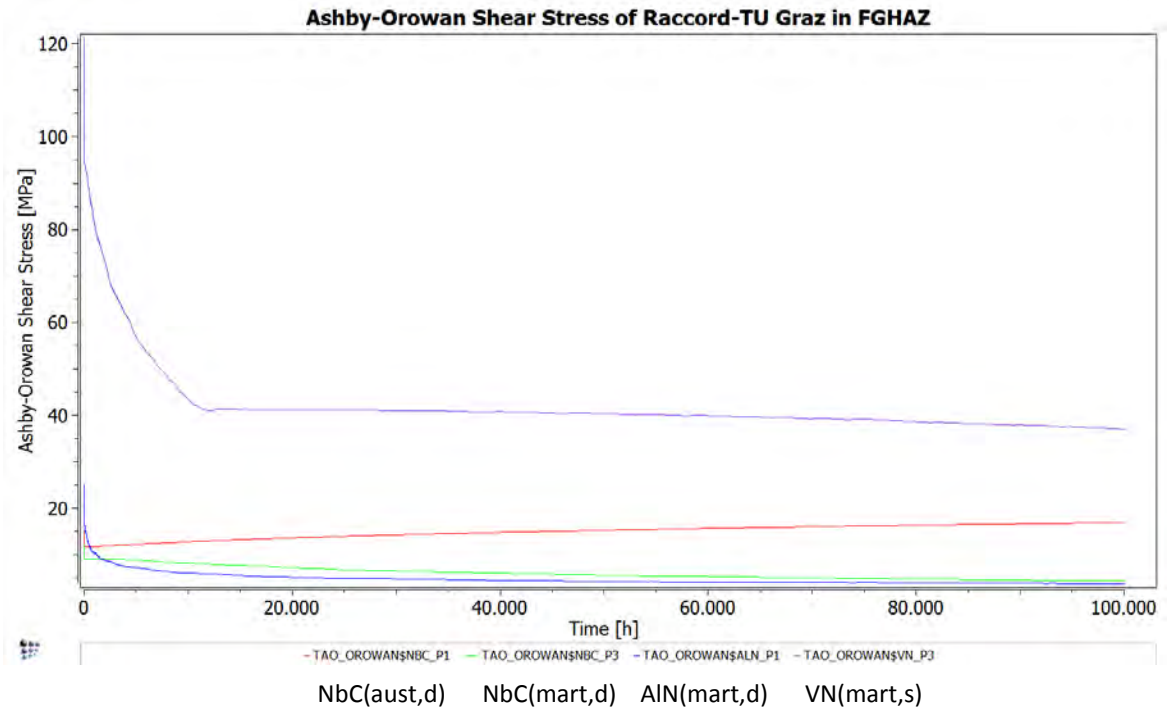

Figure 45) Ashby-Orowan shear stress over time for Gr. 91 FGHAZ during creep at 650 °C

Orowan Stress Service FGHAZ	τ (10 h)	τ (14379 h)	σ (10 h)	σ (14379 h)
NbC(aust,d)	11,5 MPa	13,3 MPa	34,5 MPa	39,9 MPa
NbC(mart,d)	9,0 MPa	7,7 MPa	27,0 MPa	23,1 MPa
AlN(mart,d)	17,3 MPa	5,7 MPa	51,9 MPa	17,1 MPa
VN(mart,s)	94,4 MPa	41,4 MPa	283,2 MPa	124,2 MPa
Sum			396,6 MPa	204,3 MPa

Table 40) Orowan stress for Gr. 91 FGHAZ during creep after 10 h and 14 379 h at 650 °C

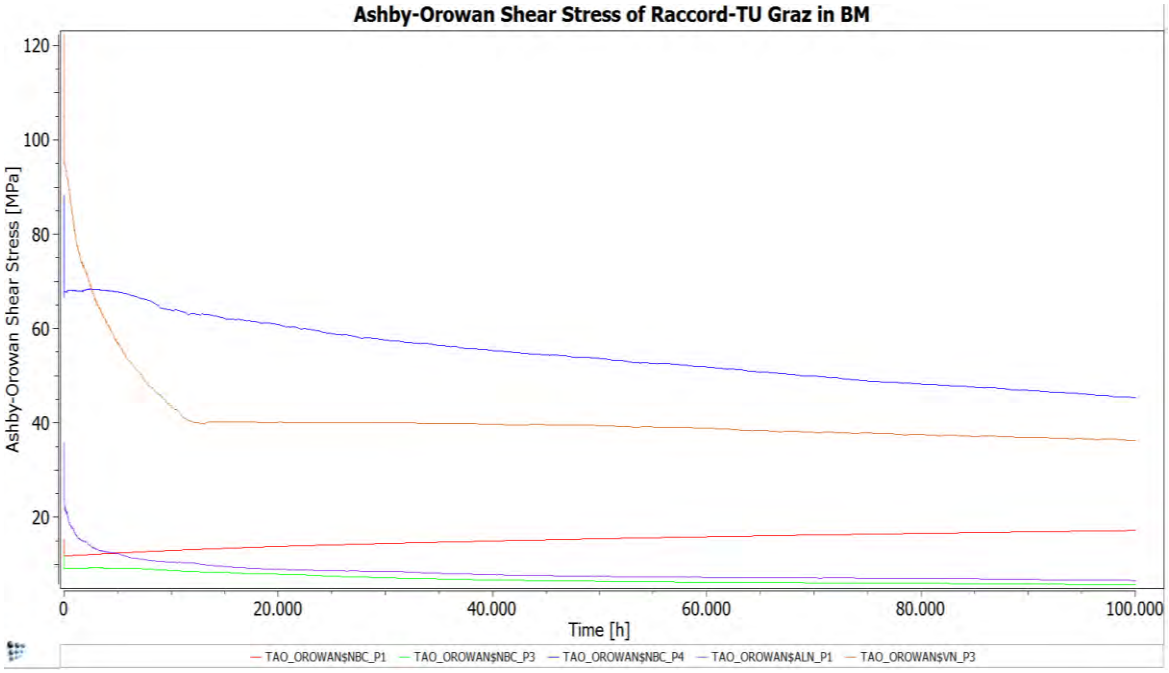

Figure 46) Ashby-Orowan shear stress over time for Gr. 91 BM during creep at 650 °C

Orowan Stress Service BM	τ (10 h)	τ (14379 h)	σ (10 h)	σ (14379 h)
NbC(aust,d)	11,8 MPa	13,4 MPa	35,4 MPa	40,2 MPa
NbC(mart,d)	9,2 MPa	8,4 MPa	27,6 MPa	25,2 MPa
AlN(mart,d)	24,6 MPa	9,7 MPa	73,8 MPa	29,1 MPa
VN(mart,s)	95,3 MPa	40,2 MPa	285,9 MPa	120,6 MPa
Sum			422,7 MPa	215,1 MPa

Table 41) Orowan stress for Gr. 91 BM during creep after 10 h and 14 379 h at 650 °C

4.3.4.4.2) Effect of Dislocation Climb

The main contributors to precipitation backstress according to Magnusson and Sandström [53] are MX and $M_{23}C_6$ particles.

They suggest a Pythagorean addition (equation 53 or equation 24 in chapter 3.5.5.2) for the interparticle distances of MX and $M_{23}C_6$ on basis of Martin [54] to calculate a total value λ_{tot}:

$$\frac{1}{\lambda_{tot}^{\ 2}} = \frac{1}{\lambda_{MX}^{\ 2}} + \frac{1}{\lambda_{M23C6}^{\ 2}} \qquad (53)$$

Finally, the authors provide a slightly different Orowan equation (number 54 or number 25 in the literature study part) for particle hardening, containing dislocation line tension T_L, Taylor factor m=3, Burger's vector b and the interparticle distance λ_{tot} from above.

$$\sigma_{part} = \frac{2T_L m}{b\lambda_{tot}} \quad (54)$$

On basis of equation 53/24 and the results for model 2 shown in table 34, the two-dimensional interparticle distances for MX and $M_{23}C_6$ were calculated both for BM and FGHAZ after 10 hours and after 14 379 hours of service at 650 °C (see table 42).

	Radius [nm]	Number Density [m^{-3}]	λ_{MX} [m]	λ_{M23C6} [m]	λ_{tot} [m]
10 hours; FGHAZ	MX: 15 $M_{23}C_6$: 94	MX: $8{,}17.10^{19}$ $M_{23}C_6$: $6{,}23.10^{18}$	$3{,}5407.10^{-7}$	$4{,}1437.10^{-7}$	$2{,}6918.10^{-7}$
14 379 hours; FGHAZ	MX: 28,4 $M_{23}C_6$: 446,4	MX: $4{,}39.10^{19}$ $M_{23}C_6$: $5{,}51.10^{16}$	$3{,}3106.10^{-7}$	$2{,}0366.10^{-6}$	$3{,}3106.10^{-7}$
10 hours; BM	MX: 14,9 $M_{23}C_6$: 51,9	MX: $8{,}24.10^{19}$ $M_{23}C_6$: $3{,}57.10^{19}$	$3{,}5387.10^{-7}$	$2{,}3409.10^{-7}$	$1{,}9524.10^{-7}$
14 379 hours; BM	MX: 28,6 $M_{23}C_6$: 217,8	MX: $4{,}39.10^{19}$ $M_{23}C_6$: $4{,}78.10^{17}$	$3{,}2948.10^{-7}$	$9{,}8892.10^{-7}$	$3{,}1258.10^{-7}$

Table 42) Interparticle distances for MX, M23C6 and total value after 10 h and 14 379 h for BM and FGHAZ @ 650 °C

Dislocation line tension T_L could be derived from the simplified equation 55 (reference [55]), which is equal to equation 26 in the literature study part:

$$T_L = \frac{Gb^2}{2} \quad (55)$$

G stands for shear modulus (app. 62 GPa for 650 °C) and b for Burger's vector (2,866e-10 m).

This dislocation line tension is particle-size independent and therefore assumes to be constant during creep. Calculation with the G and b values from above led to around $2{,}5463.10^{-9}$ N.

Hull and Bacon [55] indicate an alternative method for estimating the dislocation line tension. This more complex equation 56 (equal to equation 27 in chapter 3.5.5.2) for a changing dislocation line tension depending on evolving radii r of precipitates reads:

$$T_L = \frac{Gb^2}{4\pi K} \cdot ln\left[\frac{2\sqrt{\frac{2}{3}}r}{(1..4)b}\right] \quad (56)$$

The fraction inside the logarithm is the modified ratio of outer and inner cut-off radius.
K is a factor between 0,7 and 1. In this case 0,85 was used to consider both edge and screw dislocations.

To receive the lower bound for dislocation line tension, Burger's vector b was multiplied by 4.
First the dislocation line tensions for MX and for $M_{23}C_6$ were evaluated, then the mean value was calculated (see table 43).
Again, both BM and FGHAZ after 10 and after 14 379 hours of creep were analyzed.

	Radius [nm]	T_{L_MX} [N]	T_{L_M23C6} [N]	T_{L_tot} [N] = $(T_{L\_MX} + T_{L\_M23C6})/2$
10 hours; FGHAZ	MX: 15 $M_{23}C_6$: 94	$1{,}4547.10^{-9}$	$2{,}3260.10^{-9}$	$1{,}8904.10^{-9}$
14 379 hours; FGHAZ	MX: 28,4 $M_{23}C_6$: 446,4	$1{,}7578.10^{-9}$	$3{,}0657.10^{-9}$	$2{,}4118.10^{-9}$
10 hours; BM	MX: 14,9 $M_{23}C_6$: 51,9	$1{,}4515.10^{-9}$	$2{,}0440.10^{-9}$	$1{,}7478.10^{-9}$
14 379 hours; BM	MX: 28,6 $M_{23}C_6$: 217,8	$1{,}7611.10^{-9}$	$2{,}7250.10^{-9}$	$2{,}2431.10^{-9}$

Table 43) Dislocation line tension for MX, $M_{23}C_6$ and mean value after 10 h and 14379 h for BM and FGHAZ @ 650 °C

Finally, on basis of equation 54 the particle hardening/ precipitation strengthening backstress for BM and FGHAZ after 10 hours and 14 379 hours could be estimated as illustrated in table 44.

Additionally, the difference between obtaining dislocation line tension from equation 55 (result σ_{part2}) and from equation 56 (result σ_{part1}) is demonstrated and how this influences the backstress estimation.

	T_{L_tot} [N]	λ_{tot} [m]	σ_{part1} [MPa]	T_L [N]	λ_{tot} [m]	σ_{part2} [MPa]
10 hours; FGHAZ	$1{,}8904.10^{-9}$	$2{,}6918.10^{-7}$	147,0	$2{,}5463.10^{-9}$	$2{,}6918.10^{-7}$	198,0
14 379 hours; FGHAZ	$2{,}4118.10^{-9}$	$3{,}3106.10^{-7}$	152,5		$3{,}3106.10^{-7}$	161,0
10 hours; BM	$1{,}7478.10^{-9}$	$1{,}9524.10^{-7}$	187,4	$2{,}5463.10^{-9}$	$1{,}9524.10^{-7}$	273,
14 379 hours; BM	$2{,}2431.10^{-9}$	$3{,}1258.10^{-7}$	150,2		$3{,}1258.10^{-7}$	170,5

Table 44) Particle hardening/ precipitation strengthening calculation comparing 2 different versions of dislocation line tension

For BM after 10 hours of creep the particle hardening result was between 187,4 MPa and 273 MPa. After 14 379 hours of service, precipitate backstress for BM declined to 150,2 MPa or 170,5 MPa, depending on the method of calculating the dislocation line tension.

FGHAZ in the beginning of creep showed a backstress of between 147 MPa and 198 MPa. After 14 379 hours of service in FGHAZ this values changed to 152,5 MPa and 161 MPa. Consequently, the lower bound increased slightly, whereas the upper limit decreased significantly.

4.3.4.6) Total Backstress (Room Temperature)

Applying equation 15, the total backstress can be calculated by linear add up to achieve a so-called "athermal yield strength" [48], which leads to a final value of 1071,2 MPa after 10 hours and 474,7 MPa after 14 379 hours of creep for FGHAZ of Gr. 91 steel at 650 °C (see table 45).

Interestingly, the subgrain boundary strengthening value after 10 hours of creep for BM exceeds the one for FGHAZ due to the slightly bigger subgrain size of BM (0,56 µm) detected in FELMI/ IWS measurements compared to the FGHAZ subgrain size (namely 0,51 µm). Nevertheless, after 14 379 hours the subgrain size was assumed to coarsen faster in FGHAZ, as it is reported in literature by El-Azim and others [13].

For BM after 10 hours of creep 1066,2 MPa were achieved as well as 521,1 MPa after 14 379 hours of service (see table 45).

Method 1	Equ. Ref.	BM 10 h	BM 14379 h	FGHAZ 10 h	FGHAZ 14379 h
σ_{ρ_m}	[46]*	326,1 MPa	234,9 MPa	326,1 MPa	234,9 MPa
σ_{Or}	[51]	422,7 MPa	215,1 MPa	396,6 MPa	204,3 MPa
σ_{sgb}	[48] [45]	317,4 MPa	71,1 MPa	348,5 MPa	35,5 MPa
σ_i	*α=0,5	1066,2 MPa	521,1 MPa	1071,2 MPa	474,7 MPa

Table 45) Total "athermal" backstress of Gr. 91 in BM and FGHAZ after 10 hours and 14379 hours of service at 650 °C

4.3.4.7) Total Backstress (Service Conditions)

Following the recommendations of [65] and [49], particle hardening as well as dislocation strengthening originating from immobile or boundary dislocations (as main strength contributors at high temperatures) are added up (see table 46). Furthermore, on basis of [45] and [46] work hardening effect associated with mobile dislocations is considered and included in the inner stress.

This is done both for BM and for FGHAZ after 10 hours and 14 379 hours of creep.

After 10 hours of creep, BM backstress is estimated to lie between 223- 309 MPa, whereas FGHAZ backstress in the beginning of service amounts to 185- 236 MPa.

After 14379 hours of creep, BM backstress reduces to 180- 200 MPa, whereas FGHAZ declines to 181- 189 MPa.

Method 2	Equ. Ref.	BM 10 h	BM 14379 h	FGHAZ 10 h	FGHAZ 14379 h
σ_{ρ_m}	[45] , [46]*	13 MPa	9,4 MPa	13 MPa	9,4 MPa
σ_{ρ_im}	[65] , [46]*	22,8 MPa	20 MPa	25 MPa	19 MPa
σ_{part}	[65]	187,4- 273 MPa	150,2- 170,5 MPa	147- 198 MPa	152,5- 161 MPa
σ_i	*α=0,02	223- 309 MPa	180- 200 MPa	185- 236 MPa	181- 189 MPa

Table 46) High temperature backstress of Gr. 91 in BM and FGHAZ after 10 hours and 14379 hours of service at 650 °C

5.) Discussion

5.1) Assessment of Model 1

5.1.1) Comparison to Literature Data

5.1.1.1) Chromium Carbide ($M_{23}C_6$)

Table 47 compares model 1 results for the mean diameter of chromium carbide $M_{23}C_6$ to available data from literature.

AR stands for as-received condition, 600 for BM creep-loaded at a service temperature of 600 °C. For the meaning of the other abbreviations, please see the introduction of chapter 3.2.

Simulation values that show good agreement with literature were marked in green. Yellow means that in the simulation a deviation from literature could be observed, but still it does not exceed half or the double of the measurement. Red colour symbolizes an even bigger gap between simulation and measurements and poor agreement.

For $M_{23}C_6$ the quality of simulation was excellent, matching nearly all literature values.

Steel No.	**Temp. [°C]**	**Time [h]**	**Stress [MPa]**	**Shape**	**Nucl. sites**	**Main chem. elements**	**Diameter [nm]**	**Model 1 Results [nm]**	**Inv. method**	**Ref.**
1	AR	AR	-	CO	GB, LB	Cr	GB=124 LB=102	95,6	LOM, SEM, TEM, EDX, SAD	[17]
2	AR	AR	-	IR	GB	Cr	50-300		SEM, TEM, EDX	[18]
3	AR	AR	-	-	-	-	86 ±17		TEM	[19]
2	600	113,431	80	IR	-	Cr	150-800	426	SEM, TEM, EDX	[18]
5	AR	AR	-	IR	-	-	90-115	95,6	TEM	[21]
5	AR	AR	-	-	-	-	30-200	95,6	TEM	[22]
5	600	0-16650	0-175	-	-	-	30-300	323,7	TEM	[22]
7	AR	AR	-	-	-	-	79	95,6	TEM	[23]
7	600	250	175	-	-	-	95	93,9	TEM	[23]
7	600	2500	130	-	-	-	114	211,7	TEM	[23]

Table 47) Model 1 results vs. literature data for mean diameter of $M_{23}C_6$ in as-received condition and during creep of BM at 600 °C

5.1.1.2) MX Precipitates (VN+ NbC)

Table 48 compares mean diameters of MX in as-received condition and creep-loaded state to measurement results from literature.

The same colour system as for table 47 was used.

In as-received condition differences between simulation and measurement could be seen, just as in the beginning of service section.

Simulation tended to overestimate MX sizes compared to SEM and TEM results reported in literature.
Nevertheless, the quality of simulation improved during service section, giving very similar results in simulation as it could be observed in measurements.

Steel No.	Temp. [°C]	Time [h]	Stress [MPa]	Nucl. sites	Main chem. elements	Diameter [nm]	Model 1 Results [nm]	Inv. method	Ref.
2	AR	AR	-	LI	-	-	VN(mart,s): 45,3 NbC(mart,s): 31,1 NbC(aust,d): 33,9	SEM	[18]
3	AR	AR	-	-	-	16 ±3		TEM	[19]
7	600	50	200	-	-	19	VN(mart,s): 47,8 NbC(aust,d): 33,4 NbC(mart,s): 30,8	TEM	[23]
7	600	250	175	-	-	32	VN(mart,s): 46,6 NbC(aust,d): 33 NbC(mart,s): 30,5	TEM	[23]
7	600	2500	130	-	-	33	VN(mart,s): 56 NbC(aust,d): 33,4 NbC(mart,s): 30,5	TEM	[23]

Table 48) Model 1 results vs. literature data for mean diameter of MX in as-received condition and during creep of BM at 600 °C

5.1.1.3) Laves Phase

As far as Laves phase evolution (table 49) is concerned, agreement with reference [18] was bad.
Simulation in model 1 obviously used a too low coarsening rate for Laves phase.
The MatCalc values better fitted with source [16], reaching around half of the measurement (see figure number 47).

Steel No.	Temp. [°C]	Time [h]	Stress [MPa]	Shape	Nucleation sites	Main chem. elements	Diameter [nm]	Model 1 Results [nm]	Inv. method	Ref.
2	600	113,431	80	IR	GB	Mo	>1,000	192,6	SEM	[18]
2	600	113,431	-	IR	GB	Mo	>1,000	192,6	SEM	[18]

Table 49) Model 1 results vs. literature data for Laves diameter during creep of BM at 600 °

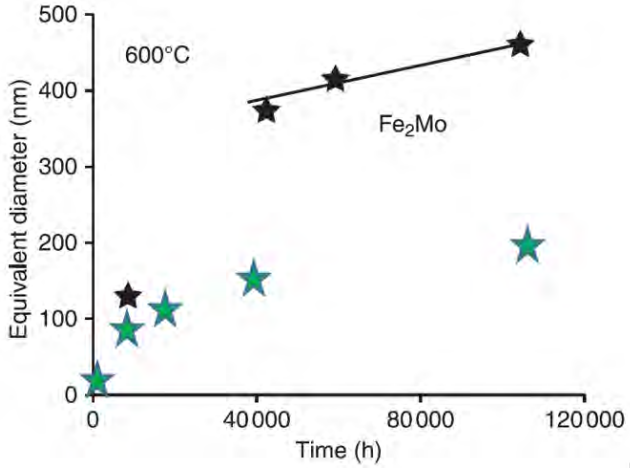

Figure 47) Evolution of equivalent diameter of Fe_2Mo Laves precipitates in P91 at 600°C [16] *and comparison to model 1 simulation (green stars)*

5.1.1.4) Modified Z Phase and AlN

Modified Z Phase did not nucleate in model 1, even though it was reported in literature (see chapter 3.2.3.4).

However, more MatCalc variations concerning this precipitate were conducted in model 2. So for a more detailed discussion about the used input parameters and the weakness of current Z phase model in MatCalc please go to chapter 6.2.1.4.

It was shown by S. Yadav and others that aluminium nitrides in P91 are often misinterpreted as creep cavities, and can reach a size of 500 nm or less after 9000 hours of creep at 650 °C. [66] Unfortunately, robust statistics about the number of particles is still missing. Moreover, comparison to model 1 is not useful, since service temperature was 600 °C.

However, H. Naoi and others [67] made investigations about aluminium nitride in a 9Cr-0.5Mo-1.8W steel with creep experiments at 600 °C, detecting one particle's diameter as around 350 nm after 3000 hours of service. Again, of course, this size cannot be taken as a representative value.

The MatCalc simulation of model 1 revealed a mean diameter of only 73 nm after 3000 hours (service temperature 600 °C).

5.2) Assessment of Model 2

5.2.1) Comparison to Literature Data

5.2.1.1) Chromium Carbide ($M_{23}C_6$)

Table 50 contains model 2 results for the mean diameter of chromium carbide $M_{23}C_6$ as well as available data from literature.

"AR" again stands for as-received condition and "FGHAZ, PWHT" for post-weld heat-treated FGHAZ. 625 or 650 means BM creep-loaded at a service temperature of 620 °C or 650 °C. "FGHAZ, PWHT, 650" includes data for FGHAZ during service section at 650 °C of operation. For the meaning of the other abbreviations, please go back to the introduction of chapter 4.

Simulation values that show good agreement with literature were once more marked in green. Yellow means that in the simulation a deviation from literature could be observed, but still it does not exceed the double of the measurement. Red colour symbolizes a big gap between simulation and measurements with poor agreement.

For $M_{23}C_6$ diameters model 2 gave very accurate predictions compared to literature.

Steel No.	Temp. [°C]	Time [h]	Stress [MPa]	Shape	Nucl. sites	Main chem. elements	Diameter [nm]	Model 2 Results [nm]	Inv. method	Ref.
1	AR	AR	-	CO	GB, LB	Cr	GB=124 LB=102	102,8	LOM, SEM, TEM, EDX, SAD	[17]
2	AR	AR	-	IR	GB	Cr	50-300		SEM, TEM, EDX	[18]
3	AR	AR	-	-	-	-	86 ±17		TEM	[19]
1	625	4292	98	CO	GB, LB	Cr	GB=255 LB=215	312 (650°C!)	LOM, SEM, TEM, EDX, SAD	[17]
5	AR	AR	-	IR	-	-	90-115	102,8	TEM	[21]
5	AR	AR	-	-	-	-	30-200	102,8	TEM	[22]
6	FGHAZ, PWHT	-	-	IR	-	Cr	158	186,6	TEM	[13]
6	FGHAZ, PWHT, 650	14379	40	IR	-	Cr	173	142,7	TEM	[13]
7	AR	AR	-	-	-	-	79	102,8	TEM	[23]
7	650	UF*	115	-	-	-	111	147,6	TEM	[23]
7	650	UF*	85	-	-	-	156	253,4	TEM	[23]

Table 50) Model 2 results vs. literature data for mean diameter of $M_{23}C_6$ in as-received condition, post-weld heat-treated (PWHT) and during creep of FGHAZ at 650 °C

* Assumption in accordance with MHI specimen 2016 due to missing data:
t_R(115 MPa)=300 h; t_R(85 MPa)=2300 h

5.2.1.2) MX Precipitates (VN+ NbC)

Table 51 compares mean diameters of MX in as-received condition, after PWHT and in creep-loaded state (both BM and FGHAZ) to measurement results from literature. The same colour system as for table 50 was used.

In as-received condition agreement was good, assuming the found particles in TEM were niobium carbide.

As far as FGHAZ after PWHT is concerned, vanadium nitride in the simulation turned out to be close to measured values. Unfortunately, niobium carbide in model 2 results (21 or 26 nm) did not fit the TEM findings at all (61 nm by TEM).

For FGHAZ after around 14000 hours of service the similarity of vanadium nitride in MatCalc model 2 (121 nm) and in TEM measurements was not perfect, but satisfactory (70 nm).

In regard to short-time creep, niobium carbide values of the simulation (which lie between 21 and 27 nm) strongly resemble to measured MX data (25 and 27 nm).

Steel No.	Temp. [°C]	Time [h]	Stress [MPa]	Shape	Nucl. sites	Main chem. elements	Diameter [nm]	Model 2 Results [nm]	Inv. method	Ref.
2	AR	AR	-	-	LI	-	-	VN(mart,s): 42,6 NbC(mart,s): 20,8	SEM	[18]
3	AR	AR	-	-	-	-	16 ±3		TEM	[19]
6	FGHAZ, PWHT	-	-	-	-	V	57	VN(mart,s): 42,6	TEM	[13]
6	FGHAZ, PWHT	-	-	-	-	Nb	61	NbC(mart,s): 20,8 NbC(aust,d): 26,4	TEM	[13]
6	FGHAZ, PWHT, 650	14379	40	-	-	V	70	VN(mart,s): 120,6	TEM	[13]
7	650	UF*	115	-	-	-	25	VN(mart,s): 42 NbC(mart,s): 20,6 NbC(aust,d): 26,5	TEM	[23]
7	650	UF*	85	-	-	-	27	VN(mart,s): 52 NbC(mart,s): 20,7 NbC(aust,d): 27	TEM	[23]

Table 51) Model 2 results vs. literature data for mean diameter of MX in as-received condition, post-weld heat-treated (PWHT) and during creep of FGHAZ at 650 °C

* Assumption in accordance with MHI specimen 2016 due to missing data:
t_R(115 MPa)=300 h; t_R(85 MPa)=2300 h

5.2.1.3) Laves Phase

For Laves phase evolution only TEM data about FGHAZ during service was available, matching fairly with the simulation result of model 2 (see table 52).

Steel No.	Temp. [°C]	Time [h]	Stress [MPa]	Shape	Nucleation Sites	Main chem. elements	Diameter [nm]	Model 2 Resuls [nm]	Inv. method	Ref.
6	FGHAZ, PWHT 650	14379	40	-	-	-	775	466	TEM	[13]

Table 52) Model 2 results vs. literature data for mean diameter of Laves phase during creep of FGHAZ at 650 °C

5.2.1.4) Modified Z Phase and AlN

An equivalent interface energy of around 0,75 was identified as threshold: Below this value, modified Z phase nucleates immediately in the beginning of normalizing section- jumping to a diameter of several hundreds of nanometers. This size (with a low phase fraction <0,01 %) stays constant in all heat treatment stages and also during service, showing no tendency for coarsening. Due to this unpromising behavior, it was decided to choose a value of 1 for the equivalent interface energy, which actually suppresses the formation of Z phase.

For that reason no direct comparison with literature is possible (see chapter 4.3.4).

The nucleation constant of 1.10^{-12} from previous scripts (Vujic's model 0 and templates from E. Kozeschnik) was not changed, but could also be a way to create a more realistic Z phase model. Further research is needed about the influence of this factor on the fragile and complicated MatCalc simulation network between Z phase activity at different nucleation sites and possible vanadium nitride depletion.

As said in chapter 6.1.1.4, S. Yadav and others [66] revealed that aluminium nitrides in P91 are often mixed up with creep cavities. A size of 500 nm or less was observed by the authors with SEM after 9000 hours of creep at 650 °C. [66]

However, the few measurements do not allow a statistical analysis for deriving a size distribution and mean diameter of AlN. Thus, comparison to BM result of model 2 (app. 122 nm after 9000 hours of creep simulation) is limited.

5.2.2) Comparison of BM Creep in Model 2 to Model 1

First of all, one has to be aware that model 1 and model 2 cannot be directly compared, as the temperature of service was increased from 600 to 650 °C.

All of the following results are also displayed in table 53.

For **$M_{23}C_6$(mart,s)** this means a 63 % larger mean diameter after 100 000 hours in model 2, reaching 696 nm with a phase fraction of around 2,25 % (almost the same as before).

Vanadium nitride at martensitic subgrain boundaries **VN(mart,s)** doubles its diameter from formerly 62 nm in model 1 to about 127 nm at the end of service stage with a phase fraction of 0,382 % (which is similar to model 1, too).

Laves phase located at martensitic subgrain boundaries **Laves(mart,s)** dramatically reduces its phase fraction from 0,447 % at 600 °C to about 0,153 % at 650 °C, which is in accordance with the stepped equilibrium calculation in figure 10.
Mean diameter grows to about 392 nm after 100 000 hours (formerly 193 nm with 600 °C).

Niobium carbide at martensitic subgrain boundaries **NbC(mart,s)** develops a phase fraction of 0,041 % (formerly 0,025 %), having a mean diameter of 24,4 nm (23 nm in model 1).
Aluminium nitride at martensitic dislocations **AlN(mart,d)** is estimated to coarsen to 211 nm after 100 000 hours at 650 °C (formerly 148 nm at 600 °C), having a phase fraction of 0,033 % (a bit higher than in model 1).

Niobium carbide at austenitic dislocations **NbC(aust,d)** nearly halves its phase fraction from 0,04 % in model 1 to 0,025 % in model 2.
Also a smaller mean diameter of 43,6 nm can be observed (formerly 51 nm).

Differences for precipitates with minor phase fraction will not be discussed, but can be seen in table 52. They are marked in yellow color.

100 000 h service, 600°C	Phase Fraction	Mean Diameter	Number Density	100 000 h service, 650°C	Phase Fraction	Mean Diameter	Number Density
$M_{23}C_6$(mart,s)	2,24 %	426 nm	$5{,}18.10^{17}$ m^{-3}	$M_{23}C_6$(mart,s)	2,249 %	695,9 nm	$1{,}19.10^{17}$ m^{-3}
Laves(mart,s)	0,447 %	192,6 nm	$1{,}05.10^{18}$ m^{-3}	VN(mart,s)	0,382 %	126,6 nm	$3{,}15.10^{18}$ m^{-3}
VN(mart,s)	0,404 %	61,9 nm	$2{,}66.10^{19}$ m^{-3}	Laves(mart,s)	0,153 %	392,4 nm	$4{,}23.10^{16}$ m^{-3}
NbC(aust,d)	0,040 %	51,3 nm	$5{,}6.10^{18}$ m^{-3}	NbC(mart,s)	0,041 %	24,4 nm	$4{,}94.10^{19}$ m^{-3}
NbC(mart,s)	0,025 %	22,5 nm	$4{,}16.10^{19}$ m^{-3}	AlN(mart,d)	0,033 %	211,4 nm	$6{,}17.10^{16}$ m^{-3}
AlN(mart,d)	0,021 %	148 nm	$1{,}13.10^{17}$ m^{-3}	NbC(aust,d)	0,025 %	43,6 nm	$5{,}55.10^{18}$ m^{-3}
NbC(mart,d)	$8{,}85.10^{-3}$ %	50,2 nm	$1{,}34.10^{18}$ m^{-3}	NbC(mart,g)	$8{,}12.10^{-3}$ %	586,4 nm	$7{,}69.10^{14}$ m^{-3}
NbC(mart,g)	$2{,}69.10^{-5}$ %	365,8 nm	$1{,}04.10^{13}$ m^{-3}	NbC(mart,d)	$1{,}28.10^{-3}$ %	27,5 nm	$1{,}09.10^{18}$ m^{-3}
NbC(aust,g)	$3{,}59.10^{-6}$ %	356 nm	$1{,}51.10^{12}$ m^{-3}	NbC(aust,g)	$9{,}07.10^{-6}$ %	479,4 nm	$1{,}57.10^{12}$ m^{-3}

Table 53) Comparison of BM creep in model 1 (left- 600 °C) to model 2 (right- 650 °C)

5.2.3) Comparison to TEM Results 2016

The mean TEM sizes (diameters) for MX and $M_{23}C_6$ seem to be close to the simulation values of model 2, having a bit higher mean radii in microscopic investigation than in MatCalc. The derived number density is lower in TEM compared to simulation (see tables 54 and 55). The phase fraction, in contrast, shows excellent agreement.

AR, BM TEM	Mean Diameter	Number Density	Phase Fraction
$M_{23}C_6$	134 nm	$1{,}73.10^{19}$ m^{-3}	2,193 %
MX	54 nm	$5{,}17.10^{19}$ m^{-3}	0,435 %

Table 54) Results of TEM measurements for Gr. 91 BM in as-received condition

AR, BM MatCalc	Mean Diameter	Number Density	Phase Fraction
$M_{23}C_6$(mart,s)	102,8 nm	$3{,}63.10^{19}$ m^{-3}	2,219 %
VN(mart,s)	42,6 nm	$9{,}55.10^{19}$ m^{-3}	0,416 %

Table 55) MatCalc model 2 results for Gr. 91 BM as-received

Interpeting $M_{23}C_6$ and MX precipitates as the main contributors to precipitation strengthening, this speaks for the reliability and trustworthiness of the new simulation model 2 at least in the as-received condition.

Unfortunately, so far (status end of July 2016) no TEM results for other heat-treatment conditions or during creep have been available. Consequently, validation of the complete results still depends on literature sources.

5.2.4) Room Temperature Backstress

Method 1	Equ. Ref.	BM 10 h	BM 14379 h	FGHAZ 10 h	FGHAZ 14379 h
σ_{ρ_m}	[46]*	326,1 MPa	234,9 MPa	326,1 MPa	234,9 MPa
σ_{Or}	[51]	422,7 MPa	215,1 MPa	396,6 MPa	204,3 MPa
σ_{sgb}	[48] [45]	317,4 MPa	71,1 MPa	348,5 MPa	35,5 MPa
σ_i	*α=0,5	1066,2 MPa	521,1 MPa	1071,2 MPa	474,7 MPa

Table 56) Total "athermal" backstress of Gr. 91 in BM and FGHAZ after 10 hours and 14379 hours of service at 650 °C

When taking a look at table 56 on basis of MatCalc model 2 results (identical to table 45), it can be seen that directly after the start of creep (10 hours of service) precipitates contribute the biggest share to the overall athermal yield strength. This is the case both in BM and FGHAZ.

After 14 379 hours of service, mobile dislocation strengthening sligthly decreases in comparison to the situation after 10 hours of creep, but nevertheless it finally starts to exceed the backstress for precipitation strengthening in room temperature condition.

The inner stress after 10 hours of FGHAZ creep is larger than for BM. This can be traced back to IWS measurements, where subgrain size in as-received FGHAZ (0,51 µm) turned out to be beyond as-received BM (0,51 µm), initially causing more subgrain strengthening for FGHAZ.

However, after 14 379 hours of creep simulation at 650 °C service, this positive effect disappears because of faster coarsening of particles and subgrains in FGHAZ, resulting in a nearly 50 MPa lower backstress of FGHAZ than in BM. Literature and experiments confirm this trend, stating the FGHAZ as the weakest zone with increased danger of void formation and damage.

It can be observed in reality that subgrain strengthening reduces dramatically during the microstructural evolution due to the phenomenon of subgrain coarsening. FGHAZ in the simulation loses even more in subgrain backstress (with remaining 10 % of strengthening) than BM after 14 379 hours, since the double subgrain size was assumed in that time of creep for FGHAZ than for BM based on [13]. It remains unclear, if the predicted subgrain sizes of 2,5 µm (BM) and 5 µm (FGHAZ) are realistic for P91 service at 650 °C, since IWS measurements were not available and the only literature data [13] for 14 379 hours of creep (40 MPa of load) was below the values detected by IWS in creep-loaded BM specimen with around 300 and 2200 hours of rupture time (100 MPa and 80 MPa of load).

As far as this precipitation strengthening is concerned, Orowan stress for BM is generally higher than for FGHAZ both after 10 hours (422,7 MPa vs. 396,6 MPa) and after 14 379 hours of creep (215,1 MPa vs. 204,3 MPa). This is in good agreement with a bigger precipitate start size for $M_{23}C_6$ in as-received condition of FGHAZ and a faster coarsening rate for $M_{23}C_6$ during service stage implemented in the MatCalc script part of FGHAZ, talking about model 2.

5.2.5) Service Temperature Backstress

Method 2	Equ. Ref.	BM 10 h	BM 14379 h	FGHAZ 10 h	FGHAZ 14379 h
σ_{ρ_m}	[45] , [46]*	13 MPa	9,4 MPa	13 MPa	9,4 MPa
σ_{ρ_im}	[65] , [46]*	22,8 MPa	20 MPa	25 MPa	19 MPa
σ_{part}	[65]	187,4- 273 MPa	150,2- 170,5 MPa	147- 198 MPa	152,5- 161 MPa
σ_i	*α=0,02	223- 309 MPa	180- 200 MPa	185- 236 MPa	181- 189 MPa

Table 57) High temperature backstress of Gr. 91 in BM and FGHAZ after 10 hours and 14379 hours of service at 650 °C

The basic idea of making an attempt to calculate a high temperature backstress was to reflect the real conditions at a temperature level of 650 °C, including climbing of dislocations and a dramatically reduced mobile dislocation strengthening. Moreover, subgrain strengthening is replaced by a concept of immobile/ boundary dislocation strengthening.

One of the fundamental differences in the approach for mobile (and also immobile) dislocations was the applied dislocation interaction factor (α=0,02), where the recommendation of Basirat [46] was followed. It is obvious that this empirical and non-physical fitting parameter is basically unknown and a big range of factors is provided by literature, most of them only focusing on calculation of room temperature backstress.

Magnusson and Sandström suggest both to apply α=0,33 to 0,5 [65] and to introduce a weighting factor for soft and hard subgrain zones to correct the immobile dislocation strengthening. Since both the weighting factors and measurements concerning the difference in dislocation density at subgrain walls and in subgrain interiors were missing, instead a reduced dislocation interaction factor of α=0,02 was preferred. Test calculations with α=0,33 furthermore led to the dilemma that immobile dislocation strengthening at high temperatures for FGHAZ (318 MPa) began to dramatically exceed subgrain strengthening at room temperature (35,5 MPa) after 14 379 hours of creep, which makes no sense and demolishes the concept of a 650 °C backstress. Consequently, α for immobile dislocations could only amount to 0,037 or less to avoid this contradiction.

Additionally, the question remains unanswered, whether interaction factor for mobile and immobile dislocations is identical (like assumed) or should significantly differ from each other.

After 10 hours of creep the BM backstress tends to be higher than for FGHAZ (but it can also be reversed), depending on the calculation method of dislocation line tension, which represents another unsolved problem and explains the range of results for particle hardening.

After 14 379 hours of creep, still the difference in backstress between BM (180- 200 MPa) and FGHAZ (181- 189 MPa) remains dissatisfying, lying extremely close to each other and possibly overestimating the FGHAZ backstress. First of all, the method of evaluating dislocation line tensions has to be critically questioned. On the other hand, possibly the dislocation interaction

factor for immobile dislocation strengthening, which was arbitrarily chosen, has to be redefined. Moreover, MX coarsening rate- in contrast to $M_{23}C_6$- in FGHAZ was the same as in BM, making different $M_{23}C_6$ sizes responsible for varying particle hardening values. However, the major part of precipitate backstress seems to originate from MX particles, and since their diameters after 14 379 hours were the same in BM and FGHAZ, the gap turned out to be small between particle hardening in BM and FGHAZ.

5.2.6) Comparison of Backstress in Room Temperature and High Temperature Condition

After 10 hours of BM creep, high temperature backstress reaches approximately 25 % of the room temperature backstress/ athermal yield strength. FGHAZ high temperature backstress after 10 hours only becomes around 20 % of the room temperature value.

After 14 379 hours of creep, high temperature backstresses both for BM and FGHAZ approach between 35 % and 40 % of the values for athermal yield strength.

5.2.7) Conclusion of Backstress Calculations

One of the original targets for high temperature backstress was to insert the effective stress at 650 °C (as the difference of external stress and high temperature backstress/ inner stress) directly into Norton's creep law for the stage of steady-state creep.

However, Norton considers a constant creep rate as long as effective stress and temperature remain constant. In general, this is not the case during service stage, because effective stress represents the difference between external load and internal backstress, which changes parallelly to the microstructural evolution. This provides potential for the future to deal with non-constant creep rates, which is closer to reality.

High temperature backstress closely resembles to the expected values for tensile strength at 600 or 650 °C- at least this seems to be valid for the BM results.

Thus the high temperature backstress managed to supplement the estimation for room temperature backstress or athermal yield strength, which led to promising results also.

All in all, the calculations demonstrated, how the microstructural changes affect the resistance of P91 material to creep and also gave an idea- especially concerning the athermal yield strength- of the significantly weaker character of FGHAZ compared to BM.

6.) Conclusion and Outlook

6.1) Advantages of Model 1 and 2 Simulations

All in all, a first attempt to improve the simulation of microstructure evolution in a 9 % Cr steel proved to be successful.

Many complex physical parameters of the MatCalc precipitation kinetic model for Gr. 91 were analyzed, modified and carefully implemented. Some values were newly introduced, others removed, and at the same time, the documentation and readability of the script was optimized line by line.

Minor bugs in the script code were detected and eliminated step by step. Measurements, automatic evaluations with software programs (OIM for instance), manual calculations, literature reviews and last but not least endless testing procedures with MatCalc served to raise the quality and reliability of P91 simulation.

6.1.1) Dislocation Density Evolution

The introduction of a reduction function for mobile dislocation density in form of a non-linear equation has already been able to solve problems with unrealistically high coarsening of $M_{23}C_6$ during service, although further improvement concerning the difference between BM and FGHAZ would be desirable.

A step function that used a variable step size to approximate this new non-linear equation replaced a formerly implemented linear reduction rate.

6.1.2) Grain Sizes

The prior austenitic grain sizes in 2016 were calculated both automatically and manually out of EBSD data, applying TSL OIM software.

A Mackenzie-based correction factor was used for PAGS that were not fully visible, leading to a result close to the measurements from the previous TU Graz/ MHI project in 2015. Subgrain size was successfully validated on basis of literature data. Additionally, the correctness of grain sizes was proven by good simulation results for model 2 after implementation into MatCalc.

6.1.3) Nucleation Sites

Although not all literature sources fully agree with the choice of nucleation sites according to Srinivas [37] (especially concerning dislocations), their introduction in models 1 and 2 had a positive effect: The MatCalc results became more diverse and accurate, considering all physically possible places of nucleation, growth and coarsening.

The detection and proof of particles located at dislocations remains the biggest issue, when it comes to TEM or SEM investigations.

6.1.4) Diffuse Interface Correction Temperature for Laves Phase

A systematic method was found and shown how to estimate the diffuse interface correction temperature for Laves phase in a reliable way. It was successfully applied for model 2, avoiding both dramatic coarsening and drastic underestimation when choosing a wrong value.

6.1.5) Precipitate Evolution

Combining new grain sizes, changed nucleation sites, a continuos dislocation density reduction and last but not least updated heating and cooling rates, the precipitation evolution for all stages of heat-treatments and service turned out to be satisfactory for BM in model 1 as well as for BM and FGHAZ in model 2.

Laves phase represents the only exception, showing stronger deviation from literature values during service in BM for model 1 and 2. Eventually, the FGHAZ results for Laves phase also closely resembled to literature data after considering accelerated diffusion.

Consequently, the main goal of the thesis was achieved, despite being aware of some remaining problems and difficult tasks for the future, as will be discussed in the next section.

6.2) Weaknesses of Model 1 and 2 Simulations and Outlook

6.2.1) Dislocation Density

Unfortunately, no experimental or modelling data was available treating the difference of mobile dislocation density reduction in base metal and in FGHAZ. For both script parts, the same function was used, which has to be critically questioned. T. Watanabe and others [68], for example, hint a lower dislocation density start value in FGHAZ and an assumed faster recovery of dislocations in the FGHAZ than in BM. However, no quantitive estimates for the order of deviations is given in this document.

Furthermore, the dislocation density evolution has to be regarded as stress-dependent (e.g. 145 MPa at 600 °C for P92 was used as basis for deriving a dislocation density reduction function). At the moment, there is no concept to consider this influence factor in MatCalc. It is unclear, how the dislocation density will look for a creep specimen loaded with 40 MPa at 650 °C, for instance.

6.2.2) Subgrain Coarsening

So far, subgrain coarsening has not been implemented in the MatCalc model, either.

First test calculations with a reduced number of size classes and only for 10 000 hours of BM creep indicated that the change of subgrain size had only very little impact at the precipitation kinetics after the nucleation stage. When incorporating an increase of subgrain size from 0,56 µm to 1 µm after 500 hours and from 1 µm to 1,3 µm after 2500 hours, no difference could be observed to the script version with a constant subgrain size value of 0,56 µm.

Consequently, the definition of a correct subgrain size seems to be much more important in the stage of nucleation.

However, to be sure about the long-term effect of implemented subgrain coarsening in MatCalc, further test calculations with 100 000 hours and a higher number of size classes is strongly recommended for the future.

6.2.3) Precipitates

Z phase simulation represents another challenge for the future which has not been solved in a satisfactory way yet.

The question why Laves phase nucleated in martensite at grain boundaries- in contrast to nucleation at subgrain boundaries- did not lead to promising results, remains unanswered. In some

templates of E. Kozeschnik also dislocations were used as nucleation site, which appears to be physically possible.

This arouses the question how the definition of combinations of nucleations sites (g+s) or (d+s) or (d+g) changes the quality of results compared to single-nucleation-site models like using only "g", only "d" or only "s" (which is currently chosen in models 1 and 2).

Moreover, research about a possible substitution or further reduction of aluminium nitride, which is of importance for the casting process during manufacturing, in martensitic chromium steels could be of interest. Grain refinement could be further restricted in that way [11] and phase fraction of MX might be increased at the same time [12], which positively affects the long term creep resistance of P91.

Furthermore, literature at the moment provides no good data about mean diameter and size distribution of aluminium nitrides. Further measurements to quantify AlN particles and to produce more reliable statistics would be another valuable task for the future.

6.2.4) Diffusion

Automatic consideration of higher diffusion rates for FGHAZ in comparison to BM instead of using a matrix diffusion enhancement factor would also be desirable. The grain-size dependence of the diffusion coefficient considered in MatCalc software seems to underestimate this effect.

6.2.5) Calculation Time

A big disadvantage of the high simulation accuracy including non-constant heating and cooling rates, changing dislocation density, a large variety of nucleation sites and the choice of a high number of precipitation size classes is the extremely long calculation time of nearly 35 hours (on the workstation computer used).

Strategies are urgently needed to decrease the calculation time- especially for computers that are not so powerful.

6.2.6) Role of CPU Types

Concerning different MatCalc simulation results on different computers with varying CPU types or operating systems, information about the cause of troubles would be useful. Still it is not clear, which role possible bugs in the software, unstable operating systems or manufacturing mistakes of CPU types play.

7.) Appendix A: MatCalc Script on 2016 Data (model 2)

```
$ ********************************************************************************************************

$ ********************************** GENERAL INFORMATION ***********************************************
$ ********************************************************************************************************
$
$ Script for simulation of multi-stage heat treatment of 9% Cr-steel (Gr. 91)
$
$
$ Database: mc_fe_v2.050.tdb, mc_fe_v2.008.ddb
$ Author: S. Vujic
$ Modified by: F. Riedlsperger
$ Creation date: 07.04.2015
$ Last revision: 21.02.2016
$ Reason for update: new databases; changed input parameters
$ This is a script for MatCalc version 5.60 (rel 1.001)
$ ********************************************************************************************************
$ ************************************ SETUP INFORMATION ***********************************************
$ ********************************************************************************************************
$ make sure we work in the correct module
use-module core $ select core module for kinetic simulation
$ close any open workspace without asking for save
close-workspace f
new-workspace $ open new workspace
$ give some information about the script:
set-workspace-info + Selected elements:
set-workspace-info + C, Si, Mn, Cu, Ni, Cr, Mo, V, Nb, Al, N
set-workspace-info +
set-workspace-info + Matrix phases: Martensite (BCC_A2), Austenite (FCC_A1)
set-workspace-info +
set-workspace-info + Precipitate phases:
set-workspace-info + NbC, AlN, Cr2N, VN, M23C6, M7C3, Cementite, Laves, Z-phase
set-workspace-info +
set-workspace-info + Samples are quenched, tempered, welded, post weld heat treated and aged
set-workspace-info +
set-workspace-info + The different compositions are considered: Raccord (=MHI1) and MHI2
set-workspace-info +
$ ********************************************************************************************************
$ ************************************ SYSTEM SETUP ****************************************************
$ ********************************************************************************************************
$ verify correct MatCalc version (is accessible as internal variable)
if (matcalc_version<5600001)
send-dialog-string "MatCalc version must be 5.60 (rel 1.001) or higher to run this script. Stopping."
stop_run_script $ stop script
endif
$ show console window and notify user to perform selection
move-gui-window c show $ bring console window to front
$ selection of calc variants
set-variable-value comp 1 $ default value for composition
set-variable-value salo 1 $ default value for sample location
set-variable-value weldcyc 1 $ default value for sample location
echo n $ do not display in console window
send-console-string
send-console-string
send-console-string Select composition
send-console-string 1 ... Raccord (MHI2- version HiMAT 2015)
send-console-string 2 ... Raccord (MHI1- version TU Graz 2015)
send-console-string settings of Raccord
send-console-string
input-variable-value comp "Please select composition (1-2): "
send-console-string
```

```
send-console-string Select sample location
send-console-string 1 ... FGHAZ
send-console-string 2 ... Base metal (BM)
send-console-string
input-variable-value salo "Please select sample location (1-2): "
if (salo==1)
send-console-string
send-console-string Select welding cycle
send-console-string 1 ... Multipass (default)
send-console-string 2 ... Singlepass (MHI data)
send-console-string
input-variable-value weldcyc "Please select welding cycle (1-2): "
endif
echo y $ reset display in console window
$ ***************************************************************************************************
$ GLOBAL VARIABLES
$ ***************************************************************************************************
$ The austenitic grain size (ags) was found from an analysis of EBSD data with OIM software, considering
$ dislocation angles between 18 and 50 degrees.
$ To account for prior austenitic grain boundaries that were not clearly visible, a correction factor was
$ introduced on the basis of Mackenzie distribution.
$ With this factor the PAGS values derived from linear intercept method (manual procedure) were corrected.
$ The equilibrium solution temperature of laves phase is close to the service temperature of 600C.
$ Therefore the interface between the matrix and laves phase becomes diffuse instead of sharp. To
$ handle this state, an interface correction temperature of 1452K for for Raccord is applied.
$ Comment: a higher interface correction temp. like 1600K causes coarsening of laves phase, which is
$ not in agreement with experimental results.
$ A good estimation for the range of Laves interface correction temperature can be made by creating a
$ binary system of Fe-Mo or Fe-W (depending on the chemical composition of Gr. 91) and finding the maximum
$ dissolution temperature for Laves phase when varying Fe- and Mo-content [wt %], which in this case gave 1477 K.
$ Further optimization of this value led to 1452 K, which now can be used at any temperature level of service.
$ 600 degress of service temperature in theory demand the same interface correction temperature as 650 degrees, e.g.
set-variable-string scale_range 1e10..1e23 $ unified scaling for histogram windows
set-variable-value npc 50 $ set number prec. classes (default is 25- lower value worsens accuracy dramatically!)
$ In general the number of required precipitation classes depends on the performance of CPU.
$ On different computers, the same number of size classes can lead to slightly different results, especially when using low values.
$ Therefore, crosschecks are recommendable.
$ Also be aware that an increase of heating and cooling rates demands higher npc values to guarantee good accuracy.
$ Once heating and cooling rates are adjusted, also the number of size classes has to checked critically.
set-variable-value npc_laves 100 $ set number prec. classes for laves phase
set-variable-value npc_m23c6 100 $ set number prec. classes for M23C6
set-variable-value npc_aln 50 $ set number prec. classes for AlN
set-variable-value npc_vn 75 $ set number prec. classes for VN(mart,s) + VN(aust,g)
set-variable-value npc_nbc 75 $ set number prec. classes for NbC(mart,d) + NbC(mart,s)
set-variable-value mdef 8 $ matrix diff. enhancement factor during PWHT and service is 1 (faster diffusion in FGHAZ)
set-variable-value eie_zet 1 $ equivalent interf. energy for Z-phase nucleation
set-variable-value nucl_const_zet 1e-12 $ nucleation constant for matrix-Z-phase
set-variable-value lav_ict 1452 $ interface correction temperature [K] for laves
set-variable-value dda 1e11 $ dislocation density in austenite
set-variable-value ddm 1.5e14 $ dislocation density in martensite after 0h service
set-variable-value ddm_100h 1.48e14 $ calculation of ddm reduction according to extrapolation formula from S. Yadav:
set-variable-value ddm_200h 1.47e14 $ ddm=2.39257*10^16*t^(-0.57315), where ddm= dislocation density and t= time.
set-variable-value ddm_300h 1.46e14 $ IMPORTANT: primary creep has to be neglected to receive good results
set-variable-value ddm_400h 1.45e14 $ Consequently, a start value of 1,5e14 m^(-2) for dislocation density is defined
set-variable-value ddm_500h 1.44e14
set-variable-value ddm_600h 1.43e14
set-variable-value ddm_700h 1.42e14
set-variable-value ddm_800h 1.41e14
set-variable-value ddm_900h 1.4e14
set-variable-value ddm_1000h 1.39e14
set-variable-value ddm_1250h 1.36e14
set-variable-value ddm_1500h 1.34e14
set-variable-value ddm_2000h 1.3e14
```

```
set-variable-value ddm_2500h 1.26e14
set-variable-value ddm_3000h 1.22e14
set-variable-value ddm_3500h 1.19e14
set-variable-value ddm_4000h 1.15e14
set-variable-value ddm_4500h 1.13e14
set-variable-value ddm_5000h 1.1e14
set-variable-value ddm_6000h 1.05e14
set-variable-value ddm_9000h 9.31e13
set-variable-value ddm_12000h 8.44e13
set-variable-value ddm_15000h 7.76e13
set-variable-value ddm_20000h 6.9e13
set-variable-value ddm_25000h 6.26e13
set-variable-value ddm_30000h 5.76e13
set-variable-value ddm_40000h 5.02e13
set-variable-value ddm_50000h 4.5e13
set-variable-value ddm_60000h 4.1e13
set-variable-value ddm_70000h 3.78e13
set-variable-value ddm_80000h 3.53e13
set-variable-value ddm_90000h 3.31e13
set-variable-value ddm_100000h 3.13e13 $ dislocation density in martensite after 100000h service
set-variable-value T_ms 400 $ martensite start temperature
set-variable-value T_weld_fghaz 950 $ virtual welding peak temperature in FGHAZ
set-variable-value T_weld_bm 800 $ virtual welding peak temperature in base metal (BM)
set-variable-value hr_weld 1 $ multipass heating rate for virtual welding (only for selection "multipass"!)
set-variable-value cr_weld 15 $ multipass cooling rate for virtual welding (only for selection "multipass"!)
set-variable-value T_serv 650 $ service temperature
if (comp==1)
$ Below the setting for the Raccord steel (version HiMAT 2015) can be found. The normalizing-,
$ tempering- and PWHT-conditions are taken from the MHI data. At the moment values for TU Graz 2015
$ version are used, as no other data is available.

set-variable-value T_trans 833 $ martensite to austenite transformation temperature
set-variable-value ags 76e-6 $ austenitic grain size [=76µm]
set-variable-value sgs 0.56e-6 $ subgrain size in BM [=0,56µm]
set-variable-value sgef 5 $ subgrain elongation factor BM
set-variable-value agsfghaz 9e-6 $ austenitic grain size of FGHAZ [=9µm]
set-variable-value sgsfghaz 0.51e-6 $ subgrain size in FGHAZ [=0,51µm]
set-variable-value sgeffghaz 1 $ subgrain elongation factor in FGHAZ [=1]
set-variable-value T_aust 1050 $ normalizing temperature
set-variable-value time_aust 2*60*60 $ normalizing time (=2h)
set-variable-value T_temp 770 $ tempering temperature
set-variable-value time_temp 2*60*60 $ tempering time (=2h)
set-variable-value T_pwht 750 $ PWHT temperature
set-variable-value time_pwht 2*60*60 $ PWHT time (=2h)

elseif(comp==2)
$ Below the setting for the Raccord steel (version TU Graz 2015) can be found. The normalizing-,
$ tempering- and PWHT-conditions are taken from the MHI data.

set-variable-value T_trans 833 $ martensite to austenite transformation temperature
set-variable-value ags 76e-6 $ austenitic grain size [=76µm]
set-variable-value sgs 0.56e-6 $ subgrain size in BM [=0,56µm]
set-variable-value sgef 5 $ subgrain elongation factor BM
set-variable-value agsfghaz 9e-6 $ austenitic grain size of FGHAZ [=9µm]
set-variable-value sgsfghaz 0.51e-6 $ subgrain size in FGHAZ [=0,51µm]
set-variable-value sgeffghaz 1 $ subgrain elongation factor in FGHAZ [=1]
set-variable-value T_aust 1050 $ normalizing temperature
set-variable-value time_aust 2*60*60 $ normalizing time (=2h)
set-variable-value T_temp 770 $ tempering temperature
set-variable-value time_temp 2*60*60 $ tempering time (=2h)
set-variable-value T_pwht 750 $ PWHT temperature
set-variable-value time_pwht 2*60*60 $ PWHT time (=2h)
endif
```

```
$ ********************************************************************************************************
$ DATABASES, CHEMICAL COMPOSITION, SELECTED PHASES
$ ********************************************************************************************************
$ if you receive an error when executing the next line, please make sure you have the database
$ in your MatCalc/database folder. The mc_fe database available for registered MatCalc customers
open-thermodyn-database mc_fe_v2.050.tdb $ open thermodynamic database- ATTENTION: updated from 039 to 050 in
February 2016
select-elements C Si Mn Ni Cr Mo V Nb Al N Co Cu $ select elements
select-phases liquid fcc_a1 bcc_a2 g_phase laves_phase $ select phases
select-phases sigma m23c6 aln zet hcp_a3 m7c3 cementite $ select phases
read-thermodyn-database $ read thermodynamic database
read-mobility-database mc_fe_v2.008.ddb $ read diffusion data- ATTENTION: updated from 005 to 008 in February 2016
$ steel composition ...
$ now come values which are dependent on the choice of steel grade
if (comp==1)
$ Raccord without S, P, Ti, B, Co = MHI2 (HiMAT 2015)
enter-composition wp C=0,118 Si=0,49 Mn=0,37 Ni=0,40 Cu=0,13
enter-composition wp Cr=8,95 Mo=0,90 V=0,183 Nb=0,061 Al=0,016 N=0,0488
elseif (comp==2)
$ Raccord without S, P, Ti, B, Co= MHI1 (TU Graz 2015)
enter-composition wp C=0,112 Si=0,48 Mn=0,37 Ni=0,37 Cu=0,13
enter-composition wp Cr=8,98 Mo=0,87 V=0,199 Nb=0,063 Al=0,016 N=0,0473
endif
$ ********************************************************************************************************
$ CHANGE PHASE STATUS ETC.
$ ********************************************************************************************************
$ suspend fcc_a1#01 is replaced by simple phases NbC, and VN
change-phase-status fcc_a1#01 f s s
create-new-phase fcc_a1#01 C :Cr,Fe,Mo,Nb%:C%,N,VA: NbC $ create new phase NbC
create-new-phase fcc_a1#01 C :Cr,Mo,V%:C,N%,VA: VN $ create new phase VN
$ suspend hcp_a3 and kids, is replaced by simple phases Mo2C and Cr2N
change-phase-status hcp_a3 f s s
change-phase-status hcp_a3#01 f s s
change-phase-status hcp_a3#02 f s s
create-new-phase hcp_a3 C :CR%,MO,NB,V:C,N%,VA: Cr2N $ Cr2-nitride
$ ********************************************************************************************************
$ HEAT TREATMENTS, VARIABLES, TABLES & FUNCTIONS (1)
$ ********************************************************************************************************
$ ------------------------------------ HEAT TREATMENTS ------------------------------------------
$ ------------------------------------ PART I: HARDENING ----------------------------------------

$ ---------------------------------- END OF PART I: HARDENING ----------------------------------
create-heat-treatment hardening $ create heat treatment part I:
$ austenitization and quenching
append-ht-segment hardening $ casting process (START)
edit-ht-segment hardening . d n austenite $ define precipitation domain
edit-ht-segment hardening . s 1500 $ define start temperature
edit-ht-segment hardening . 1 T_ms 0.1 $ Tend + cooling rate
edit-ht-segment hardening . c cooling from solution treatment to martensite start $ comment
append-ht-segment hardening $ casting process- change to martensite (END)
edit-ht-segment hardening . d n martensite $ define precipitation domain
edit-ht-segment hardening . 1 25 0.1 $ Tend + cooling rate
edit-ht-segment hardening . c cooling from martensite start to room temperature $ comment

append-ht-segment hardening $ heating to normalize (START)
edit-ht-segment hardening . 1 40 0.0083 $ Point T2 (=Tend) + heating rate
edit-ht-segment hardening . c heating from room temperature 40 degrees $ comment
append-ht-segment hardening $ heating to normalize
edit-ht-segment hardening . 1 T_trans 0.0444 $ T_trans (=Tend) + heating rate
edit-ht-segment hardening . c heating from 40 degrees to A3 temperature $ comment
append-ht-segment hardening $ heating to normalize- change to austenite
edit-ht-segment hardening . d n austenite $ define precipitation domain
edit-ht-segment hardening . 1 920 0.0444 $ Point T3 (=Tend) + heating rate
```

```
edit-ht-segment hardening . c heating from A3 temperature to 920 degrees $ comment

append-ht-segment hardening $ heating to normalize
edit-ht-segment hardening . 1 T_aust 0.0181 $ T_aust (=Tend) + heating rate
edit-ht-segment hardening . c heating from 920 degrees to austenitization temperature $ comment
append-ht-segment hardening $ normalizing (HOLDING)
edit-ht-segment hardening . 2 0 time_aust $ Tdot + delta_t
edit-ht-segment hardening . c isothermal holding for 2 h at austenitization temperature $ comment

append-ht-segment hardening $ cooling process
edit-ht-segment hardening . 1 800 0.0694 $ Point T4 (=Tend) + cooling rate
edit-ht-segment hardening . c cooling from austenitization temperature to 800 degrees $ comment

append-ht-segment hardening $ cooling process
edit-ht-segment hardening . 1 600 0.0556 $ Point T5 (=Tend) + cooling rate
edit-ht-segment hardening . c cooling from 800 degrees to 600 degrees $ comment

append-ht-segment hardening $ cooling process
edit-ht-segment hardening . 1 460 0.0389 $ Point T6 (=Tend) + cooling rate
edit-ht-segment hardening . c cooling from 600 degrees to 460 degrees $ comment
append-ht-segment hardening $ cooling process
edit-ht-segment hardening . 1 T_ms 0.0278 $ T_ms (=Tend) + cooling rate
edit-ht-segment hardening . c quenching to martensite start temperature $ comment
append-ht-segment hardening $ cooling process- change to martensite
edit-ht-segment hardening . d n martensite $ define precipitation domain
edit-ht-segment hardening . 1 360 0.0278 $ Point T7 (=Tend) + cooling rate
edit-ht-segment hardening . c cooling from martensite start temperature to 360 degrees $ comment

append-ht-segment hardening $ cooling process
edit-ht-segment hardening . 1 320 0.0111 $ Point T8 (=Tend) + cooling rate
edit-ht-segment hardening . c cooling from 360 degrees to 320 degrees $ comment

append-ht-segment hardening $ cooling process
edit-ht-segment hardening . 1 260 0.0167 $ Point T9 (=Tend) + cooling rate
edit-ht-segment hardening . c cooling from 320 to 260 degrees

append-ht-segment hardening $ cooling process (END)
edit-ht-segment hardening . 1 25 0.013 $ T10 (=room temperature) + cooling rate (extrapolated)
edit-ht-segment hardening . c cooling from 260 degrees to room temperature
$ ---------------------------------------- PART II: TEMPERING ----------------------------------------
create-heat-treatment tempering $ second heat treatment
append-ht-segment tempering $ heating to temper (START)
edit-ht-segment tempering . s 25 $ define start temperature for HT
edit-ht-segment tempering . d n martensite $ define precipitation domain
edit-ht-segment tempering . 1 80 0.0306 $ Point T2 (=Tend) + heating rate
edit-ht-segment tempering . c heating from room temperature to 80 degrees $ comment

append-ht-segment tempering $ heating to temper
edit-ht-segment tempering . 1 T_temp 0.0295 $ T_temp (=Tend) + heating rate
edit-ht-segment tempering . c heating from 80 degrees to tempering temperature
append-ht-segment tempering $ tempering (HOLDING)
edit-ht-segment tempering . 2 0 time_temp $ Tdot + delta_t
edit-ht-segment tempering . c annealing for 2 h $ comment

append-ht-segment tempering $ cooling process
edit-ht-segment tempering . 1 550 0.0244 $ Point T3 (=Tend) + cooling rate
edit-ht-segment tempering . c cooling from tempering temperature to 550 degrees $ comment
append-ht-segment tempering $ cooling process
edit-ht-segment tempering . 1 420 0.0181 $ Point T4 (=Tend) + cooling rate
edit-ht-segment tempering . c cooling from 550 degrees to 420 degrees $ comment
append-ht-segment tempering $ cooling process
edit-ht-segment tempering . 1 360 0.0111 $ Point T5 (=Tend) + cooling rate
edit-ht-segment tempering . c cooling from 420 degrees to 360 degrees $ comment
```

```
append-ht-segment tempering $ cooling process
edit-ht-segment tempering . 1 250 0.0134 $ Point T6 (=Tend) + cooling rate
edit-ht-segment tempering . c cooling from 360 degrees to 250 degrees $ comment
append-ht-segment tempering $ append segment 2
edit-ht-segment tempering . d n martensite $ change precipitation domain
edit-ht-segment tempering . 1 25 0.01 $ Tend + cooling rate (extrapolated)
edit-ht-segment tempering . c cooling to room temperature $ comment
$ ---------------------------------- END OF PART II: TEMPERING -----------------------------------
if (salo==1)

$ ---------------------------------- PART III: VIRTUAL WELDING -----------------------------------
$ "salo" ... sample location; 1...FGHAZ; 2...Base metal;
$ "weldcyc" ... welding cycle; 1...Multipass; 2...Singlepass
if (weldcyc==1)
create-heat-treatment welding $ third heat treatment
append-ht-segment welding $ append segment 0 "heating to A3"
edit-ht-segment welding . s 25 $ define start temperature for HT
edit-ht-segment welding . d n martensite $ define precipitation domain
edit-ht-segment welding . 1 T_trans hr_weld $ Tend + heating rate
edit-ht-segment welding . c heating from room temperature to A3 temperature $ comment
append-ht-segment welding $ append segment 1
edit-ht-segment welding . d n austenite $ define precipitation domain
edit-ht-segment welding . 1 T_weld_fghaz hr_weld $ Tend + heating rate
edit-ht-segment welding . o +set-precipitation-parameter austenite t g agsfghaz $ modification of austenitic grain size;
transformation of BM in FGHAZ
edit-ht-segment welding . c heating from A3 to austenitization temperature $ comment
append-ht-segment welding $ segment 2 (quenching)
edit-ht-segment welding . 1 T_ms cr_weld $ Tend + cooling rate
edit-ht-segment welding . o +set-precipitation-parameter martensite t g agsfghaz $ modification of martensite grain size in
FGHAZ !!! NEW !!!
edit-ht-segment welding . o +set-precipitation-parameter martensite t s sgsfghaz $ modification of martensite lath size in FGHAZ
edit-ht-segment welding . o +set-precipitation-parameter martensite t o sgeffghaz $ modification of martensite lath elongation
factor in FGHAZ
edit-ht-segment welding . c quenching to martensite start temperature $ comment
append-ht-segment welding $ append segment 3 "cooling to RT"
edit-ht-segment welding . d n martensite $ define precipitation domain
edit-ht-segment welding . 1 25 cr_weld $ Tend + cooling rate
edit-ht-segment welding . c cooling to room temperature $ comment
elseif (weldcyc==2)
create-heat-treatment welding $ third heat treatment
append-ht-segment welding $ heating to welding peak (START)
edit-ht-segment welding . s 25 $ define start temperature for HT
edit-ht-segment welding . d n martensite $ define precipitation domain
edit-ht-segment welding . 1 T_trans 37.848 $ T_trans (=Tend) + heating rate (37,848 °C/s)
edit-ht-segment welding . c heating from room temperature to A3 temperature $ comment
append-ht-segment welding $ heating to welding peak- change to austenite
edit-ht-segment welding . d n austenite $ define precipitation domain
edit-ht-segment welding . 1 T_weld_fghaz 37.848 $ T_weld_fghaz (=950°C) + heating rate (37,848 °C/s)
edit-ht-segment welding . c heating from A3 to welding peak temperature $ comment

append-ht-segment welding $ welding peak (HOLDING)
edit-ht-segment welding . 2 0 5 $ Tdot + delta_t
edit-ht-segment welding . o +set-precipitation-parameter austenite t g agsfghaz $ modification of austenitic grain size in FGHAZ
edit-ht-segment welding . c exposed to welding peak temperature for 5 s

append-ht-segment welding $ cooling process
edit-ht-segment welding . 1 600 11.25 $ Point T2 (=Tend) + cooling rate
edit-ht-segment welding . c cooling from peak weld temperature to 600 degrees $ comment
append-ht-segment welding $ cooling process
edit-ht-segment welding . 1 T_ms 6.188 $ T_ms (=Tend) + cooling rate
edit-ht-segment welding . o +set-precipitation-parameter martensite t g agsfghaz $ modification of martensite grain size in
FGHAZ
```

```
edit-ht-segment welding . o +set-precipitation-parameter martensite t s sgsfghaz $ modification of martensite lath size in FGHAZ
edit-ht-segment welding . o +set-precipitation-parameter martensite t o sgeffghaz $ modification of martensite lath elongation factor in FGHAZ
edit-ht-segment welding . c quenching from 600 degrees to martensite start temperature $ comment

append-ht-segment welding $ cooling process- change to martensite
edit-ht-segment welding . d n martensite $ define precipitation domain
edit-ht-segment welding . 1 325 6.188 $ Point T3 (=Tend) + cooling rate
edit-ht-segment welding . c cooling form martensite start temperature to 325 degrees $ comment

append-ht-segment welding $ cooling process
edit-ht-segment welding . 1 109 1.836 $ Point T4 (=Tend) + cooling rate
edit-ht-segment welding . c cooling from 325 degrees to 109 degrees
append-ht-segment welding $ cooling process (END)
edit-ht-segment welding . 1 25 1 $ Tend + cooling rate (extrapolated)
edit-ht-segment welding . c cooling to room temperature $ comment
endif
$ ------------------------------ END OF PART III: VIRTUAL WELDING ------------------------------
$ ---------------------------------------- PART IV: PWHT ----------------------------------------
$ The heating-, cooling-rates as well as holding-temperature and -time for the PWHT are out of the
$ "Chart of PWHT for JFE.pdf"
create-heat-treatment pwht $ fourth heat treatment
append-ht-segment pwht $ append segment 0 "tempering"
edit-ht-segment pwht . s 25 $ define start temperature for HT
edit-ht-segment pwht . d n martensite $ define precipitation domain
edit-ht-segment pwht . 1 T_pwht 0.03 $ Tend + heating rate (=110C/h)
edit-ht-segment pwht . c Heating to PWHT temperature with 110C/h $ comment
append-ht-segment pwht $ append segment 1
edit-ht-segment pwht . 2 0 time_pwht $ Tdot + delta_t
edit-ht-segment pwht . c annealing for 120min $ comment
append-ht-segment pwht $ append segment 2
edit-ht-segment pwht . 1 650 0,036 $ Tend + cooling rate(=130C/h)
edit-ht-segment pwht . c cooling to 650C $ comment
append-ht-segment pwht $ append segment 3
edit-ht-segment pwht . 1 560 0.022 $ Tend + cooling rate(=80C/h)
edit-ht-segment pwht . c cooling to 560C $ comment
append-ht-segment pwht $ append segment 4
edit-ht-segment pwht . 1 510 0.014 $ Tend + cooling rate(=50C/h)
edit-ht-segment pwht . c cooling to 510C $ comment
append-ht-segment pwht $ append segment 5
edit-ht-segment pwht . 1 470 0.011 $ Tend + cooling rate(=40C/h)
edit-ht-segment pwht . c cooling to 470C $ comment
append-ht-segment pwht $ append segment 6
edit-ht-segment pwht . 1 25 0.008 $ Tend + cooling rate(=30C/h)
edit-ht-segment pwht . c cooling to room temperature $ comment
$ ---------------------------------- END OF PART IV: PWHT ----------------------------------

$ ---------------------------------------- PART V: SERVICE ----------------------------------------
create-heat-treatment service $ fifth heat treatment
append-ht-segment service $ append segment 1 "tempering"
edit-ht-segment service . s 25 $ define start temperature for HT
edit-ht-segment service . d n martensite $ define precipitation domain
edit-ht-segment service . 1 T_serv 0.033 $ Tend + heating rate
edit-ht-segment service . c Heating to service temperature $ comment
append-ht-segment service $ append segment 2
edit-ht-segment service . 2 0 100*60*60 $ Tdot + delta_t
edit-ht-segment service . o +set-precipitation-parameter martensite t d e ddm_100h $ change dislocation density
edit-ht-segment service . c isothermal service at 600C $ comment: sum=100h
append-ht-segment service $ append segment 3
edit-ht-segment service . 2 0 100*60*60 $ Tdot + delta_t
edit-ht-segment service . o +set-precipitation-parameter martensite t d e ddm_200h $ change dislocation density
edit-ht-segment service . c isothermal service at 600C $ comment: sum=200h
append-ht-segment service $ append segment 4
```

```
edit-ht-segment service . 2 0 100*60*60 $ Tdot + delta_t
edit-ht-segment service . o +set-precipitation-parameter martensite t d e ddm_300h $ change dislocation density
edit-ht-segment service . c isothermal service at 600C $ comment: sum=300h
append-ht-segment service $ append segment 5
edit-ht-segment service . 2 0 100*60*60 $ Tdot + delta_t
edit-ht-segment service . o +set-precipitation-parameter martensite t d e ddm_400h $ change dislocation density
edit-ht-segment service . c isothermal service at 600C $ comment: sum=400h

append-ht-segment service $ append segment 6
edit-ht-segment service . 2 0 100*60*60 $ Tdot + delta_t
edit-ht-segment service . o +set-precipitation-parameter martensite t d e ddm_500h $ change dislocation density
edit-ht-segment service . c isothermal service at 600C $ comment: sum=500h

append-ht-segment service $ append segment 7
edit-ht-segment service . 2 0 100*60*60 $ Tdot + delta_t
edit-ht-segment service . o +set-precipitation-parameter martensite t d e ddm_600h $ change dislocation density
edit-ht-segment service . c isothermal service at 600C $ comment: sum=600h

append-ht-segment service $ append segment 8
edit-ht-segment service . 2 0 100*60*60 $ Tdot + delta_t
edit-ht-segment service . o +set-precipitation-parameter martensite t d e ddm_700h $ change dislocation density
edit-ht-segment service . c isothermal service at 600C $ comment: sum=700h

append-ht-segment service $ append segment 9
edit-ht-segment service . 2 0 100*60*60 $ Tdot+delta_t
edit-ht-segment service . o +set-precipitation-parameter martensite t d e ddm_800h $ change dislocation density
edit-ht-segment service . c isothermal service at 600C $ comment: sum=800h

append-ht-segment service $ append segment 10
edit-ht-segment service . 2 0 100*60*60 $ Tdot+delta_t
edit-ht-segment service . o +set-precipitation-parameter martensite t d e ddm_900h $ change dislocation density
edit-ht-segment service . c isothermal service at 600C $ comment: sum=900h

append-ht-segment service $ append segment 11
edit-ht-segment service . 2 0 100*60*60 $ Tdot+delta_t
edit-ht-segment service . o +set-precipitation-parameter martensite t d e ddm_1000h $ change dislocation density
edit-ht-segment service . c isothermal service at 600C $ comment: sum=1000h

append-ht-segment service $ append segment 12
edit-ht-segment service . 2 0 250*60*60 $ Tdot+delta_t
edit-ht-segment service . o +set-precipitation-parameter martensite t d e ddm_1250h $ change dislocation density
edit-ht-segment service . c isothermal service at 600C $ comment: sum=1250h

append-ht-segment service $ append segment 13
edit-ht-segment service . 2 0 250*60*60 $ Tdot+delta_t
edit-ht-segment service . o +set-precipitation-parameter martensite t d e ddm_1500h $ change dislocation density
edit-ht-segment service . c isothermal service at 600C $ comment: sum=1500h

append-ht-segment service $ append segment 14
edit-ht-segment service . 2 0 500*60*60 $ Tdot+delta_t
edit-ht-segment service . o +set-precipitation-parameter martensite t d e ddm_2000h $ change dislocation density
edit-ht-segment service . c isothermal service at 600C $ comment: sum=2000h

append-ht-segment service $ append segment 15
edit-ht-segment service . 2 0 500*60*60 $ Tdot+delta_t
edit-ht-segment service . o +set-precipitation-parameter martensite t d e ddm_2500h $ change dislocation density
edit-ht-segment service . c isothermal service at 600C $ comment: sum=2500h

append-ht-segment service $ append segment 16
edit-ht-segment service . 2 0 500*60*60 $ Tdot+delta_t
edit-ht-segment service . o +set-precipitation-parameter martensite t d e ddm_3000h $ change dislocation density
edit-ht-segment service . c isothermal service at 600C $ comment: sum=3000h
```

append-ht-segment service $ append segment 17
edit-ht-segment service . 2 0 500*60*60 $ Tdot+delta_t
edit-ht-segment service . o +set-precipitation-parameter martensite t d e ddm_3500h $ change dislocation density
edit-ht-segment service . c isothermal service at 600C $ comment: sum=3500h

append-ht-segment service $ append segment 18
edit-ht-segment service . 2 0 500*60*60 $ Tdot+delta_t
edit-ht-segment service . o +set-precipitation-parameter martensite t d e ddm_4000h $ change dislocation density
edit-ht-segment service . c isothermal service at 600C $ comment: sum=4000h

append-ht-segment service $ append segment 19
edit-ht-segment service . 2 0 500*60*60 $ Tdot+delta_t
edit-ht-segment service . o +set-precipitation-parameter martensite t d e ddm_4500h $ change dislocation density
edit-ht-segment service . c isothermal service at 600C $ comment: sum=4500h

append-ht-segment service $ append segment 20
edit-ht-segment service . 2 0 500*60*60 $ Tdot+delta_t
edit-ht-segment service . o +set-precipitation-parameter martensite t d e ddm_5000h $ change dislocation density
edit-ht-segment service . c isothermal service at 600C $ comment: sum=5000h

append-ht-segment service $ append segment 21
edit-ht-segment service . 2 0 1000*60*60 $ Tdot+delta_t
edit-ht-segment service . o +set-precipitation-parameter martensite t d e ddm_6000h $ change dislocation density
edit-ht-segment service . c isothermal service at 600C $ comment: sum=6000h

append-ht-segment service $ append segment 22
edit-ht-segment service . 2 0 3000*60*60 $ Tdot+delta_t
edit-ht-segment service . o +set-precipitation-parameter martensite t d e ddm_9000h $ change dislocation density
edit-ht-segment service . c isothermal service at 600C $ comment: sum=9000h

append-ht-segment service $ append segment 23
edit-ht-segment service . 2 0 3000*60*60 $ Tdot+delta_t
edit-ht-segment service . o +set-precipitation-parameter martensite t d e ddm_12000h $ change dislocation density
edit-ht-segment service . c isothermal service at 600C $ comment: sum=12000h

append-ht-segment service $ append segment 24
edit-ht-segment service . 2 0 3000*60*60 $ Tdot+delta_t
edit-ht-segment service . o +set-precipitation-parameter martensite t d e ddm_15000h $ change dislocation density
edit-ht-segment service . c isothermal service at 600C $ comment: sum=15000h

append-ht-segment service $ append segment 25
edit-ht-segment service . 2 0 5000*60*60 $ Tdot+delta_t
edit-ht-segment service . o +set-precipitation-parameter martensite t d e ddm_20000h $ change dislocation density
edit-ht-segment service . c isothermal service at 600C $ comment: sum=20000h

append-ht-segment service $ append segment 26
edit-ht-segment service . 2 0 5000*60*60 $ Tdot+delta_t
edit-ht-segment service . o +set-precipitation-parameter martensite t d e ddm_25000h $ change dislocation density
edit-ht-segment service . c isothermal service at 600C $ comment: sum=25000h

append-ht-segment service $ append segment 27
edit-ht-segment service . 2 0 5000*60*60 $ Tdot+delta_t
edit-ht-segment service . o +set-precipitation-parameter martensite t d e ddm_30000h $ change dislocation density
edit-ht-segment service . c isothermal service at 600C $ comment: sum=30000h

append-ht-segment service $ append segment 28
edit-ht-segment service . 2 0 10000*60*60 $ Tdot+delta_t
edit-ht-segment service . o +set-precipitation-parameter martensite t d e ddm_40000h $ change dislocation density
edit-ht-segment service . c isothermal service at 600C $ comment: sum=40000h

append-ht-segment service $ append segment 29
edit-ht-segment service . 2 0 10000*60*60 $ Tdot+delta_t
edit-ht-segment service . o +set-precipitation-parameter martensite t d e ddm_50000h $ change dislocation density

```
edit-ht-segment service . c isothermal service at 600C $ comment: sum=50000h

append-ht-segment service $ append segment 30
edit-ht-segment service . 2 0 10000*60*60 $ Tdot+delta_t
edit-ht-segment service . o +set-precipitation-parameter martensite t d e ddm_60000h $ change dislocation density
edit-ht-segment service . c isothermal service at 600C $ comment: sum=60000h

append-ht-segment service $ append segment 31
edit-ht-segment service . 2 0 10000*60*60 $ Tdot+delta_t
edit-ht-segment service . o +set-precipitation-parameter martensite t d e ddm_70000h $ change dislocation density
edit-ht-segment service . c isothermal service at 600C $ comment: sum=70000h

append-ht-segment service $ append segment 32
edit-ht-segment service . 2 0 10000*60*60 $ Tdot+delta_t
edit-ht-segment service . o +set-precipitation-parameter martensite t d e ddm_80000h $ change dislocation density
edit-ht-segment service . c isothermal service at 600C $ comment: sum=80000h

append-ht-segment service $ append segment 33
edit-ht-segment service . 2 0 10000*60*60 $ Tdot+delta_t
edit-ht-segment service . o +set-precipitation-parameter martensite t d e ddm_90000h $ change dislocation density
edit-ht-segment service . c isothermal service at 600C $ comment: sum=90000h

append-ht-segment service $ append segment 34
edit-ht-segment service . 2 0 10000*60*60 $ Tdot+delta_t
edit-ht-segment service . o +set-precipitation-parameter martensite t d e ddm_100000h $ change dislocation density
edit-ht-segment service . c isothermal service at 600C $ comment: sum=100000h


$ ---------------------------------- END OF PART V: SERVICE ----------------------------------
$ ********************************************************************************************************
$ PRECIPITATION DOMAINS, PRECIPITATES
$ ********************************************************************************************************
$ --------------------------------- PRECIPITATION DOMAINS ----------------------------------------
create-precipitation-domain austenite $ austenite is precipitation domain = matrix
set-precipitation-parameter austenite x fcc_a1 $ matrix phase of domain austenite
set-precipitation-parameter austenite t d e dda $ dislocation density (=1e11 m^-2)
set-precipitation-parameter austenite t g ags $ austenite grain size
create-precipitation-domain martensite $ new matrix: martensite
set-precipitation-parameter martensite x bcc_a2 $ define matrix structure
set-precipitation-parameter martensite t d e ddm $ dislocation density (=1e14 m^-2)
set-precipitation-parameter martensite t g ags $ austenite grain size
set-precipitation-parameter martensite t s sgs $ subgrain size
set-precipitation-parameter martensite t o sgef $ subgrain elongation factor
$ ------------------------------ PRECIPITATE PHASES IN AUSTENITE ----------------------------------
create-new-phase nbc p NbC(aust,g) $ new precipitate phase in austenite
set-precipitation-parameter nbc_p0 c npc $ use variable for prec. classes
set-precipitation-parameter nbc_p0 d austenite $ precipitation domain (matrix phase)
set-precipitation-parameter nbc_p0 n s g $ nucleation sites are grain boundaries
set-precipitation-parameter nbc_p0 n j y $ nucleate only with valid major constituents
set-precipitation-parameter nbc_p0 n p y austenite $ restrict nucleation to precipitation domain

create-new-phase nbc p NbC(aust,d) $ new precipitate phase in austenite
set-precipitation-parameter nbc_p1 c npc $ use variable for prec. classes
set-precipitation-parameter nbc_p1 d austenite $ precipitation domain (matrix phase)
set-precipitation-parameter nbc_p1 n s d $ nucleation sites are dislocations
set-precipitation-parameter nbc_p1 n j y $ nucleate only with valid major constituents
set-precipitation-parameter nbc_p1 n p y austenite $ restrict nucleation to precipitation domain

create-new-phase aln p AlN(aust,d) $ new precipitate phase in austenite
set-precipitation-parameter aln_p0 c npc_aln $ use variable for prec. classes
set-precipitation-parameter aln_p0 d austenite $ precipitation domain (austenite phase)
set-precipitation-parameter aln_p0 n s d $ nucleation sites are dislocations
set-precipitation-parameter aln_p0 n f y $ account for coherent misfit stress
```

```
set-precipitation-parameter aln_p0 t m n 0.27 $ use volumetric misfit value of 0.27
set-precipitation-parameter aln_p0 n p y austenite $ restrict nucleation to precipitation domain
create-new-phase cr2n p Cr2N(aust,d) $ new precipitate phase in austenite
set-precipitation-parameter cr2n_p0 c npc $ use variable for prec. classes
set-precipitation-parameter cr2n_p0 d austenite $ precipitation domain (austenite phase)
set-precipitation-parameter cr2n_p0 n s d $ nucleation sites are dislocations
set-precipitation-parameter cr2n_p0 n p y austenite $ restrict nucleation to precipitation domai

create-new-phase VN p VN(aust,g) $ new precipitate phase VN in martensite
set-precipitation-parameter vn_p0 c npc_vn $ use variable npc for # of prec. classes
set-precipitation-parameter vn_p0 d austenite $ precipitation domain (matrix phase)
set-precipitation-parameter vn_p0 n s g $ nucleation sites at grain boundaries
set-precipitation-parameter vn_p0 n j y $ nucleate only with valid major constituents
set-precipitation-parameter vn_p0 n p y austenite $ restrict nucleation to precipitation domain
$ --------------------------------- PRECIPITATE PHASES IN MARTENSITE ---------------------------------
$ The M7C3 and Cementite precipitates are not stable at 600C, nevertheless they have to be considered
$ in the calculation due to the influence on the M23C6 evolution during heating and cooling treatments.
$ Better agreement with experimental values of M23C6 diameter is achieved by considering the M7C3 and
$ Cementite in the calculation.
create-new-phase nbc p NbC(mart,g) $ new precipitate phase in martensite
set-precipitation-parameter nbc_p2 c npc $ use variable for prec. classes
set-precipitation-parameter nbc_p2 d martensite $ precipitation domain (matrix phase)
set-precipitation-parameter nbc_p2 n s g $ nucleation sites are grain boundaries
set-precipitation-parameter nbc_p2 n j y $ nucleate only with valid major constituents
set-precipitation-parameter nbc_p2 n p y martensite $ restrict nucleation to precipitation domain

create-new-phase nbc p NbC(mart,d) $ new precipitate phase in martensite
set-precipitation-parameter nbc_p3 c npc_nbc $ use variable for prec. classes
set-precipitation-parameter nbc_p3 d martensite $ precipitation domain (matrix phase)
set-precipitation-parameter nbc_p3 n s d $ nucleation sites are dislocations
set-precipitation-parameter nbc_p3 n j y $ nucleate only with valid major constituents
set-precipitation-parameter nbc_p3 n p y martensite $ restrict nucleation to precipitation domain

create-new-phase nbc p NbC(mart,s) $ new precipitate phase in martensite
set-precipitation-parameter nbc_p4 c npc_nbc $ use variable for prec. classes
set-precipitation-parameter nbc_p4 d martensite $ precipitation domain (matrix phase)
set-precipitation-parameter nbc_p4 n s s $ nucleation sites are subgrain boundaries
set-precipitation-parameter nbc_p4 n j y $ nucleate only with valid major constituents
set-precipitation-parameter nbc_p4 n p y martensite $ restrict nucleation to precipitation domain
create-new-phase aln p AlN(mart,d) $ new precipitate phase in martensite
set-precipitation-parameter aln_p1 c npc_aln $ use variable for prec. classes
set-precipitation-parameter aln_p1 d martensite $ precipitation domain (matrix phase)
set-precipitation-parameter aln_p1 n s d $ nucleation sites are dislocations
set-precipitation-parameter aln_p1 n f y $ account for coherent misfit stress
set-precipitation-parameter aln_p1 t m n 0.27 $ use volumetric misfit value of 0.27
set-precipitation-parameter aln_p1 n p y martensite $ restrict nucleation to precipitation domain
create-new-phase VN p VN(mart,g) $ new precipitate phase VN in martensite
set-precipitation-parameter vn_p1 c npc $ use variable npc for # of prec. classes
set-precipitation-parameter vn_p1 d martensite $ precipitation domain (matrix phase)
set-precipitation-parameter vn_p1 n s g $ nucleation sites at grain boundaries
set-precipitation-parameter vn_p1 n j y $ nucleate only with valid major constituents
set-precipitation-parameter vn_p1 n p y martensite $ restrict nucleation to precipitation domain

create-new-phase VN p VN(mart,d) $ new precipitate phase VN in martensite
set-precipitation-parameter vn_p2 c npc $ use variable npc for # of prec. classes
set-precipitation-parameter vn_p2 d martensite $ precipitation domain (matrix phase)
set-precipitation-parameter vn_p2 n s d $ nucleation sites at dislocations
set-precipitation-parameter vn_p2 n j y $ nucleate only with valid major constituents
set-precipitation-parameter vn_p2 n p y martensite $ restrict nucleation to precipitation domain

create-new-phase VN p VN(mart,s) $ new precipitate phase VN in martensite
set-precipitation-parameter vn_p3 c npc_vn $ use variable npc for # of prec. classes
set-precipitation-parameter vn_p3 d martensite $ precipitation domain (matrix phase)
```

```
set-precipitation-parameter vn_p3 n s s $ nucleation sites at subgrain boundaries
set-precipitation-parameter vn_p3 n j y $ nucleate only with valid major constituents
set-precipitation-parameter vn_p3 n p y martensite $ restrict nucleation to precipitation domain
create-new-phase m23c6 p M23C6(mart,s) $ new precipitate phase in martensite
set-precipitation-parameter m23c6_p0 c npc_m23c6 $ use variable for prec. classes
set-precipitation-parameter m23c6_p0 d martensite $ precipitation domain (matrix phase)
set-precipitation-parameter m23c6_p0 n s s $ nucleation sites are subgrains
set-precipitation-parameter m23c6_p0 n p y martensite $ restrict nucleation to precipitation domain

create-new-phase m23c6 p M23C6(mart,g) $ new precipitate phase in martensite
set-precipitation-parameter m23c6_p1 c npc_m23c6 $ use variable for prec. classes
set-precipitation-parameter m23c6_p1 d martensite $ precipitation domain (matrix phase)
set-precipitation-parameter m23c6_p1 n s g $ nucleation sites are grain boundaries
set-precipitation-parameter m23c6_p1 n p y martensite $ restrict nucleation to precipitation domain
create-new-phase m7c3 p M7C3(mart,s) $ new precipitate phase M7C3 in martensite
set-precipitation-parameter m7c3_p0 c npc $ use variable for prec. classes
set-precipitation-parameter m7c3_p0 d martensite $ precipitation domain (matrix phase)
set-precipitation-parameter m7c3_p0 n s s $ nucleation sites at subgrain boundaries
set-precipitation-parameter m7c3_p0 n p y martensite $ restrict nucleation to precipitation domain
create-new-phase cementite p Cem(mart,s) $ new precipitate cementite in martensite
set-precipitation-parameter cementite_p0 c npc $ use variable for prec. classes
set-precipitation-parameter cementite_p0 d martensite $ precipitation domain (matrix phase)
set-precipitation-parameter cementite_p0 n s s $ nucleation sites at grain boundaries
set-precipitation-parameter cementite_p0 n p y martensite $ restrict nucleation to prec. domain
create-new-phase cr2n p Cr2N(mart,d) $ new precipitate phase in martensite
set-precipitation-parameter cr2n_p1 c npc $ use variable for prec. classes
set-precipitation-parameter cr2n_p1 d martensite $ precipitation domain (matrix phase)
set-precipitation-parameter cr2n_p1 n s d $ nucleation sites are dislocations
set-precipitation-parameter cr2n_p1 n p y martensite $ restrict nucleation to precipitation domai
create-new-phase laves_phase p Laves(mart,s) $ new precipitate phase in martensite
set-precipitation-parameter laves_phase_p0 c npc_laves $ use variable for prec. classes
set-precipitation-parameter laves_phase_p0 d martensite $ precipitation domain (matrix phase)
set-precipitation-parameter laves_phase_p0 n s s $ nucleation sites are subgrains
set-precipitation-parameter laves_phase_p0 n p y martensite $ restrict nucleation to precipitation domain
set-precipitation-parameter laves_phase_p0 f y lav_ict $ diffuse interface correction is set on
$ Zet-phase has special settings due to the fact that it nucleates within the VN precipitates
$ and nucleation is defined as special nucleation model for precipitation on particles with
$ equivalent interfacial energy. Make sure that 'direct particle transformation' is selected as
$ nucleation model
$ IMPORTANT: The value for the equivalent interfacial energy is basically unknown and must
$ be considered as a fitting parameter!!! Presently, no physical model for Z-phase nucleation
$ is available!!!
create-new-phase zet p Z(m,vn_a_g) $ new prec. phase for Zet-phase in martensite
set-precipitation-parameter zet_p0 c npc $ use variable for prec. classes
set-precipitation-parameter zet_p0 d martensite $ precipitation domain (matrix phase)
set-precipitation-parameter zet_p0 n s p vn_p0 $ nucleation sites are existing VN prec.
set-precipitation-parameter zet_p0 n o e eie_zet $ use equiv. intf. energy with value 1
set-precipitation-parameter zet_p0 n n d $ use direct particle transf. nucl. model
set-precipitation-parameter zet_p0 n p y martensite $ restrict nucleation to precipitation domain

create-new-phase zet p Z(m,vn_m_g) $ new prec. phase for Zet-phase in martensite
set-precipitation-parameter zet_p1 c npc $ use variable for prec. classes
set-precipitation-parameter zet_p1 d martensite $ precipitation domain (matrix phase)
set-precipitation-parameter zet_p1 n s p vn_p1 $ nucleation sites are existing VN prec.
set-precipitation-parameter zet_p1 n o e eie_zet $ use equiv. intf. energy with value 1
set-precipitation-parameter zet_p1 n n d $ use direct particle transf. nucl. model
set-precipitation-parameter zet_p1 n p y martensite $ restrict nucleation to precipitation domain

create-new-phase zet p Z(mart,vn_m_d) $ new prec. phase for Zet-phase in martensite
set-precipitation-parameter zet_p2 c npc $ use variable for prec. classes
set-precipitation-parameter zet_p2 d martensite $ precipitation domain (matrix phase)
set-precipitation-parameter zet_p2 n s p vn_p2 $ nucleation sites are existing VN prec.
set-precipitation-parameter zet_p2 n o e eie_zet $ use equiv. intf. energy with value 1
```

```
set-precipitation-parameter zet_p2 n n d $ use direct particle transf. nucl. model
set-precipitation-parameter zet_p2 n p y martensite $ restrict nucleation to precipitation domain

create-new-phase zet p Z(mart,vn_m_s) $ new prec. phase for Zet-phase in martensite
set-precipitation-parameter zet_p3 c npc $ use variable for prec. classes
set-precipitation-parameter zet_p3 d martensite $ precipitation domain (matrix phase)
set-precipitation-parameter zet_p3 n s p vn_p3 $ nucleation sites are existing VN prec.
set-precipitation-parameter zet_p3 n o e eie_zet $ use equiv. intf. energy with value 1
set-precipitation-parameter zet_p3 n n d $ use direct particle transf. nucl. model
set-precipitation-parameter zet_p3 n p y martensite $ restrict nucleation to precipitation domain
$ Zet-phase can also nucleate directly from the matrix. However, its nuclei with rather complex
$ crystal structure is in direct competition with the MX phase with simple fcc. For that reason,
$ the probability of Z-phase nucleation is extremely low, because Cr, V and N will nucleate the simple
$ structure much easier than the double-layer structure of Zet. Estimates (Sonderegger/Danielsen/
$ Kozeschnik, 2005, unpublished) deliver a factor of 1e-12. This value is entered as nucleation
$ constant, to reflect this competitive (entropic) effect
create-new-phase zet p Z(mart,d) $ new prec. phase for Zet-phase in martensite
set-precipitation-parameter zet_p4 c npc $ use variable for prec. classes
set-precipitation-parameter zet_p4 d martensite $ precipitation domain (matrix phase)
set-precipitation-parameter zet_p4 n s d $ nucleation sites are dislocation
set-precipitation-parameter zet_p4 z n $ no ie size correction for Z-Phase
set-precipitation-parameter zet_p4 n u nucl_const_zet $ nucleation constant for matrix Z-phase
set-precipitation-parameter zet_p4 n p y martensite $ restrict nucleation to precipitation domain
$ ****************************************************************************************************
$ ********************************** OUTPUT WINDOWS, PLOTS, ETC. ***********************************
$ ****************************************************************************************************
$ -------------------------------- Hardening (Normalizing) plot ----------------------------------
$ create one frame displaying the service part, with no exp data
new-gui-window p1 $ generate new plot: Hardening
$ remember window ID to address it correctly later in the script
set-variable-value window_id_hardening active_frame_id $ save windows id to variable
set-gui-window-property . x stepvalue $ default x-axis variable (time)
set-gui-window-property . s u y $ use default x-axis for all plots: yes
set-gui-window-property . s t time / min $ default x-axis title
set-gui-window-property . s f 1/60 $ scaling factor is 1/60 for min
set-gui-window-property . n 2 $ 2 plot columns
set-plot-option . s n b t$c $ add series: temperature
set-plot-option . s m -1 t$c T $ define series legend
set-plot-option . a y 1 t temperature / C $ y-axis title
if (comp==1)
set-plot-option . t Raccord-HiMAT-Normalizing $ define plot title
elseif (comp==2)
set-plot-option . t Raccord-TUGraz-Normalizing $ define plot title
endif
create-new-plot x . $ create new plot: phase fractions
set-plot-option . l a y $ replace variable names by kinetic alias
set-plot-option . s n b f_prec$* $ add all series: phase fractions of prec.
set-plot-option . a y 1 t phase fraction / % $ y-axis title
set-plot-option . a y 1 y log $ use logarithmic scale for y-axis
set-plot-option . a y 1 f 100 $ scaling factor is 100 for %
set-plot-option . a y 1 s 1e-4.. $ scale the y-axis from 1e-4..
create-new-plot x . $ create new plot: mean diameter
set-plot-option . l a y $ replace variable names by kinetic alias
set-plot-option . s n b d_mean$* $ add all series: mean diameter of precipitates
set-plot-option . a y 1 t mean diameter / nm $ change y-axis title
set-plot-option . a y 1 y lin $ use linear scale for y-axis
set-plot-option . a y 1 f 1e9 $ scaling factor is 1e9 for nm
create-new-plot x . $ create new plot: number densities
set-plot-option . l a y $ replace all variable names by kinetic alias
set-plot-option . s n b num_part$* $ add all series: number densities of precipitates
set-plot-option . a y 1 t number density / m<sup>-3</sup> $ change y-axis title
set-plot-option . a y 1 y log $ use logarithmic scale for y-axis
set-plot-option . a y 1 s 1e10.. $ scale the y-axis from 1e10..
```

```
move-gui-window . 70 30 700 980 $ move window to new position and resize
update-gui-windows . $ update the GUI window
move-gui-window . hide $ hide plot
$ ---------------------------------------- Tempering ----------------------------------------
$ create one frame displaying the service part, with no exp data
new-gui-window p1 $ generate new plot: Tempering
$ remember window ID to address it correctly later in the script
set-variable-value window_id_tempering active_frame_id $ save windows id to variable
set-gui-window-property . x stepvalue $ default x-axis variable (time)
set-gui-window-property . s u y $ use default x-axis for all plots: yes
set-gui-window-property . s t time / min $ default x-axis title
set-gui-window-property . s f 1/60 $ scaling factor is 1/60 for min
set-gui-window-property . n 2 $ 2 plot columns
set-plot-option . s n b t$c $ add series: temperature
set-plot-option . s m -1 t$c T $ define series legend
set-plot-option . a y 1 t temperature / C $ y-axis title
if (comp==1)
set-plot-option . t Raccord-HiMAT-Tempering $ define plot title
elseif (comp==2)
set-plot-option . t Raccord-TUGraz-Tempering $ define plot title
endif
create-new-plot x . $ create new plot: phase fractions
set-plot-option . l a y $ replace variable names by kinetic alias
set-plot-option . s n b f_prec$* $ add all series: phase fractions of prec.
set-plot-option . a y 1 t phase fraction / % $ y-axis title
set-plot-option . a y 1 y log $ use logarithmic scale for y-axis
set-plot-option . a y 1 f 100 $ scaling factor is 100 for %
set-plot-option . a y 1 s 1e-4.. $ scale the y-axis from 1e-4..
create-new-plot x . $ create new plot: mean diameter
set-plot-option . l a y $ replace variable names by kinetic alias
set-plot-option . s n b d_mean$* $ add all series: mean diameter of precipitates
set-plot-option . a y 1 t mean diameter / nm $ change y-axis title
set-plot-option . a y 1 y lin $ use linear scale for y-axis
set-plot-option . a y 1 f 1e9 $ scaling factor is 1e9 for nm
create-new-plot x . $ create new plot: number densities
set-plot-option . l a y $ replace all variable names by kinetic alias
set-plot-option . s n b num_part$* $ add all series: number densities of precipitates
set-plot-option . a y 1 t number density / m<sup>-3</sup> $ change y-axis title
set-plot-option . a y 1 y log $ use logarithmic scale for y-axis
set-plot-option . a y 1 s 1e10.. $ scale the y-axis from 1e10..
move-gui-window . 90 50 700 980 $ move window to new position and resize
update-gui-windows . $ update the GUI window
move-gui-window . hide $ hide plot
$ ---------------------------------------- Welding ----------------------------------------
$ create one frame displaying the service part, with no exp data
new-gui-window p1 $ generate new plot: Welding
$ remember window ID to address it correctly later in the script
set-variable-value window_id_welding active_frame_id $ save windows id to variable
set-gui-window-property . x stepvalue $ default x-axis variable (time)
set-gui-window-property . s u y $ use default x-axis for all plots: yes
set-gui-window-property . s t time / min $ default x-axis title
set-gui-window-property . s f 1/60 $ scaling factor is 1/60 for min
set-gui-window-property . n 2 $ 2 plot columns
set-plot-option . s n b t$c $ add series: temperature
set-plot-option . s m -1 t$c T $ define series legend
set-plot-option . a y 1 t temperature / C $ y-axis title
if (comp==1)
set-plot-option . t Raccord-HiMAT-Welding-FGHAZ $ define plot title
elseif (comp==2)
set-plot-option . t Raccord-TUGraz-Welding-FGHAZ $ define plot title
endif

create-new-plot x . $ create new plot: phase fractions
```

```
set-plot-option . l a y $ replace variable names by kinetic alias
set-plot-option . s n b f_prec$* $ add all series: phase fractions of prec.
set-plot-option . a y 1 t phase fraction / % $ y-axis title
set-plot-option . a y 1 y log $ use logarithmic scale for y-axis
set-plot-option . a y 1 f 100 $ scaling factor is 100 for %
set-plot-option . a y 1 s 1e-4.. $ scale the y-axis from 1e-4..
create-new-plot x . $ create new plot: mean diameter
set-plot-option . l a y $ replace variable names by kinetic alias
set-plot-option . s n b d_mean$* $ add all series: mean diameter of precipitates
set-plot-option . a y 1 t mean diameter / nm $ change y-axis title
set-plot-option . a y 1 y lin $ use linear scale for y-axis
set-plot-option . a y 1 f 1e9 $ scaling factor is 1e9 for nm
create-new-plot x . $ create new plot: number densities
set-plot-option . l a y $ replace all variable names by kinetic alias
set-plot-option . s n b num_part$* $ add all series: number densities of precipitates
set-plot-option . a y 1 t number density / m<sup>-3</sup> $ change y-axis title
set-plot-option . a y 1 y log $ use logarithmic scale for y-axis
set-plot-option . a y 1 s 1e10.. $ scale the y-axis from 1e10..
move-gui-window . 110 70 700 980 $ move window to new position and resize
update-gui-windows . $ update the GUI window
move-gui-window . hide $ hide plot
$ ----------------------------------------- PWHT -----------------------------------------
$ create one frame displaying the service part, with no exp data
new-gui-window p1 $ generate new plot: PWHT
$ remember window ID to address it correctly later in the script
set-variable-value window_id_pwht active_frame_id $ save windows id to variable
set-gui-window-property . x stepvalue $ default x-axis variable (time)
set-gui-window-property . s u y $ use default x-axis for all plots: yes
set-gui-window-property . s t time / min $ default x-axis title
set-gui-window-property . s f 1/60 $ scaling factor is 1/60 for min
set-gui-window-property . n 2 $ 2 plot columns
set-plot-option . s n b t$c $ add series: temperature
set-plot-option . s m -1 t$c T $ define series legend
set-plot-option . a y 1 t temperature / C $ y-axis title
if (comp==1)
set-plot-option . t Raccord-HiMAT-PWHT-FGHAZ $ define plot title
elseif (comp==2)
set-plot-option . t Raccord-TUGraz-PWHT-FGHAZ $ define plot title
endif
create-new-plot x . $ create new plot: phase fractions
set-plot-option . l a y $ replace variable names by kinetic alias
set-plot-option . s n b f_prec$* $ add all series: phase fractions of prec.
set-plot-option . a y 1 t phase fraction / % $ y-axis title
set-plot-option . a y 1 y log $ use logarithmic scale for y-axis
set-plot-option . a y 1 f 100 $ scaling factor is 100 for %
set-plot-option . a y 1 s 1e-4.. $ scale the y-axis from 1e-4..
create-new-plot x . $ create new plot: mean diameter
set-plot-option . l a y $ replace variable names by kinetic alias
set-plot-option . s n b d_mean$* $ add all series: mean diameter of precipitates
set-plot-option . a y 1 t mean diameter / nm $ change y-axis title
set-plot-option . a y 1 y lin $ use linear scale for y-axis
set-plot-option . a y 1 f 1e9 $ scaling factor is 1e9 for nm
create-new-plot x . $ create new plot: number densities
set-plot-option . l a y $ replace all variable names by kinetic alias
set-plot-option . s n b num_part$* $ add all series: number densities of precipitates
set-plot-option . a y 1 t number density / m<sup>-3</sup> $ change y-axis title
set-plot-option . a y 1 y log $ use logarithmic scale for y-axis
set-plot-option . a y 1 s 1e10.. $ scale the y-axis from 1e10..
move-gui-window . 130 90 700 980 $ move window to new position and resize
update-gui-windows . $ update the GUI window
move-gui-window . hide $ hide plot
$ ----------------------------------------- Service -----------------------------------------
$ create one frame displaying the service part, with no exp data
```

```
new-gui-window p1 $ generate new plot: Service
$ remember window ID to address it correctly later in the script
set-variable-value window_id_service active_frame_id $ save windows id to variable
set-gui-window-property . x stepvalue $ default x-axis variable (time)
set-gui-window-property . s u y $ use default x-axis for all plots: yes
set-gui-window-property . s t time / h $ default x-axis title
set-gui-window-property . s f 1/3600 $ scaling factor is 1/3600 for h
set-gui-window-property . n 2 $ 2 plot columns
set-plot-option . s n b t$c $ add series: temperature
set-plot-option . s m -1 t$c T $ define series legend
set-plot-option . a y 1 t temperature / C $ y-axis title
if (comp==1)
set-plot-option . t Raccord-HiMAT-Service-FGHAZ $ define plot title
elseif (comp==2)
set-plot-option . t Raccord-TUGraz-Service-FGHAZ $ define plot title
endif
create-new-plot x . $ create new plot: phase fractions
set-plot-option . l a y $ replace variable names by kinetic alias
set-plot-option . s n b f_prec$* $ add all series: phase fractions of prec.
set-plot-option . a y 1 t phase fraction / % $ y-axis title
set-plot-option . a y 1 y log $ use logarithmic scale for y-axis
set-plot-option . a y 1 f 100 $ scaling factor is 100 for %
set-plot-option . a y 1 s 1e-4.. $ scale the y-axis from 1e-4..
create-new-plot x . $ create new plot: mean diameter
set-plot-option . l a y $ replace variable names by kinetic alias
set-plot-option . s n b d_mean$* $ add all series: mean diameter of precipitates
set-plot-option . a y 1 t mean diameter / nm $ change y-axis title
set-plot-option . a y 1 y lin $ use linear scale for y-axis
set-plot-option . a y 1 f 1e9 $ scaling factor is 1e9 for nm
create-new-plot x . $ create new plot: number densities
set-plot-option . l a y $ replace all variable names by kinetic alias
set-plot-option . s n b num_part$* $ add all series: number densities of precipitates
set-plot-option . a y 1 t number density / m<sup>-3</sup> $ change y-axis title
set-plot-option . a y 1 y log $ use logarithmic scale for y-axis
set-plot-option . a y 1 s 1e10.. $ scale the y-axis from 1e10..
move-gui-window . 150 110 700 980 $ move window to new position and resize
update-gui-windows . $ update the GUI window
move-gui-window . hide $ hide plot
$ ********************************************************************************************************
$ ************************** START PRECIPITATE SIMULATION ***********************************************
$ ********************************************************************************************************
set-temperature-celsius 2000 $ define something
set-automatic-startvalues $ initiate equil. calc. (estimate variables)
calculate-equilibrium $ calculate equilibrium state
$ speed up simulations, modify numerical parameters
set-simulation-parameter c n f 1.0 $ maximum radius growth from 0.2 to 1.0
set-simulation-parameter u 1000
$ ------------------------ START PRECIPITATE SIMULATION PART I (HARDENING) -------------------------
rename-current-buffer hardening $ rename buffer for heat treatment
set-gui-window-property window_id_hardening b hardening $ attach to buffer window
set-simulation-parameter t h hardening 10 $ temperature profile from HT, max. T-step
set-simulation-parameter s r $ starting condition for prec. sim.: reset
move-gui-window window_id_hardening show $ bring plot to front
$ hide console window to make plots visible
move-gui-window c hide $ hide console window
start-precipitate-simulation $ let's go with part I
$ save state after simulation. Is starting point for next simulation part II
create-calc-state after_hardening
$ ---------------------- START PRECIPITATE SIMULATION PART II (TEMPERING)----------------------------
create-calc-buffer tempering $ create buffer for HT
select-calc-buffer tempering $ select calc buffer
set-gui-window-property window_id_tempering b tempering $ attach to buffer window
set-simulation-parameter t h tempering 10 $ temperature profile from HT, max. T-step
```

```
set-simulation-parameter s l after_hardening $ starting condition for prec. sim.: reset
move-gui-window window_id_tempering show $ bring plot to front
start-precipitate-simulation $ let's go with part II
$ save state after simulation. Is starting point for next simulation part III
create-calc-state after_tempering
$ ---------- START PRECIPITATE SIMULATION PART III (WELDING)----------
create-calc-buffer welding $ create buffer for HT
select-calc-buffer welding $ select calc buffer
set-gui-window-property window_id_welding b welding $ attach to buffer window
set-simulation-parameter t h welding 10 $ temperature profile from HT, max. T-step
set-simulation-parameter s l after_tempering $ starting condition for prec. sim.: reset
move-gui-window window_id_welding show $ bring plot to front
start-precipitate-simulation $ let's go with part II
$ save state after simulation. Is starting point for next simulation part IV
create-calc-state after_welding

$ increase matrix diffusion enhancement factor to 8 before start of PWHT

$set-precipitation-parameter nbc_p0 s m s mdef $ individual matrix diff. enh. factor
$set-precipitation-parameter nbc_p1 s m s mdef $ individual matrix diff. enh. factor
$set-precipitation-parameter nbc_p2 s m s mdef $ individual matrix diff. enh. factor
$set-precipitation-parameter nbc_p3 s m s mdef $ individual matrix diff. enh. factor
$set-precipitation-parameter nbc_p4 s m s mdef $ individual matrix diff. enh. factor
set-precipitation-parameter aln_p0 s m s mdef $ individual matrix diff. enh. factor
set-precipitation-parameter aln_p1 s m s mdef $ individual matrix diff. enh. factor
$set-precipitation-parameter cr2n_p0 s m s mdef $ individual matrix diff. enh. factor
$set-precipitation-parameter cr2n_p1 s m s mdef $ individual matrix diff. enh. factor
$set-precipitation-parameter vn_p0 s m s mdef $ individual matrix diff. enh. factor
$set-precipitation-parameter vn_p1 s m s mdef $ individual matrix diff. enh. factor
$set-precipitation-parameter vn_p2 s m s mdef $ individual matrix diff. enh. factor
$set-precipitation-parameter vn_p3 s m s mdef $ individual matrix diff. enh. factor
set-precipitation-parameter m23c6_p0 s m s mdef $ individual matrix diff. enh. factor
set-precipitation-parameter m23c6_p1 s m s mdef $ individual matrix diff. enh. factor
$set-precipitation-parameter m7c3_p0 s m s mdef $ individual matrix diff. enh. factor
$set-precipitation-parameter cementite_p0 s m s mdef $ individual matrix diff. enh. factor
set-precipitation-parameter laves_phase_p0 s m s mdef $ individual matrix diff. enh. factor
$set-precipitation-parameter zet_p0 s m s mdef $ individual matrix diff. enh. factor
$set-precipitation-parameter zet_p1 s m s mdef $ individual matrix diff. enh. factor
$set-precipitation-parameter zet_p2 s m s mdef $ individual matrix diff. enh. factor
$set-precipitation-parameter zet_p3 s m s mdef $ individual matrix diff. enh. factor
$set-precipitation-parameter zet_p4 s m s mdef $ individual matrix diff. enh. factor
$ ---------- START PRECIPITATE SIMULATION PART IV (PWHT)----------
create-calc-buffer pwht $ create buffer for HT
select-calc-buffer pwht $ select calc buffer
set-gui-window-property window_id_pwht b pwht $ attach to buffer window
set-simulation-parameter t h pwht 10 $ temperature profile from HT, max. T-step
set-simulation-parameter s l after_welding $ starting condition for prec. sim.: reset
move-gui-window window_id_pwht show $ bring plot to front
start-precipitate-simulation $ let's go with part II
$ save state after simulation. Is starting point for next simulation part V
create-calc-state after_pwht
$ ---------- START PRECIPITATE SIMULATION PART V (SERVICE)----------
create-calc-buffer service $ create buffer for HT
select-calc-buffer service $ select calc buffer
set-gui-window-property window_id_service b service $ attach to buffer window
set-simulation-parameter t h service 10 $ temperature profile from HT, max. T-step
set-simulation-parameter s l after_pwht $ starting condition for prec. sim.: reset
move-gui-window window_id_service show $ bring plot to front
start-precipitate-simulation $ let's go with part III
$ save state after simulation.
create-calc-state after_service
if (comp==1)
set-working-directory C:/Users/Florian/Desktop/Diplomarbeit/Unterlagen_Schlachi/JFE Steel
```

```
save-workspace JFE_5_service
elseif(comp==2)
set-working-directory C:/Users/students/Desktop/FinalVersion4/Results
save-workspace P91_FGHAZ_76_9_0.5_ict_laves1452K_agsfghaz950C_650C_100000h_mdef8
endif

$ ****************************** PRECIPITATE SIMULATION FINISHED
(FGHAZ)******************************
$ ********************************************************************************************************************
elseif (salo==2)
$ ------------------------------------- PART III: SERVICE ----------------------------------------
create-heat-treatment service $ fifth heat treatment
append-ht-segment service $ append segment 1 "tempering"
edit-ht-segment service . s 25 $ define start temperature for HT
edit-ht-segment service . d n martensite $ define precipitation domain
edit-ht-segment service . 1 T_serv 0.033 $ Tend + heating rate
edit-ht-segment service . c Heating to service temperature $ comment
append-ht-segment service $ append segment 2
edit-ht-segment service . 2 0 100*60*60 $ Tdot + delta_t
edit-ht-segment service . o +set-precipitation-parameter martensite t d e ddm_100h $ change dislocation density
edit-ht-segment service . c isothermal service at 600C $ comment: sum=100h
append-ht-segment service $ append segment 3
edit-ht-segment service . 2 0 100*60*60 $ Tdot + delta_t
edit-ht-segment service . o +set-precipitation-parameter martensite t d e ddm_200h $ change dislocation density
edit-ht-segment service . c isothermal service at 600C $ comment: sum=200h
append-ht-segment service $ append segment 4
edit-ht-segment service . 2 0 100*60*60 $ Tdot + delta_t
edit-ht-segment service . o +set-precipitation-parameter martensite t d e ddm_300h $ change dislocation density
edit-ht-segment service . c isothermal service at 600C $ comment: sum=300h
append-ht-segment service $ append segment 5
edit-ht-segment service . 2 0 100*60*60 $ Tdot + delta_t
edit-ht-segment service . o +set-precipitation-parameter martensite t d e ddm_400h $ change dislocation density
edit-ht-segment service . c isothermal service at 600C $ comment: sum=400h

append-ht-segment service $ append segment 6
edit-ht-segment service . 2 0 100*60*60 $ Tdot + delta_t
edit-ht-segment service . o +set-precipitation-parameter martensite t d e ddm_500h $ change dislocation density
edit-ht-segment service . c isothermal service at 600C $ comment: sum=500h

append-ht-segment service $ append segment 7
edit-ht-segment service . 2 0 100*60*60 $ Tdot + delta_t
edit-ht-segment service . o +set-precipitation-parameter martensite t d e ddm_600h $ change dislocation density
edit-ht-segment service . c isothermal service at 600C $ comment: sum=600h

append-ht-segment service $ append segment 8
edit-ht-segment service . 2 0 100*60*60 $ Tdot + delta_t
edit-ht-segment service . o +set-precipitation-parameter martensite t d e ddm_700h $ change dislocation density
edit-ht-segment service . c isothermal service at 600C $ comment: sum=700h

append-ht-segment service $ append segment 9
edit-ht-segment service . 2 0 100*60*60 $ Tdot+delta_t
edit-ht-segment service . o +set-precipitation-parameter martensite t d e ddm_800h $ change dislocation density
edit-ht-segment service . c isothermal service at 600C $ comment: sum=800h

append-ht-segment service $ append segment 10
edit-ht-segment service . 2 0 100*60*60 $ Tdot+delta_t
edit-ht-segment service . o +set-precipitation-parameter martensite t d e ddm_900h $ change dislocation density
edit-ht-segment service . c isothermal service at 600C $ comment: sum=900h

append-ht-segment service $ append segment 11
edit-ht-segment service . 2 0 100*60*60 $ Tdot+delta_t
edit-ht-segment service . o +set-precipitation-parameter martensite t d e ddm_1000h $ change dislocation density
edit-ht-segment service . c isothermal service at 600C $ comment: sum=1000h
```

```
append-ht-segment service $ append segment 12
edit-ht-segment service . 2 0 250*60*60 $ Tdot+delta_t
edit-ht-segment service . o +set-precipitation-parameter martensite t d e ddm_1250h $ change dislocation density
edit-ht-segment service . c isothermal service at 600C $ comment: sum=1250h

append-ht-segment service $ append segment 13
edit-ht-segment service . 2 0 250*60*60 $ Tdot+delta_t
edit-ht-segment service . o +set-precipitation-parameter martensite t d e ddm_1500h $ change dislocation density
edit-ht-segment service . c isothermal service at 600C $ comment: sum=1500h

append-ht-segment service $ append segment 14
edit-ht-segment service . 2 0 500*60*60 $ Tdot+delta_t
edit-ht-segment service . o +set-precipitation-parameter martensite t d e ddm_2000h $ change dislocation density
edit-ht-segment service . c isothermal service at 600C $ comment: sum=2000h

append-ht-segment service $ append segment 15
edit-ht-segment service . 2 0 500*60*60 $ Tdot+delta_t
edit-ht-segment service . o +set-precipitation-parameter martensite t d e ddm_2500h $ change dislocation density
edit-ht-segment service . c isothermal service at 600C $ comment: sum=2500h

append-ht-segment service $ append segment 16
edit-ht-segment service . 2 0 500*60*60 $ Tdot+delta_t
edit-ht-segment service . o +set-precipitation-parameter martensite t d e ddm_3000h $ change dislocation density
edit-ht-segment service . c isothermal service at 600C $ comment: sum=3000h

append-ht-segment service $ append segment 17
edit-ht-segment service . 2 0 500*60*60 $ Tdot+delta_t
edit-ht-segment service . o +set-precipitation-parameter martensite t d e ddm_3500h $ change dislocation density
edit-ht-segment service . c isothermal service at 600C $ comment: sum=3500h

append-ht-segment service $ append segment 18
edit-ht-segment service . 2 0 500*60*60 $ Tdot+delta_t
edit-ht-segment service . o +set-precipitation-parameter martensite t d e ddm_4000h $ change dislocation density
edit-ht-segment service . c isothermal service at 600C $ comment: sum=4000h

append-ht-segment service $ append segment 19
edit-ht-segment service . 2 0 500*60*60 $ Tdot+delta_t
edit-ht-segment service . o +set-precipitation-parameter martensite t d e ddm_4500h $ change dislocation density
edit-ht-segment service . c isothermal service at 600C $ comment: sum=4500h

append-ht-segment service $ append segment 20
edit-ht-segment service . 2 0 500*60*60 $ Tdot+delta_t
edit-ht-segment service . o +set-precipitation-parameter martensite t d e ddm_5000h $ change dislocation density
edit-ht-segment service . c isothermal service at 600C $ comment: sum=5000h

append-ht-segment service $ append segment 21
edit-ht-segment service . 2 0 1000*60*60 $ Tdot+delta_t
edit-ht-segment service . o +set-precipitation-parameter martensite t d e ddm_6000h $ change dislocation density
edit-ht-segment service . c isothermal service at 600C $ comment: sum=6000h

append-ht-segment service $ append segment 22
edit-ht-segment service . 2 0 3000*60*60 $ Tdot+delta_t
edit-ht-segment service . o +set-precipitation-parameter martensite t d e ddm_9000h $ change dislocation density
edit-ht-segment service . c isothermal service at 600C $ comment: sum=9000h

append-ht-segment service $ append segment 23
edit-ht-segment service . 2 0 3000*60*60 $ Tdot+delta_t
edit-ht-segment service . o +set-precipitation-parameter martensite t d e ddm_12000h $ change dislocation density
edit-ht-segment service . c isothermal service at 600C $ comment: sum=12000h

append-ht-segment service $ append segment 24
edit-ht-segment service . 2 0 3000*60*60 $ Tdot+delta_t
```

```
edit-ht-segment service . o +set-precipitation-parameter martensite t d e ddm_15000h $ change dislocation density
edit-ht-segment service . c isothermal service at 600C $ comment: sum=15000h

append-ht-segment service $ append segment 25
edit-ht-segment service . 2 0 5000*60*60 $ Tdot+delta_t
edit-ht-segment service . o +set-precipitation-parameter martensite t d e ddm_20000h $ change dislocation density
edit-ht-segment service . c isothermal service at 600C $ comment: sum=20000h

append-ht-segment service $ append segment 26
edit-ht-segment service . 2 0 5000*60*60 $ Tdot+delta_t
edit-ht-segment service . o +set-precipitation-parameter martensite t d e ddm_25000h $ change dislocation density
edit-ht-segment service . c isothermal service at 600C $ comment: sum=25000h

append-ht-segment service $ append segment 27
edit-ht-segment service . 2 0 5000*60*60 $ Tdot+delta_t
edit-ht-segment service . o +set-precipitation-parameter martensite t d e ddm_30000h $ change dislocation density
edit-ht-segment service . c isothermal service at 600C $ comment: sum=30000h

append-ht-segment service $ append segment 28
edit-ht-segment service . 2 0 10000*60*60 $ Tdot+delta_t
edit-ht-segment service . o +set-precipitation-parameter martensite t d e ddm_40000h $ change dislocation density
edit-ht-segment service . c isothermal service at 600C $ comment: sum=40000h

append-ht-segment service $ append segment 29
edit-ht-segment service . 2 0 10000*60*60 $ Tdot+delta_t
edit-ht-segment service . o +set-precipitation-parameter martensite t d e ddm_50000h $ change dislocation density
edit-ht-segment service . c isothermal service at 600C $ comment: sum=50000h

append-ht-segment service $ append segment 30
edit-ht-segment service . 2 0 10000*60*60 $ Tdot+delta_t
edit-ht-segment service . o +set-precipitation-parameter martensite t d e ddm_60000h $ change dislocation density
edit-ht-segment service . c isothermal service at 600C $ comment: sum=60000h

append-ht-segment service $ append segment 31
edit-ht-segment service . 2 0 10000*60*60 $ Tdot+delta_t
edit-ht-segment service . o +set-precipitation-parameter martensite t d e ddm_70000h $ change dislocation density
edit-ht-segment service . c isothermal service at 600C $ comment: sum=70000h

append-ht-segment service $ append segment 32
edit-ht-segment service . 2 0 10000*60*60 $ Tdot+delta_t
edit-ht-segment service . o +set-precipitation-parameter martensite t d e ddm_80000h $ change dislocation density
edit-ht-segment service . c isothermal service at 600C $ comment: sum=80000h

append-ht-segment service $ append segment 33
edit-ht-segment service . 2 0 10000*60*60 $ Tdot+delta_t
edit-ht-segment service . o +set-precipitation-parameter martensite t d e ddm_90000h $ change dislocation density
edit-ht-segment service . c isothermal service at 600C $ comment: sum=90000h

append-ht-segment service $ append segment 34
edit-ht-segment service . 2 0 10000*60*60 $ Tdot+delta_t
edit-ht-segment service . o +set-precipitation-parameter martensite t d e ddm_100000h $ change dislocation density
edit-ht-segment service . c isothermal service at 600C $ comment: sum=100000h
$ ---------------------------------- END OF PART V: SERVICE ----------------------------------
$ ********************************************************************************************************
$ PRECIPITATION DOMAINS, PRECIPITATES
$ ********************************************************************************************************

create-precipitation-domain austenite $ austenite is precipitation domain = matrix
set-precipitation-parameter austenite x fcc_a1 $ matrix phase of domain austenite
set-precipitation-parameter austenite t d e dda $ dislocation density (=1e11 m^-2)
set-precipitation-parameter austenite t g ags $ austenite grain size
create-precipitation-domain martensite $ new matrix: martensite
set-precipitation-parameter martensite x bcc_a2 $ define matrix structure
```

```
set-precipitation-parameter martensite t d e ddm $ dislocation density (=1e14 m^-2)
set-precipitation-parameter martensite t g ags $ austenite grain size !!! NEW !!!
set-precipitation-parameter martensite t s sgs $ subgrain size
set-precipitation-parameter martensite t o sgef $ subgrain elongation factor
$ ------------------------------ PRECIPITATE PHASES IN AUSTENITE ----------------------------------
create-new-phase nbc p NbC(aust,g) $ new precipitate phase in austenite
set-precipitation-parameter nbc_p0 c npc $ use variable for prec. classes
set-precipitation-parameter nbc_p0 d austenite $ precipitation domain (matrix phase)
set-precipitation-parameter nbc_p0 n s g $ nucleation sites are grain boundaries
set-precipitation-parameter nbc_p0 n j y $ nucleate only with valid major constituents
set-precipitation-parameter nbc_p0 n p y austenite $ restrict nucleation to precipitation domain

create-new-phase nbc p NbC(aust,d) $ new precipitate phase in austenite
set-precipitation-parameter nbc_p1 c npc $ use variable for prec. classes
set-precipitation-parameter nbc_p1 d austenite $ precipitation domain (matrix phase)
set-precipitation-parameter nbc_p1 n s d $ nucleation sites are dislocations
set-precipitation-parameter nbc_p1 n j y $ nucleate only with valid major constituents
set-precipitation-parameter nbc_p1 n p y austenite $ restrict nucleation to precipitation domain

create-new-phase aln p AlN(aust,d) $ new precipitate phase in austenite
set-precipitation-parameter aln_p0 c npc_aln $ use variable for prec. classes
set-precipitation-parameter aln_p0 d austenite $ precipitation domain (austenite phase)
set-precipitation-parameter aln_p0 n s d $ nucleation sites are dislocations
set-precipitation-parameter aln_p0 n f y $ account for coherent misfit stress
set-precipitation-parameter aln_p0 t m n 0.27 $ use volumetric misfit value of 0.27
set-precipitation-parameter aln_p0 n p y austenite $ restrict nucleation to precipitation domain
create-new-phase cr2n p Cr2N(aust,d) $ new precipitate phase in austenite
set-precipitation-parameter cr2n_p0 c npc $ use variable for prec. classes
set-precipitation-parameter cr2n_p0 d austenite $ precipitation domain (austenite phase)
set-precipitation-parameter cr2n_p0 n s d $ nucleation sites are dislocations
set-precipitation-parameter cr2n_p0 n p y austenite $ restrict nucleation to precipitation domai

create-new-phase VN p VN(aust,g) $ new precipitate phase VN in martensite
set-precipitation-parameter vn_p0 c npc_vn $ use variable npc for # of prec. classes
set-precipitation-parameter vn_p0 d austenite $ precipitation domain (matrix phase)
set-precipitation-parameter vn_p0 n s g $ nucleation sites at grain boundaries
set-precipitation-parameter vn_p0 n j y $ nucleate only with valid major constituents
set-precipitation-parameter vn_p0 n p y austenite $ restrict nucleation to precipitation domain
$ ------------------------------- PRECIPITATE PHASES IN MARTENSITE -------------------------------
$ The M7C3 and Cementite precipitates are not stable at 600C, nevertheless they have to be considered
$ in the calculation due to the influence on the M23C6 evolution during heating and cooling treatments.
$ Better agreement with experimental values of M23C6 diameter is achieved by considering the M7C3 and
$ Cementite in the calculation.
create-new-phase nbc p NbC(mart,g) $ new precipitate phase in martensite
set-precipitation-parameter nbc_p2 c npc $ use variable for prec. classes
set-precipitation-parameter nbc_p2 d martensite $ precipitation domain (matrix phase)
set-precipitation-parameter nbc_p2 n s g $ nucleation sites are grain boundaries
set-precipitation-parameter nbc_p2 n j y $ nucleate only with valid major constituents
set-precipitation-parameter nbc_p2 n p y martensite $ restrict nucleation to precipitation domain

create-new-phase nbc p NbC(mart,d) $ new precipitate phase in martensite
set-precipitation-parameter nbc_p3 c npc_nbc $ use variable for prec. classes
set-precipitation-parameter nbc_p3 d martensite $ precipitation domain (matrix phase)
set-precipitation-parameter nbc_p3 n s d $ nucleation sites are dislocations
set-precipitation-parameter nbc_p3 n j y $ nucleate only with valid major constituents
set-precipitation-parameter nbc_p3 n p y martensite $ restrict nucleation to precipitation domain

create-new-phase nbc p NbC(mart,s) $ new precipitate phase in martensite
set-precipitation-parameter nbc_p4 c npc_nbc $ use variable for prec. classes
set-precipitation-parameter nbc_p4 d martensite $ precipitation domain (matrix phase)
set-precipitation-parameter nbc_p4 n s s $ nucleation sites are subgrain boundaries
set-precipitation-parameter nbc_p4 n j y $ nucleate only with valid major constituents
set-precipitation-parameter nbc_p4 n p y martensite $ restrict nucleation to precipitation domain
```

```
create-new-phase aln p AlN(mart,d) $ new precipitate phase in martensite
set-precipitation-parameter aln_p1 c npc_aln $ use variable for prec. classes
set-precipitation-parameter aln_p1 d martensite $ precipitation domain (matrix phase)
set-precipitation-parameter aln_p1 n s d $ nucleation sites are dislocations
set-precipitation-parameter aln_p1 n f y $ account for coherent misfit stress
set-precipitation-parameter aln_p1 t m n 0.27 $ use volumetric misfit value of 0.27
set-precipitation-parameter aln_p1 n p y martensite $ restrict nucleation to precipitation domain
create-new-phase VN p VN(mart,g) $ new precipitate phase VN in martensite
set-precipitation-parameter vn_p1 c npc $ use variable npc for # of prec. classes
set-precipitation-parameter vn_p1 d martensite $ precipitation domain (matrix phase)
set-precipitation-parameter vn_p1 n s g $ nucleation sites at grain boundaries
set-precipitation-parameter vn_p1 n j y $ nucleate only with valid major constituents
set-precipitation-parameter vn_p1 n p y martensite $ restrict nucleation to precipitation domain

create-new-phase VN p VN(mart,d) $ new precipitate phase VN in martensite
set-precipitation-parameter vn_p2 c npc $ use variable npc for # of prec. classes
set-precipitation-parameter vn_p2 d martensite $ precipitation domain (matrix phase)
set-precipitation-parameter vn_p2 n s d $ nucleation sites at dislocations
set-precipitation-parameter vn_p2 n j y $ nucleate only with valid major constituents
set-precipitation-parameter vn_p2 n p y martensite $ restrict nucleation to precipitation domain

create-new-phase VN p VN(mart,s) $ new precipitate phase VN in martensite
set-precipitation-parameter vn_p3 c npc_vn $ use variable npc for # of prec. classes
set-precipitation-parameter vn_p3 d martensite $ precipitation domain (matrix phase)
set-precipitation-parameter vn_p3 n s s $ nucleation sites at subgrain boundaries
set-precipitation-parameter vn_p3 n j y $ nucleate only with valid major constituents
set-precipitation-parameter vn_p3 n p y martensite $ restrict nucleation to precipitation domain
create-new-phase m23c6 p M23C6(mart,s) $ new precipitate phase in martensite
set-precipitation-parameter m23c6_p0 c npc_m23c6 $ use variable for prec. classes
set-precipitation-parameter m23c6_p0 d martensite $ precipitation domain (matrix phase)
set-precipitation-parameter m23c6_p0 n s s $ nucleation sites are subgrains
set-precipitation-parameter m23c6_p0 n p y martensite $ restrict nucleation to precipitation domain

create-new-phase m23c6 p M23C6(mart,g) $ new precipitate phase in martensite
set-precipitation-parameter m23c6_p1 c npc_m23c6 $ use variable for prec. classes
set-precipitation-parameter m23c6_p1 d martensite $ precipitation domain (matrix phase)
set-precipitation-parameter m23c6_p1 n s g $ nucleation sites are grain boundaries
set-precipitation-parameter m23c6_p1 n p y martensite $ restrict nucleation to precipitation domain
create-new-phase m7c3 p M7C3(mart,s) $ new precipitate phase M7C3 in martensite
set-precipitation-parameter m7c3_p0 c npc $ use variable for prec. classes
set-precipitation-parameter m7c3_p0 d martensite $ precipitation domain (matrix phase)
set-precipitation-parameter m7c3_p0 n s s $ nucleation sites at subgrain boundaries
set-precipitation-parameter m7c3_p0 n p y martensite $ restrict nucleation to precipitation domain
create-new-phase cementite p Cem(mart,s) $ new precipitate cementite in martensite
set-precipitation-parameter cementite_p0 c npc $ use variable for prec. classes
set-precipitation-parameter cementite_p0 d martensite $ precipitation domain (matrix phase)
set-precipitation-parameter cementite_p0 n s s $ nucleation sites at grain boundaries
set-precipitation-parameter cementite_p0 n p y martensite $ restrict nucleation to prec. domain
create-new-phase cr2n p Cr2N(mart,d) $ new precipitate phase in martensite
set-precipitation-parameter cr2n_p1 c npc $ use variable for prec. classes
set-precipitation-parameter cr2n_p1 d martensite $ precipitation domain (matrix phase)
set-precipitation-parameter cr2n_p1 n s d $ nucleation sites are dislocations
set-precipitation-parameter cr2n_p1 n p y martensite $ restrict nucleation to precipitation domai
create-new-phase laves_phase p Laves(mart,s) $ new precipitate phase in martensite
set-precipitation-parameter laves_phase_p0 c npc_laves $ use variable for prec. classes
set-precipitation-parameter laves_phase_p0 d martensite $ precipitation domain (matrix phase)
set-precipitation-parameter laves_phase_p0 n s s $ nucleation sites are subgrains
set-precipitation-parameter laves_phase_p0 n p y martensite $ restrict nucleation to precipitation domain
set-precipitation-parameter laves_phase_p0 f y lav_ict $ diffuse interface correction is set on
$ Zet-phase has special settings due to the fact that it nucleates within the VN precipitates
$ and nucleation is defined as special nucleation model for precipitation on particles with
$ equivalent interfacial energy. Make sure that 'direct particle transformation' is selected as
$ nucleation model
```

```
$ IMPORTANT: The value for the equivalent interfacial energy is basically unknown and must
$ be considered as a fitting parameter!!! Presently, no physical model for Z-phase nucleation
$ is available!!!
create-new-phase zet p Z(m,vn_a_g) $ new prec. phase for Zet-phase in martensite
set-precipitation-parameter zet_p0 c npc $ use variable for prec. classes
set-precipitation-parameter zet_p0 d martensite $ precipitation domain (matrix phase)
set-precipitation-parameter zet_p0 n s p vn_p0 $ nucleation sites are existing VN prec.
set-precipitation-parameter zet_p0 n o e eie_zet $ use equiv. intf. energy with value 1
set-precipitation-parameter zet_p0 n n d $ use direct particle transf. nucl. model
set-precipitation-parameter zet_p0 n p y martensite $ restrict nucleation to precipitation domain

create-new-phase zet p Z(m,vn_m_g) $ new prec. phase for Zet-phase in martensite
set-precipitation-parameter zet_p1 c npc $ use variable for prec. classes
set-precipitation-parameter zet_p1 d martensite $ precipitation domain (matrix phase)
set-precipitation-parameter zet_p1 n s p vn_p1 $ nucleation sites are existing VN prec.
set-precipitation-parameter zet_p1 n o e eie_zet $ use equiv. intf. energy with value 1
set-precipitation-parameter zet_p1 n n d $ use direct particle transf. nucl. model
set-precipitation-parameter zet_p1 n p y martensite $ restrict nucleation to precipitation domain

create-new-phase zet p Z(mart,vn_m_d) $ new prec. phase for Zet-phase in martensite
set-precipitation-parameter zet_p2 c npc $ use variable for prec. classes
set-precipitation-parameter zet_p2 d martensite $ precipitation domain (matrix phase)
set-precipitation-parameter zet_p2 n s p vn_p2 $ nucleation sites are existing VN prec.
set-precipitation-parameter zet_p2 n o e eie_zet $ use equiv. intf. energy with value 1
set-precipitation-parameter zet_p2 n n d $ use direct particle transf. nucl. model
set-precipitation-parameter zet_p2 n p y martensite $ restrict nucleation to precipitation domain

create-new-phase zet p Z(mart,vn_m_s) $ new prec. phase for Zet-phase in martensite
set-precipitation-parameter zet_p3 c npc $ use variable for prec. classes
set-precipitation-parameter zet_p3 d martensite $ precipitation domain (matrix phase)
set-precipitation-parameter zet_p3 n s p vn_p3 $ nucleation sites are existing VN prec.
set-precipitation-parameter zet_p3 n o e eie_zet $ use equiv. intf. energy with value 1
set-precipitation-parameter zet_p3 n n d $ use direct particle transf. nucl. model
set-precipitation-parameter zet_p3 n p y martensite $ restrict nucleation to precipitation domain
$ Zet-phase can also nucleate directly from the matrix. However, its nuclei with rather complex
$ crystal structure is in direct competition with the MX phase with simple fcc. For that reason,
$ the probability of Z-phase nucleation is extremely low, because Cr, V and N will nucleate the simple
$ structure much easier than the double-layer structure of Zet. Estimates (Sonderegger/Danielsen/
$ Kozeschnik, 2005, unpublished) deliver a factor of 1e-12. This value is entered as nucleation
$ constant, to reflect this competitive (entropic) effect
create-new-phase zet p Z(mart,d) $ new prec. phase for Zet-phase in martensite
set-precipitation-parameter zet_p4 c npc $ use variable for prec. classes
set-precipitation-parameter zet_p4 d martensite $ precipitation domain (matrix phase)
set-precipitation-parameter zet_p4 n s d $ nucleation sites are dislocation
set-precipitation-parameter zet_p4 z n $ no ie size correction for Z-Phase
set-precipitation-parameter zet_p4 n u nucl_const_zet $ nucleation constant for matrix Z-phase
set-precipitation-parameter zet_p4 n p y martensite $ restrict nucleation to precipitation domain
$ ****************************************************************************************************
$ ********************************* OUTPUT WINDOWS, PLOTS, ETC. ************************************
$ ****************************************************************************************************
$ ---------------------------------- Hardening (Normalizing) plot ----------------------------------
$ create one frame displaying the service part, with no exp data
new-gui-window p1 $ generate new plot: Hardening
$ remember window ID to address it correctly later in the script
set-variable-value window_id_hardening active_frame_id $ save windows id to variable
set-gui-window-property . x stepvalue $ default x-axis variable (time)
set-gui-window-property . s u y $ use default x-axis for all plots: yes
set-gui-window-property . s t time / min $ default x-axis title
set-gui-window-property . s f 1/60 $ scaling factor is 1/60 for min
set-gui-window-property . n 2 $ 2 plot columns
set-plot-option . s n b t$c $ add series: temperature
set-plot-option . s m -1 t$c T $ define series legend
set-plot-option . a y 1 t temperature / C $ y-axis title
```

```
if (comp==1)
set-plot-option . t Raccord-HiMAT-Normalizing $ define plot title
elseif (comp==2)
set-plot-option . t Raccord-TUGraz-Normalizing $ define plot title
endif
create-new-plot x . $ create new plot: phase fractions
set-plot-option . l a y $ replace variable names by kinetic alias
set-plot-option . s n b f_prec$* $ add all series: phase fractions of prec.
set-plot-option . a y 1 t phase fraction / % $ y-axis title
set-plot-option . a y 1 y log $ use logarithmic scale for y-axis
set-plot-option . a y 1 f 100 $ scaling factor is 100 for %
set-plot-option . a y 1 s 1e-4.. $ scale the y-axis from 1e-4..
create-new-plot x . $ create new plot: mean diameter
set-plot-option . l a y $ replace variable names by kinetic alias
set-plot-option . s n b d_mean$* $ add all series: mean diameter of precipitates
set-plot-option . a y 1 t mean diameter / nm $ change y-axis title
set-plot-option . a y 1 y lin $ use linear scale for y-axis
set-plot-option . a y 1 f 1e9 $ scaling factor is 1e9 for nm
create-new-plot x . $ create new plot: number densities
set-plot-option . l a y $ replace all variable names by kinetic alias
set-plot-option . s n b num_part$* $ add all series: number densities of precipitates
set-plot-option . a y 1 t number density / m<sup>-3</sup> $ change y-axis title
set-plot-option . a y 1 y log $ use logarithmic scale for y-axis
set-plot-option . a y 1 s 1e10.. $ scale the y-axis from 1e10..
move-gui-window . 70 30 700 980 $ move window to new position and resize
update-gui-windows . $ update the GUI window
move-gui-window . hide $ hide plot
$ ---------------------------------------- Tempering ----------------------------------------
$ create one frame displaying the service part, with no exp data
new-gui-window p1 $ generate new plot: Tempering
$ remember window ID to address it correctly later in the script
set-variable-value window_id_tempering active_frame_id $ save windows id to variable
set-gui-window-property . x stepvalue $ default x-axis variable (time)
set-gui-window-property . s u y $ use default x-axis for all plots: yes
set-gui-window-property . s t time / min $ default x-axis title
set-gui-window-property . s f 1/60 $ scaling factor is 1/60 for min
set-gui-window-property . n 2 $ 2 plot columns
set-plot-option . s n b t$c $ add series: temperature
set-plot-option . s m -1 t$c T $ define series legend
set-plot-option . a y 1 t temperature / C $ y-axis title
if (comp==1)
set-plot-option . t Raccord-HiMAT-Tempering $ define plot title
elseif (comp==2)
set-plot-option . t Raccord-TUGraz-Tempering $ define plot title
endif
create-new-plot x . $ create new plot: phase fractions
set-plot-option . l a y $ replace variable names by kinetic alias
set-plot-option . s n b f_prec$* $ add all series: phase fractions of prec.
set-plot-option . a y 1 t phase fraction / % $ y-axis title
set-plot-option . a y 1 y log $ use logarithmic scale for y-axis
set-plot-option . a y 1 f 100 $ scaling factor is 100 for %
set-plot-option . a y 1 s 1e-4.. $ scale the y-axis from 1e-4..
create-new-plot x . $ create new plot: mean diameter
set-plot-option . l a y $ replace variable names by kinetic alias
set-plot-option . s n b d_mean$* $ add all series: mean diameter of precipitates
set-plot-option . a y 1 t mean diameter / nm $ change y-axis title
set-plot-option . a y 1 y lin $ use linear scale for y-axis
set-plot-option . a y 1 f 1e9 $ scaling factor is 1e9 for nm
create-new-plot x . $ create new plot: number densities
set-plot-option . l a y $ replace all variable names by kinetic alias
set-plot-option . s n b num_part$* $ add all series: number densities of precipitates
set-plot-option . a y 1 t number density / m<sup>-3</sup> $ change y-axis title
set-plot-option . a y 1 y log $ use logarithmic scale for y-axis
```

```
set-plot-option . a y 1 s 1e10.. $ scale the y-axis from 1e10..
move-gui-window . 90 50 700 980 $ move window to new position and resize
update-gui-windows . $ update the GUI window
move-gui-window . hide $ hide plot
$ ---------------------------------------- Service ----------------------------------------
$ create one frame displaying the service part, with no exp data
new-gui-window p1 $ generate new plot: Service
$ remember window ID to address it correctly later in the script
set-variable-value window_id_service active_frame_id $ save windows id to variable
set-gui-window-property . x stepvalue $ default x-axis variable (time)
set-gui-window-property . s u y $ use default x-axis for all plots: yes
set-gui-window-property . s t time / h $ default x-axis title
set-gui-window-property . s f 1/3600 $ scaling factor is 1/3600 for h
set-gui-window-property . n 2 $ 2 plot columns
set-plot-option . s n b t$c $ add series: temperature
set-plot-option . s m -1 t$c T $ define series legend
set-plot-option . a y 1 t temperature / C $ y-axis title
if (comp==1)
set-plot-option . t Raccord-HiMAT-Service-BM $ define plot title
elseif (comp==2)
set-plot-option . t Raccord-TUGraz-Service-BM $ define plot title
endif
create-new-plot x . $ create new plot: phase fractions
set-plot-option . l a y $ replace variable names by kinetic alias
set-plot-option . s n b f_prec$* $ add all series: phase fractions of prec.
set-plot-option . a y 1 t phase fraction / % $ y-axis title
set-plot-option . a y 1 y log $ use logarithmic scale for y-axis
set-plot-option . a y 1 f 100 $ scaling factor is 100 for %
set-plot-option . a y 1 s 1e-4.. $ scale the y-axis from 1e-4..
create-new-plot x . $ create new plot: mean diameter
set-plot-option . l a y $ replace variable names by kinetic alias
set-plot-option . s n b d_mean$* $ add all series: mean diameter of precipitates
set-plot-option . a y 1 t mean diameter / nm $ change y-axis title
set-plot-option . a y 1 y lin $ use linear scale for y-axis
set-plot-option . a y 1 f 1e9 $ scaling factor is 1e9 for nm
create-new-plot x . $ create new plot: number densities
set-plot-option . l a y $ replace all variable names by kinetic alias
set-plot-option . s n b num_part$* $ add all series: number densities of precipitates
set-plot-option . a y 1 t number density / m<sup>-3</sup> $ change y-axis title
set-plot-option . a y 1 y log $ use logarithmic scale for y-axis
set-plot-option . a y 1 s 1e10.. $ scale the y-axis from 1e10..
move-gui-window . 110 70 700 980 $ move window to new position and resize
update-gui-windows . $ update the GUI window
move-gui-window . hide $ hide plot

$ ********************************************************************************************************
$ ***************************** START PRECIPITATE SIMULATION ******************************************
$ ********************************************************************************************************
set-temperature-celsius 2000 $ define something
set-automatic-startvalues $ initiate equil. calc. (estimate variables)
calculate-equilibrium $ calculate equilibrium state
$ speed up simulations, modify numerical parameters
set-simulation-parameter c n f 1.0 $ maximum radius growth from 0.2 to 1.0
set-simulation-parameter u 1000
$ ------------------------ START PRECIPITATE SIMULATION PART I (HARDENING) -------------------------
rename-current-buffer hardening $ rename buffer for heat treatment
set-gui-window-property window_id_hardening b hardening $ attach to buffer window
set-simulation-parameter t h hardening 10 $ temperature profile from HT, max. T-step
set-simulation-parameter s r $ starting condition for prec. sim.: reset
move-gui-window window_id_hardening show $ bring plot to front
$ hide console window to make plots visible
move-gui-window c hide $ hide console window
start-precipitate-simulation $ let's go with part I
```

```
$ save state after simulation. Is starting point for next simulation part II
create-calc-state after_hardening
$ ---------- START PRECIPITATE SIMULATION PART II (TEMPERING)----------
create-calc-buffer tempering $ create buffer for HT
select-calc-buffer tempering $ select calc buffer
set-gui-window-property window_id_tempering b tempering $ attach to buffer window
set-simulation-parameter t h tempering 10 $ temperature profile from HT, max. T-step
set-simulation-parameter s l after_hardening $ starting condition for prec. sim.: reset
move-gui-window window_id_tempering show $ bring plot to front
start-precipitate-simulation $ let's go with part II
$ save state after simulation. Is starting point for next simulation part III
create-calc-state after_tempering
$ ---------- START PRECIPITATE SIMULATION PART V (SERVICE)----------
create-calc-buffer service $ create buffer for HT
select-calc-buffer service $ select calc buffer
set-gui-window-property window_id_service b service $ attach to buffer window
set-simulation-parameter t h service 10 $ temperature profile from HT, max. T-step
set-simulation-parameter s l after_tempering $ starting condition for prec. sim.: reset
move-gui-window window_id_service show $ bring plot to front
start-precipitate-simulation $ let's go with part III
$ save state after simulation.
create-calc-state after_service
if (comp==1)
set-working-directory C:/Users/Florian/Desktop/Diplomarbeit/Unterlagen_Schlachi/JFE Steel
save-workspace JFE_5_service
elseif(comp==2)
set-working-directory C:/Users/students/Desktop/FinalVersion4/Results
save-workspace P91_BM_76_9_0.5_ict_laves1452K_agsfghaz950C_650C_100000h
endif
$ ********************************************************************************************************
$ ****************************** PRECIPITATE SIMULATION FINISHED (BM) ******************************
$ ********************************************************************************************************
endif
```

8.) Literature

[1] D. R. Jara, „State of the art and objective of the work," in *PhD Thesis: 9-12% Cr heat resistant steels: alloy design, TEM characterisation of microstructure evolution and creep response at 650 °C*, Bochum, 2011, pp. 3-9.

[2] D. R. Jara, „Metallurgy of 9-12 % Cr steels," in *PhD Thesis: 9-12% Cr heat resistant steels: alloy design, TEM characterisation of microstructure evolution and creep response at 650 °C*, Bochum, 2011, pp. 10-24.

[3] I. Holzer, „Strength and structure of martensitic 9-12 % Cr steels," in *PhD Thesis: Modelling and Simulation of Strengthening in Complex Martensitic 9-12 % Cr Steel and a Binary Fe-Cu Alloy*, Graz, May 2010, pp. 13-32.

[4] B. Sonderegger, „Charakterisierung der Substruktur in modernen Kraftwerkswerkstoffen mittels der EBSD Methode," Graz University of Technology, Februar 2004, pp. 119- 122.

[5] F. Abe und M. Tabuchi, „Microstructure and creep strength of welds in advanced ferritic power plant steels; DOI: 10.1179/136217104225017107," *Science and Technology of Welding and Joining, 9:1,* pp. 22-30, 2004.

[6] P. Mayr, „PhD Thesis: Evolution of microstructure and mechanical properties of the heat affected zone in B-containing 9 % chromium steels," Graz, Institute of Materials Science and Welding, July 2007, pp. 23-31.

[7] J. Hald, „Microstructure and long-term creep properties of 9-12% Cr steels; doi: 10.1016/j.ijpvp.2007.06.010," *International Journal of Pressure Vessels and Piping 85 (2008),* pp. 30-37.

[8] I. Holzer, E. Kozeschnik und H. Cerjak, „New approach to predict the long-term creep behaviour and evolution of precipitate back-stress of 9-12% chromium steels; DOI: 10.1007/s12666-010-0019-8," *Transactions of the Indian Institute of Metals,* Bde. %1 von %2vol. 63, issues 2-3, pp. 137- 143, April- June 2010.

[9] Handelsblatt, „Zukunft der Energie- Umstrittene Technik CCS," 7th December 2015. [Online]. Available: http://www.handelsblatt.com/technik/zukunftderenergie/umstrittene-technik-ccs-lippenbekenntnisse-der-kohleindustrie/12687956-2.html. [Zugriff am 20th June 2016].

[10] I. BrightSource Energy, „Ivanpah- Solar Electric Generating System," 2013. [Online]. Available: http://www.ivanpahsolar.com/.

[11] H. Naoi, M. Ohgami, X. Liu und T. Fujita, „Effects of Aluminum Content on the Mechanical Properties of a 9Cr-0.5Mo-1.8W Steel," *Metallurgical and materials transactions A, vol. 28A,* pp. 1195-1203, May 1997.

[12] H. Magnusson und R. Sandström, „Influence of aluminium on creep strength of 9–12% Cr steels; doi:10.1016/j.msea.2009.07.060," *Materials Science and Engineering A 527,* p. 118–125, 2009.

[13] M. A. El-Azim, O. Ibrahim und O. El-Desoky, „Long term creep behaviour of welded joints of P91 steel at 650 C," *Materials Science and Engineering: A,* Bd. 560, pp. 678-684, 2013.

[14] B. Sonderegger, Habilitationsschrift: Aspects on measurement, modeling and impact of precipitates in alloys, Graz, July 2012.

[15] B. Krenmayr und B. Sonderegger, „Development of a creep strength estimation method based on microstructural simulation in mod. 9Cr-1Mo steels (Unpublished)," in *Literature Review*, Graz University of Technology, Institute of Materials Science and Welding, 2016.

[16] F. Abe, „Grade 91 heat-resistant martensitic steel," *Coal Power Plant Materials and Life Assessment: Developments and Applications, vol. 91, Elsevier,* pp. 3- 51, 2014.

[17] S. C. Bose, K. Singh, J. Swaminathan und D. S. Sarma, „Prediction of creep life of X10CrMoVNbN-91 (P-91) steel through short term stress relaxation test methodology," *Mat. Sci. Tech., vol. 20, no. 10,* pp. 1290- 1296, October 2004.

[18] C. G. Panait, W. Bendick, A. Fuchsmann, A.-F. Gourgues-Lorenzon und J. Besson, „Study of the microstructure of the Grade 91 steel after more than 100,000 h of creep exposure at 600 °C," *Int. J. Press. Vessel. Pip.,* Bd. 87, Nr. 6, pp. 326-335, 2010.

[19] A. Zielinska-Lipiec und A. Czyrska-Filemonowicz, „Characterisation of the Micro- and Nanoscale Structure of New Creep-Resistant Steels for Use in Advanced USC Steam Power Plants," *Material Trans.,* Bd. 48, Nr. 5, pp. 931-935, 2007.

[20] C. G. Panait, A. Zielinska-Lipiec, T. Koziel, A. Czyrska-Filemonowicz, A.-F. Gourgues-Lorenzon und W. Bendick, „Evolution of dislocation density, size of subgrains and MX-type precipitates in a P91 steel during creep and during thermal ageing at 600C for more than 100,000h," *Mater. Sci. Eng. A, vol. 527, no. 16- 17,* pp. 4062- 4069, June 2010.

[21] A. Orlova, J. Bursk, K. Kucharova und V. Sklenicka, „Microstructural development during high temperature creep of 9 % Cr steel," *Materials Science and Engineering: A,* Bd. 245, Nr. 1, pp. 39-48, 1998.

[22] P. Polcik, T. Sailer, W. Blum, S. Straub, J. Bursik und A. Orlova, „On the microstructural development of the tempered martensitic Cr-steel P 91 during long-term creep - a comparison of data," *Materials Science and Engineering: A,* Bd. 260, Nr. 1-2, pp. 252-259, 1999.

[23] E. Cerri, E. Evangelista, S. Spigarelli und P. Bianchi, „Evolution of microstructure in a modified 9Cr1Mo steel during short term creep," *Materials Science and Engineering: A ,* Bd. 245, Nr. 2, pp. 285-292, 1998.

[24] J. Pesicka, R. Kuzel, A. Dronhofer und G. Eggeler, „The evolution of dislocation density during heat treatment and creep of tempered martensite ferritic steels," *Acta Materialia,* 2003.

[25] K. Maruyama, K. Sawada und J. Koike, „Strengthening Mechanisms of Creep Resistant Tempered Martensitic Steel," *ISIJ International,* Bd. 41, Nr. 6, pp. 641-653, 2001.

[26] H. B. Callen, Thermodynamics and an Introduction to Thermostatistics; ISBN 978-0471862567, New York / Chichester / Brisbane / Toronto / Singapore: John Wiley & Sons, 1985.

[27] M. Klell und R. Almbauer, „Lecture Script: Höhere Thermodynamik (Advanced Thermodynamics)," pp. 51-74, 2013.

[28] P. Koukkari, Introduction to constrained Gibbs energy methods in process and materials research; ISBN 978-951-38-8134-4, Kuopio: VTT Technical Research Centre of Finland, 2014.

[29] R. Clausius, „Über eine veränderte Form des zweiten Hauptsatzes der mechanischen Wärmetheorie," *Annalen der Physik (Poggendoff) xciii,* pp. 481-506, 1854.

[30] K. Russell, „Nucleation in Solids: The induction and steady state effects; DOI: 10.1016/0001-8686(80)80003-0," *Adv. Coll. Interf. Sci.,* Bd. 13, Nr. 3-4, pp. 205-318, September 1980.

[31] B. Sonderegger, „Modeling precipitation kinetics," in *Habilitation: Aspects on measurement, modeling and impact of precipitates in alloys*, Graz, University of Technology, 2012, pp. 19-36.

[32] F. Riedlsperger, Bachelor Thesis: Thermodynamische Modellierung von Keimbildung, Graz: University of Technology, 2013.

[33] A. Fick, „Über Diffusion; DOI: 10.1002/andp.18551700105," *Annalen der Physik,* Bd. 170, pp. 59-86, 1855.

[34] C. Zener, „Theory of Growth of Spherical Precipitates from Solid Solution; http://dx.doi.org/10.1063/1.1698258," *J. Appl. Phys. 20, 950 (1949),* pp. 950-953.

[35] I. M. Lifshitz und V. V. Slyozov, „The Kinetics of Precipitation from Supersaturated Solid Solutions; doi:10.1016/0022-3697(61)90054-3," *Journal of Physics and Chemistry of Solids,* Bd. 19, Nr. 1-2, pp. 35- 50, April 1961.

[36] J. Svoboda, F. D. Fischer, P. Fratzl und E. Kozeschnik, „Modelling of kinetics in multi-component multi-phase systems with spherical precipitates: I: Theory; doi:10.1016/j.msea.2004.06.018," *Mater. Sci. Eng. A 385 (2004),* pp. 166-174, November 2004.

[37] B. S. Srinivas Prasad, V. B. Rajkumar und H. Kumar, „Numerical simulation of precipitate evolution in ferritic–martensitic power plant steels," *Calphad, vol. 36,* March 2012.

[38] I. Holzer, „Modelling multi-particle precipitation kinetics with the software MatCalc," in *PhD Thesis-Modelling and Simulation of Strengthening in Complex Martensitic 9-12 % Cr Steel and a Binary Fe-Cu Alloy*, Graz, Monographic Series TU/ Advanced Materials Science, vol. 2, May 2010, pp. 35-40.

[39] K. Janssens, D. Raabe, E. Kozeschnik, M. Miodownik und B. Nestler, in *Computational Materials Engineering- An Introduction to Microstructure Evolution*, Burlington, Elsevier Academic Press, October 2007, pp. 179-217.

[40] S. Vujic, E. Plesiutschnig, C. Schlacher und C. Sommitsch, „Microstructure evolution of Gr. 91 steel- microstructure investigations," Graz University of Technology, April 2015.

[41] S. Vujic, E. Plesiutschnig, C. Schlacher und C. Sommitsch, „Simulation of precipitation evolution in Gr. 91 steel- precipitation report," Graz University of Technology, June 2015.

[42] S. Vujic, „MatCalc Script for simulation of precipitation kinetics in Gr. 91 steel," Graz University of Technology, 2015.

[43] I. Holzer, „The back-stress concept," in *PhD Thesis: Modelling and Simulation of Strengthening in Complex Martensitic 9-12 % Cr Steel and a Binary Fe-Cu Alloy*, Graz, University of Technology, 2010, p. 30.

[44] G. Dimmler, PhD Thesis: Quantification of the creep strength and the creep rupture strength of 9-12% Cr-steels on a microstructural basis, Graz: University of Technology, 2012.

[45] F. Abe, „Strengthening mechanisms in steel for creep and creep rupture (DOI: 10.1533/9781845694012.2.279)," pp. 279- 304, March 2008.

[46] M. Basirat, T. Shrestha, G. Potirniche, I. Charit und K. Rink, „A study of the creep behavior of modified 9Cr-1Mo steel using continuum-damage modeling," *International Journal of Plasticity,* Bd. 37, pp. 95-107, 2012.

[47] G. Gupta und G. S. Was, „Improved Creep Behavior of Ferritic-Martensitic Alloy T91 by Subgrain Boundary Density Enhancement; DOI: 10.1007/s11661-007-9411-3," *Metallurgical and Materials Transactions A, vol. 39A (2008),* pp. 150-164.

[48] K. Maruyama, K. Sawada und J. Koike, „Strengthening Mechanisms of Creep Resistant Tempered Martensitic Steel," *ISIJ International, Vol. 41 (2001), No. 6,* p. 641–653.

[49] H. Magnusson und R. Sandström, „Creep Strain Modeling of 9 to 12 Pct Cr Steels Based on Microstructure Evolution; DOI: 10.1007/s11661-007-9256-9," *Metallurgical and Materials Transactions A, vol. 38A (2007),* pp. 2033-2039.

[50] M. McLean, „On the threshold stress for dislocation creep in particle strengthened alloys; doi:10.1016/0001-6160(85)90018-5," *Acta Metallurgica,* Bd. 33, Nr. 4, pp. 545-556, April 1985.

[51] M. Ahmadi, E. Povoden-Karadeniz, K. Öksüz, A. Falahati und E. Kozeschnik, „A model for precipitation strengthening in multi-particle systems (doi:10.1016/j.commatsci.2014.04.025)," *Computational Materials Science,* Bd. vol. 91, pp. 173- 186, 2014.

[52] B. Sonderegger, I. Holzer, E. Kozeschnik und C. Sommitsch, „Particle distance distributions and their effect on precipitation strengthening," *Computer Methods in Materials Science,* Bd. vol. 11, pp. 148- 153, 2011.

[53] H. Magnusson und R. Sandström, „The Role of Dislocation Climb across Particles at Creep Conditions in 9 to 12 Pct Cr Steels; DOI: 10.1007/s11661-007-9280-9," *Metallurgical and Materials Transactions A- vol. 38 A,* pp. 2428-2434, October 2007.

[54] J. Martin, Precipitation Hardening, 2nd ed., Oxford, UK: Butterworth-Heinemann, 1998.

[55] D. Hull und D. J. Bacon, „Chapter 4," in *Introduction to Dislocations- 3rd edition*, Oxford, Pergamon Press, 1984, p. 73.

[56] B. Sonderegger und E. Kozeschnik, „Interfacial energy of diffuse phase boundaries in the generalized broken-bond approach; DOI: 10.1007/s11661-010-0370-8," *Metall. Mater. Trans. A, 41 (12),* pp. 3262-3269, 2010.

[57] S. Yadav, B. Sonderegger, M. Stracey und C. Poletti, „Modelling the creep behaviour of tempered martensitic steel based on a hybrid approach," *Materials Science and Engineering A, vol. 662,* pp. 330- 341, April 2016.

[58] E. Kozeschnik, „MatCalc Documentation," MatCalc Engineering, 7 July 2016. [Online]. Available: http://matcalc.tuwien.ac.at/wiki/doku.php?id=techpapers:nucleation:het_nucl_sites. [Zugriff am 7 July 2016].

[59] R. Radis und E. Kozeschnik, „Kinetics of AlN precipitation in microalloyed steel; doi:10.1088/0965-0393/18/5/055003," *Modelling Simul. Mater. Sci. Eng. 18 (2010),* pp. 1-16.

[60] B. Sonderegger, Dissertation: Charakterisierung der Substruktur in modernen Kraftwerkswerkstoffen mittels der EBSD Methode, Graz: Technische Universität, 2005.

[61] J. K. Mason und C. A. Schuh, „The generalized Mackenzie distribution: Disortientation angle distributions for arbitrary textures," *Acta Materialia 57,* p. 4186– 4197, 2009.

[62] S. Yadav, S. Kalacska, M. Domankova, D. C. Yubero, R. Resel, I. Groma, C. Beal, B. Sonderegger, C. Sommitsch und C. Poletti, „Evolution of the substructure of a novel 12 % Cr steel under creep conditions," *Materials Characterization 115,* pp. 23- 31, 2016.

[63] B. Sonderegger und E. Kozeschnik, „Particle strengthening in fcc crystals with prolate and oblate precipitates; doi:10.1016/j.scriptamat.2011.10.003," *Scripta Materialia 66 (2012),* pp. 52- 55, October 2011.

[64] Y. Hasegawa, „Grade 92 creep-strength-enhanced ferritic steel (doi:10.1533/9780857097323.1.52)," in *Coal Power Plant Materials and Life Assessment- Developments and Applications*, Japan, Elsevier, 2014, p. 52–86.

[65] H. Magnusson und R. Sandström, „Modeling Creep Strength of Welded 9 to 12 Pct Cr Steels; DOI: 10.1007/s11661-010-0449-2," *Metallurgical and Materials Transactions A, vol. 41 A,* pp. 3340-3347, December 2010.

[66] S. D. Yadav, B. Sonderegger, B. Sartory, C. Sommitsch und C. Poletti, „Characterisation and quantification of cavities in 9Cr martensitic steel for power plants; DOI: 10.1179/1743284714Y.0000000635," *Materials Science and Technology, 31:5,* pp. 554-564, 2015.

[67] H. Naoi, M. Ohgami, X. Liu und T. Fujita, „Effects of Aluminum Content on the Mechanical Properties of a 9Cr-0.5Mo-1.8W Steel," *Metallurgical and materials transactions A, vol. 28 A (1997),* pp. 1195-1203.

[68] T. Watanabe, M. Tabuchi, M. Yamazaki, H. Hongo und T. Tanabe, „Creep damage evaluation of 9Cr-1Mo-V-Nb steel welded joints showing Type IV fracture; DOI: 10.1016/j.ijpvp.2005.09.004," *International Journal of Vessels and Piping 83 (2006),* pp. 63-71.